The development of a semi-empirical electrowinning model to predict process performance

by

Mandy Tucker

Thesis presented in partial fulfilment
of the requirements for the Degree

of

MASTER OF ENGINEERING
(EXTRACTIVE METALLURGICAL ENGINEERING)

in the Faculty of Engineering
at Stellenbosch University

Supervisor

Dr Margreth Tadie

Co-Supervisor

Prof. Christie Dorfling

December 2019

DECLARATION

By submitting this thesis electronically, I declare that the entirety of the work contained therein is my own, original work, that I am the sole author thereof (save to the extent explicitly otherwise stated), that reproduction and publication thereof by Stellenbosch University will not infringe any third party rights and that I have not previously in its entirety or in part submitted it for obtaining any qualification.

Date: December 2019

PLAGIARISM DECLARATION

1. Plagiarism is the use of ideas, material and other intellectual property of another's work and to present is as my own.

2. I agree that plagiarism is a punishable offence because it constitutes theft.

3. I also understand that direct translations are plagiarism.

4. Accordingly all quotations and contributions from any source whatsoever (including the internet) have been cited fully. I understand that the reproduction of text without quotation marks (even when the source is cited) is plagiarism.

5. I declare that the work contained in this assignment, except where otherwise stated, is my original work and that I have not previously (in its entirety or in part) submitted it for grading in this module/assignment or another module/assignment.

Student number:

Initials and surname: M. Tucker

Signature: ……..

Date: ……..

ABSTRACT

Electrowinning is the final step in the hydrometallurgical production of high purity copper and comprises passing an electric current through a copper-containing electrolyte to plate solid copper onto a cathode. Key electrowinning performance indicators are current efficiency, specific energy consumption, yield and metal quality. The high energy demand and associated cost make performance determination critical during operation, but online measurement is impractical due to the delayed nature of the measurements and corrosive environment caused by acid mist. The current manual approach to process control in industrial tankhouses requires improvement, through the shift towards a pre-emptive approach to attaining plant performance data. The development of a semi-empirical electrowinning model to predict process performance was considered in this research as a first step towards a dynamic model and the implementation of control in electrowinning practice. The objectives were to develop a model to predict electrowinning performance, to develop a parameter fitting approach to calibrate the model to bench-scale experimental data, and to apply the model to an industrial operation.

The scope entailed a steady state model to predict current efficiency, specific energy consumption and solid copper yield based on operational and geometrical input variables. Model development constituted the design of a conceptual circuit diagram of an electrowinning cell consisting of up to hundreds of parallel pairs of electrodes, hardware and electrolyte resistances and a current loss parameter. The electrochemical reactions incorporated were copper reduction, water evolution and the cyclic reduction and oxidation of ferric and ferrous ions as an impurity. The model was coded in MATLAB through a first principles approach, combining a series of reaction rate and mass transfer kinetics, mass balances, electrochemical and thermodynamic equations and property correlations. The parameter fitting approach comprised the design of bench-scale experiments in which the input copper, sulphuric acid and iron concentrations, and current density were varied. The experimental data were used to calibrate parameters (for reaction and mass transfer rates and current loss) to the model through nonlinear regressions. The experiments revealed a constant rate of plating over time which validated the steady state assumption.

Average current loss over the bench-scale experiments was 0.145 A (about 1 - 5% of total current), accounting for current loss due to stray currents, ineffective electrode contact and possible side reactions. The rate kinetics parameters fit relatively well to the experimental data, with an R^2_{adj} of 0.864 for copper reduction, 0.739 for water oxidation, 0.724 for iron reduction and 0.661 for iron oxidation. While the performance data for different industrial tankhouses were scattered, the electrowinning model accurately predicted the performance of the bench-scale setup, demonstrating the potential of the model to accurately predict performance in an electrowinning system with specifically fit parameters. The average absolute errors between the model and experimental data were 3.2% for current efficiency, 3.0% for specific energy consumption and 7.0% for copper plating rate. The model could be used directly for operator training or

combined with the parameter fitting approach as a first step towards process control in an industrial electrowinning tankhouse.

OPSOMMING

Elektroherwinning is die finale stap in die hidrometallurgiese produksie van hoë suiwerheid koper en behels die vloei van ’n elektriese stroom deur ’n elektroliet wat koper bevat om vaste koper op ’n katode te plateer. Sleutel elektroherwinning werkverrigting aanwysers is stroom doeltreffendheid, spesifieke energie verbruik, opbrengs en metaal kwaliteit. Die hoë energie vereiste en meegaande koste maak die bepaling van doeltreffendheid krities gedurende bedryf, maar aanlynmeting is onprakties as gevolg van vertraging van die afmetings en korroderende omgewing veroorsaak deur suurmis. Die huidige handbenadering om die proses te beheer in industriële tenkhuise vereis verbetering, deur die skuif na ’n voorkomende benadering om data van aanlegdoeltreffendheid te verkry. Die ontwikkeling van ’n elektroherwinningmodel om prosesdoeltreffendheid te voorspel is oorweeg in hierdie navorsing as ’n eerste stap na ’n dinamiese model en die implementasie van beheer in elektroherwinningpraktyk. Die doelwitte was om ’n model te ontwikkel wat elektroherwinning se doeltreffendheid voorspel, om ’n parameter-passing-benadering te ontwikkel om die model met banktoetsskaal eksperimentele data te kalibreer, en om die model op ’n industriële bedryf toe te pas.

Die omvang het ’n bestendige toestand model bevat om stroomeffektiwiteit, spesifieke energie verbruik en vastestof koper opbrengs op bedryfs- en geometriese inset veranderlikes te voorspel. Modelontwikkeling het die ontwerp van ’n konsepsionele stroombaandiagram van ’n elektroherwinningsel behels, wat bestaan uit tot en met honderde parallelle pare elektrodes, hardeware en elektroliet weerstande en ’n stroomverlies parameter. Die elektrochemiese reaksies geïnkorporeer was koperreduksie, waterevolusie en die sikliese reduksie en oksidasie van ferri- en ferro-ione as ’n onsuiwerheid. Die model is gekodeer in MATLAB deur ’n eerste beginsels-benadering, wat ’n reeks reaksietempo en massa-oordragkinetika, massa-balanse, elektrochemiese en termodinamiese vergelykings en eienskap korrelasies, kombineer. Die parameter-passing-benadering het die ontwerp van banktoetsskaalekperimente behels, waarin die inset koper-, salpetersuur- en ysterkonsentrasies, en stroomdigtheid gevarieer het. Die eksperimentele data is gebruik om parameters te kalibreer (vir reaksie en massa-oordragtempo’s en stroomverlies) na die model deur nie-liniêre regressies. Die eksperimente het ’n konstante tempo van platering oor tyd bekend gemaak, wat die bestendige toestand aanname valideer.

Gemiddelde stroomverlies oor die banktoetsskaaleksperimente was 0.145 A (omtrent 1–5% van totale stroom), wat verantwoording doen vir stroomverlies as gevolg van swerfstrome, oneffektiewe elektrode kontak en moontlike newereaksies. Die tempokinetika parameters pas relatief goed met die eksperimentele data, met ’n R^2_{adj} van 0.864 vir koperreduksie, 0.739 vir wateroksidasie, 0.724 vir ysterreduksie en 0.661 vir ysteroksidasie. Terwyl die doeltreffendheiddata vir verskillende tenkhuise onreëlmatig was, het die elektroherwinningmodel die doeltreffendheid van die banktoetsskaalopset akkuraat voorspel, wat potensiaal vir die model om doeltreffendheid akkuraat te voorspel in ’n elektroherwinningsisteem met

spesifieke gepaste parameters, demonstreer. Die gemiddelde absolute afwyking tussen die model en eksperimentele data was 3.2% vir stroomdoeltreffendheid, 3.0% vir spesifieke energie verbruik en 7.0% vir koperplateringtempo. Die model kan direk gebruik word vir bedryfsopleiding of gekombineer word met die parameter-passing-benadering as ’n eerste stap na prosesbeheer in ’n industriële elektroherwinning tenkhuis.

ACKNOWLEDGEMENTS

I am grateful for the following people who helped and guided me throughout my Masters journey:

- My supervisors, Dr Margreth Tadie and Prof. Christie Dorfling, for providing exceptional support and technical expertise, for hours of thought-provoking electrowinning discussions, providing opportunities for personal and professional growth and for always inspiring me with their passion for mineral processing.
- The South African Minerals to Metals Research Institute (SAMMRI) for funding the research and providing valuable insights from an industry perspective.
- Technical officers and assistants of the workshop, laboratories and analytical facilities, and the administration and support staff within Process Engineering at Stellenbosch University.
- My family for supporting me throughout my university experience and for always encouraging me to succeed, and my friends and family who listened as I deliberated over problems and motivated me throughout the process.

TABLE OF CONTENTS

NOMENCLATURE

Category	Symbol	Description	Unit
Numerical symbols	a	Activity	-
	A	Area	m^2
	A	A parameter from Debye-Hückel activity model	-
	B	B parameter from Debye-Hückel activity model	-
	C	Molar concentration	mol/l
	d	Interelectrode distance	m
	D	Diffusion coefficient	cm^2/s
	e^0	Electric charge of one electron	$1.602 \times 10^{-19}\ C$
	E	Reduction potential	V
	E^0	Standard reaction potential	V
	F	Faraday's constant	96485 $C/equivalent\ mole$
	G^0	Standard Gibbs free energy	J
	i	Current density	A/m^2
	i^0	Exchange current density	A/m^2
	I	Current	A
	$\boldsymbol{J}$	Flux	$mol/(cm^2 \cdot s)$
	L	Length	m
	m	Mass	g
	m	Mass transfer coefficient (when used in the diffusion equation)	cm/s
	M	Molar mass	g/mol
	n	Number of electrons in reaction	-
	n	Sample size (when used in statistics)	-
	N	Number of cathodes in cell	-
	P	Plating rate, or rate of generation	g/s
	Q	Volumetric flow rate	m^3/h
	r	Species radius	m
	R	Universal Gas Constant	$8.314\ J/(mol \cdot K)$
	$R_{subscript}$	Resistance	Ω
	t	Time	s
	T	Temperature	K or $°C$
	U	Applied potential	V
	u	Interfacial velocity	$m^3/(h \cdot m^2)$ or m/s

Category	Symbol	Description	Unit
Numerical symbols	v	Fluid velocity	m/s
	V	Volume	l
	x	Concentration	g/l
	z	Charge number of ion	-
Greek symbols	α	Charge transfer coefficient	-
	β	Current efficiency	%
	δ	Diffusion layer thickness	cm
	Δ	Change in (variable)	-
	ϵ_i	Species permittivity	F/m
	ϵ_0	Permittivity of vacuum	$8.85 \times 10^{-12}\ F/m$
	ϵ_r	Species dielectric constant	-
	γ	Activity coefficient	-
	η	Overpotential	V
	κ	Ionic conductivity	S/m
	$\boldsymbol{\nabla}$	Gradient operator	-
	ϕ	Potential	V
	ρ	Density	g/l
	υ	Stoichiometric coefficient	-
Subscripts and superscripts	a	Anode	
	(aq)	Aqueous	
	c	Cathode	
	(g)	Gas	
	h	Hardware	
	i	Species	
	in	Advance electrolyte	
	j	Specific experiment	
	(l)	Liquid	
	out	Spent electrolyte	
	s	Electrolyte	
	(s)	Solid	
	T	Total	
	0	Standard/equilibrium	

Category	Symbol	Description	Unit
Acronyms and other symbols	AAS	Atomic Absorption Spectroscopy	
	BMR	Base Metal Refinery	
	CFD	Computational Fluid Dynamics	
	e^-	Electron	
	EW	Electrowinning	
	IHP	Inner Helmholtz Plane	
	IS	Ionic strength	
	O	Oxidised species	
	OHP	Outer Helmholtz Plane	
	R	Reduced species	
	SEC	Specific Energy Consumption	MWh/t
	SX	Solvent Extraction	

GLOSSARY

Word/Phrase	Definition
Advance electrolyte	Metal rich aqueous phase that enters the electrowinning process.
Anode	The positive electrode, at which oxidation occurs.
Busbar	Conductive material that joins adjacent electrowinning cells.
Cathode	The negative electrode, at which reduction occurs.
Cell	An electrowinning process unit, housing numerous pairs of electrodes.
Conductivity	A measure of the electricity conducting capacity of a material.
Convection	Mass transfer of ions through the bulk electrolyte solution by natural or forced means.
Counter electrode	The electrode that is not of primary interest.
Current density	Current (flux of charge) per unit area perpendicular to direction of flow.
Current efficiency	Percentage of total current that is used in the metal plating reaction.
Dendrite	Abnormal growth of metal deposit on the electrode.
Diffusion	Mass transfer of ions in solution to the electrode surface, due to a concentration gradient.
Electrochemical reaction	A chemical reaction involving the transfer of electrons (either oxidation or reduction).
Electrochemistry	The branch of chemistry that focuses on the relationship between chemical and electrical principles.
Electrode	A metal through which electrons flow, and the location of an electrochemical reaction.
Electrodeposition	The process of the deposition or plating of a solid metal onto an electrode.
Electrolyte	A solution which is a conductor of ions.
Electrorefining	The plating of pure metal onto a cathode, with the anode as the impure metal. Electrorefining is the final step in a pyrometallurgical process.
Electrowinning	The plating of pure metal onto a cathode, from a metal-containing electrolyte. Electrowinning is the final step in a hydrometallurgical process.
Hydrometallurgy	A process of recovering metals from their ores using an aqueous, metal-containing solution.
Migration	Mass transfer of ions in solution due to an electrical gradient.
Morphology	Physical form of the metal deposited onto the electrode.
Nucleation	Growth of solid metal crystals as part of the deposition process.
Overpotential	The magnitude of the difference in potential from equilibrium conditions, considered the driving force for an electrochemical reaction to occur.

Word/Phrase	Definition
Oxidation	An electrochemical reaction in which a species loses electrons.
Polarisation	Difference in potential from equilibrium conditions.
Pyrometallurgy	A process of recovering metals from their ores through the application of high temperatures.
Reaction mechanism	The steps involved in the chemical reaction of a species.
Rectifier	Piece of electrical equipment that converts an alternating current to a direct current.
Reduction potential	Measure of the tendency of a species to undergo reduction.
Redox reaction	See *Electrochemical reaction.*
Reduction	An electrochemical reaction in which a species gains electrons.
Resistance	Measure of opposition to the flow of current.
Reversible electrode potential	Reduction potential at equilibrium.
Short circuit	Unintended electrical circuit caused by a lower resistance path for current to flow.
Solvent extraction	Process in which the aqueous pregnant leach solution is contacted with an organic phase to which the metal is transferred. Solvent extraction (and stripping) is the step prior to electrowinning in a hydrometallurgical process.
Stray current	The flow of current between objects that are not part of the electrical circuit.
Spent electrolyte	Metal barren aqueous phase that exits the electrowinning operation.
Stripping	*(with reference to solvent extraction)* Process in which an organic, metal-containing phase is contacted with an aqueous phase (usually the spent electrolyte) to which the metal is transferred.
Tankhouse	The physical building or location in which the electrowinning operation is situated.
Working electrode	The electrode of interest.

LIST OF FIGURES

LIST OF TABLES

1

INTRODUCTION

1.1 Background

The commercial processing of copper-containing ore bodies to produce high purity copper includes either a pyrometallurgical or hydrometallurgical procedure, in which the final step is the formation of pure copper sheets. The hydrometallurgical production of high purity copper contributes approximately 20% to the total copper processed (Schlesinger *et al.*, 2011), with approximately 75 hydrometallurgical copper processing plants globally that each produce more than 10 000 tonnes per annum (Robinson *et al.*, 2013a). The growth of hydrometallurgy as an option for copper processing can be accredited to its ability to process mixed-sulphide ores, with lower environmental consequences and beneficial economical and practical factors (Paynter, 1973).

The most common sequential processing steps in the hydrometallurgical production of high purity copper are comminution, leaching, solvent extraction (SX) and electrowinning (EW). Electrowinning entails the passage of electric current through an electrolyte containing cupric ions, and the subsequent plating of solid copper sheets. Copper plating occurs through the reduction of cupric ions to solid copper at the cathode, with the simultaneous oxidation of water to hydrogen ions and oxygen bubbles at the anode. Electrowinning is a highly energy intensive process, with approximately 2 MWh of power required to produce each tonne of copper cathode (Wiechmann *et al.*, 2010).

The determination of key performance indicators for electrowinning is vital in ensuring the energy intensive and costly process remains as efficient and effective as possible. Performance indicators relating to the energy consumption are the current efficiency (percentage of total current used in the copper plating reaction) and specific energy consumption (MWh/t copper produced). Not all the power input is utilised in the plating of copper, but lost, for example, to hardware and electrolyte resistance, electrochemical reactions of impurities such as iron and short circuits, all of which have a negative practical and economic implication. Another key performance indicator is the yield of copper product which is required to meet industry demand, and quality which is measured by the purity and smoothness of the copper cathode produced.

1.2 Problem Statement

In order to maximise efficient electrowinning operation and plant profitability, key performance indicators are required to be measured continually and are critical to the success of the plant. Currently, in industry, electrowinning performance is only measured after copper cathodes have been harvested after spending

anywhere between 4 and 14 days undergoing electrowinning (Robinson *et al.*, 2013b). Should the measured performance not meet the required standard, only then would input variables be altered and possible faults investigated so that the subsequent cathodes produced would be of a higher quality. This reactive approach to process control is inefficient, with suboptimal use of time, labour and operating costs relating to the high energy intensity of electrowinning. Online measurement of performance indicators is considered impractical due to the nature of the performance calculations which require analysis of the completed copper plates after removal from the electrowinning system. In addition, the tankhouse environment is corrosive to equipment and toxic to plant operators due to acid mist generated from the electrowinning operation.

There is scope for the shift towards a pre-emptive approach to plant performance determination, through a predictive model. The accurate prediction of key performance indicators could be used as a benchmark with which to compare actual performance data, to ensure that the required standard is maintained and to facilitate control and fault monitoring. Process automation and automated monitoring and control systems would also decrease the time spent by plant operators in the toxic tankhouse environment, forming a potential solution to occupational health problems (Robinson *et al.*, 2013a). Increasing safety regulations require a less manual approach to electrowinning performance control and optimisation, therefore the creation of a predictive electrowinning model for plant performance is a necessary step for the future of the electrowinning operation. The safety, economic and efficiency factors of current electrowinning plants require improvement, motivating the requirement for a predictive model which makes up this research.

1.3 Research Aim and Objectives

The overall aim of this research was to develop a semi-empirical electrowinning model for the prediction of process performance. There were four major objectives that were required to be met for the overall aim to be achieved, which are listed as follows:

1. Develop a semi-empirical electrowinning model to predict process performance.
2. Conduct bench-scale electrowinning experiments to generate data to be used in the fitting of model parameters.
3. Calibrate the bench-scale experimental data to the electrowinning model through a parameter fitting approach.
4. Compare the model predicted electrowinning performance indicators with data obtained from industrial plants.

1.4 Scope and Approach to Research

The scope of the electrowinning model created in this research was a steady state simulation of the key performance indicators of yield, current efficiency and specific energy consumption. The performance

indicator for copper deposit quality fell beyond the scope of this research. However, the electrowinning model was required to be able to be modified to incorporate quality indicators in the future, and form a basis for the future conversion to a dynamic model for application in process control (which is not utilised in current industrial practice).

The approach to completing the four major objectives of this research, and in so doing develop an electrowinning model for the prediction of process performance, was divided into a model development phase and a parameter fitting phase. The model development was approached using a top-down modelling strategy, by forming a conceptual electrowinning model and translating the physical electrowinning phenomena into mathematical equations which were programmed into MATLAB. This first principles approach to model development formed the first objective of this research. The parameter fitting phase was conducted by finding relevant parameters, devising an appropriate experimental procedure to generate data that would be used to fit the parameters, and using regression to fit parameters. This parameter fitting phase made up the second and third research objectives, to conduct bench-scale electrowinning experiments and calibrate the model to the experimental data generated.

The fourth objective, to compare the model predicted electrowinning performance indicators with data obtained from industrial plants, was approached by reviewing the ability of the model to predict average performance of global industrial electrowinning tankhouses using the parameters found from the bench-scale electrowinning experiments. In addition, a strategy was provided for the implementation of the parameter fitting approach to an industrial tankhouse.

1.5 Thesis Structure

The thesis consists of seven chapters, each of which contain a key aspect of the research, followed by the appendices. Chapter 1 is the introduction to the research, which includes the background of electrowinning, problem statement, the overall aim and objectives of the research, project scope and approach to the achievement of the objectives. Chapter 2 is the literature review, where fundamental electrowinning principles are presented, practical electrowinning considerations are discussed, and models developed in previous studies are evaluated.

A description of the model development forms Chapter 3, which outlines the approach to the creation of the electrowinning model from fundamental principles. The function of the model is discussed, the physical electrowinning concept translated into fundamental principles through a circuit diagram, and major assumptions provided with a breakdown of the programming. Thereafter, Chapter 4 provides details on the parameter fitting, which includes the design of the electrowinning experimental procedure in the bench-scale cell, and the approach to fitting parameters to the experimental data.

In Chapter 5, the results and discussion, the bench-scale electrowinning experiments and parameter fit are evaluated. The performance of the electrowinning model, that is its ability to predict electrowinning data, is reviewed for the bench-scale experiments and the application to industrial tankhouses. Conclusions and recommendations are provided in Chapter 6, followed by references in Chapter 7. Finally, appendices are provided for sample calculations, experimental procedure and experimental and model results.

2

LITERATURE REVIEW

2.1 Process Overview

2.1.1 Electrometallurgy

Electrometallurgy is the branch of extractive metallurgy comprising the extraction of high purity metals from their low-grade ores through the application of an electric current. Pyrometallurgy and hydrometallurgy are both electrometallurgical processing techniques that have been used in the commercial production of high grade copper for over a hundred years (Anderson, 2014). The final step in each of these processes consists of the production of solid copper sheets through electrochemical reactions brought about by the supply of energy in the form of electricity. The copper sheets are sold and subsequently melted and cast into their desired form (Davenport *et al.*, 2002).

The copper contained in sulphide ores (such as chalcopyrite, chalcocite and bornite) is extracted using the pyrometallurgical process. The pyrometallurgical process usually entails comminution, froth flotation, smelting into molten matte, casting and finally the plating of pure copper by electrorefining (Davenport *et al.*, 2002).

The hydrometallurgical process is usually used to extract copper from oxide ores and chalcocite (Najminoori *et al.*, 2015). Steps in the hydrometallurgical process usually include grinding or comminution, leaching, solvent extraction and electrowinning (Panda and Das, 2001). The processing of copper through hydrometallurgy was refined after the pyrometallurgical processing route as a more environmentally friendly option, as the hydrometallurgical process produced much lower sulphur dioxide emissions than its pyrometallurgical counterpart (Murray *et al.*, 2016). According to Davenport *et al.* (2002), about 20% of all copper processed is extracted through hydrometallurgy.

2.1.2 The Hydrometallurgical Process

A typical hydrometallurgical process for the extraction of high purity, solid copper is shown in the block flow diagram of *Figure 2.1*. Once the ore has been crushed and ground in the comminution step, it undergoes leaching. In the leaching process, sulphuric acid is used as lixiviant to dissolve copper and produce a leach solution rich in cupric ions, and takes place in either a heap or in a reactor. The aqueous pregnant leach solution enters a solvent extraction-stripping circuit in order to further purify the solution. In the solvent extraction step, the pregnant leach solution is contacted with an immiscible organic phase containing a

copper-selective extractant. Copper complexes with and is transferred to the organic phase. Following phase separation, the raffinate is returned to the leaching process and the copper loaded organic phase enters the stripping unit where it is contacted with an aqueous phase recycled from electrowinning, known as the spent electrolyte. Cupric ions are stripped into the spent electrolyte and a copper rich advance electrolyte is formed. The stripped organic is returned to the solvent extraction stage; the advance electrolyte undergoes electrowinning, where an electric current is applied to the solution and solid copper is plated onto cathodes (Schlesinger *et al.*, 2011). The copper depleted solution is the spent electrolyte that is returned to the stripping section.

It is important to note that not all hydrometallurgical processing plants include the solvent extraction-stripping circuit. Should solvent extraction and stripping be excluded from the process, the pregnant leach solution becomes the advance electrolyte entering the electrowinning process and consists of more impurities that have been carried through from the ore.

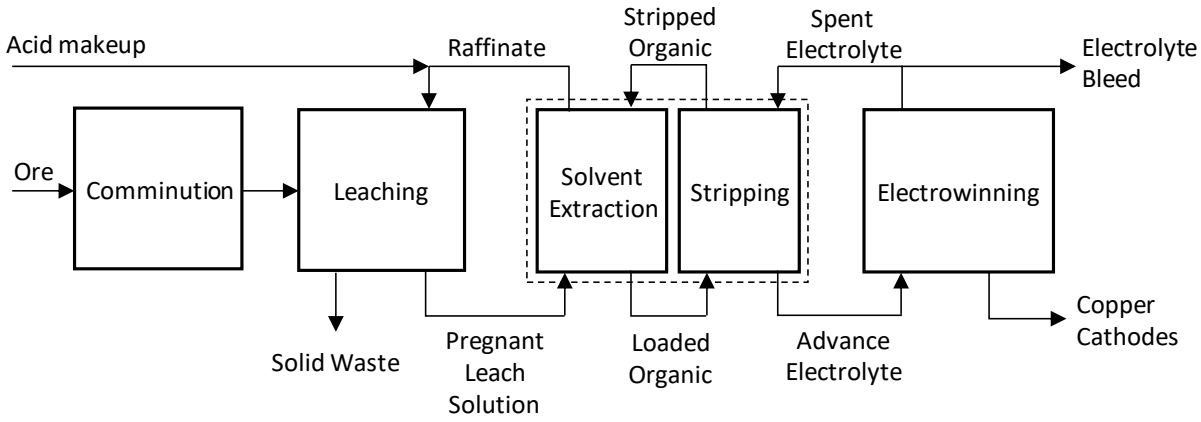

Figure 2.1: *Block flow diagram of hydrometallurgical processes to produce high grade copper.*

2.2 Electrochemical Principles

2.2.1 The Electrolytic Cell

2.2.1.1 Electrochemical Reactions

Electrochemical (redox) reactions comprise the transfer of electrons between species and the consequent conversion between electrical and chemical energy. Electrochemical reactions occur at the interface of electrodes, or electrically conductive metal, submerged in a solution. At least two electrodes are required for the electrochemical reaction to occur: a cathode and an anode. The overall electrochemical reaction can be split into reduction at the cathode and oxidation at the anode (Lower, 1994). The general form of an electrochemical equation is provided in Equation 1 (Bard and Faulkner, 2001).

$$O^{n+} + ne^- \leftrightarrow R \quad [1]$$

Where O = Oxidised species

R = Reduced species

n = Number of electrons involved in reaction (stoichiometric coefficient)

e^- = Electron

Every electrochemical reaction is associated with a standard reduction potential, which is the tendency of a species to undergo reduction. A reaction with a more positive reduction potential will undergo reduction in preference of a reaction with a lower reduction potential. The overall cell potential is the voltage when no current flows through the cell, and represents the maximum possible work that can be obtained from the system (Newman and Thomas-Alyea, 2004). The overall cell potential can be calculated as the difference in reduction potentials of the electrochemical reactions occurring at the anode and cathode, as indicated in Equation 2 (Bard and Faulkner, 2001).

$$E^0_{cell} = E^0_{cathode} - E^o_{anode} \quad [2]$$

Where E^0 = Standard reduction potential (V)

The overall reduction potential of the cell is related to the change in Gibbs free energy, as indicated in Equation 3 (Bard and Faulkner, 2001).

$$\Delta G^0 = -nFE^0_{cell} \quad [3]$$

Where ΔG^0 = Change in standard Gibbs free energy (J)

n = Number of electrons involved in reaction

F = Faraday's Constant (96485 C/equivalent mol)

A negative change in Gibbs free energy is indicative of a spontaneous pair of redox reactions. Consequently, the reduction potential of the cell would be positive.

For solid copper to be plated during an electrometallurgical process, cupric ions need to be reduced at the cathode. The oxidation of water, or water evolution, occurs simultaneously at the anode. The redox half reactions for copper reduction and water oxidation with their respective standard reduction potentials are shown in Equations 4 and 5, written in the standard convention of reduction format.

$$Cu^{2+}_{(aq)} + 2e^- \rightarrow Cu_{(s)} \qquad E^0 = +0.34\,V \quad [4]$$

$$2H^+_{(aq)} + \frac{1}{2}O_{2(g)} + 2e^- \rightarrow H_2O_{(l)} \qquad E^0 = +1.23\,V \quad [5]$$

Therefore,

$$E^0_{cell} = 0.34 - 1.23 = -0.89\,V$$

The negative overall reduction potential of -0.89 V, hence positive change in Gibbs free energy, implies that the reaction is non-spontaneous. An external potential would therefore need to be applied for the copper plating reaction to occur, classifying the cell as electrolytic (Bard and Faulkner, 2001).

2.2.1.2 The Basic Electrolytic Cell

A basic electrolytic cell illustrating the fundamental electrochemistry of copper plating by electrowinning is given in *Figure 2.2*. The cell consists of two electrodes (the anode and cathode) placed in a solution of cupric ions and sulphuric acid (the electrolyte) and connected by an external power source.

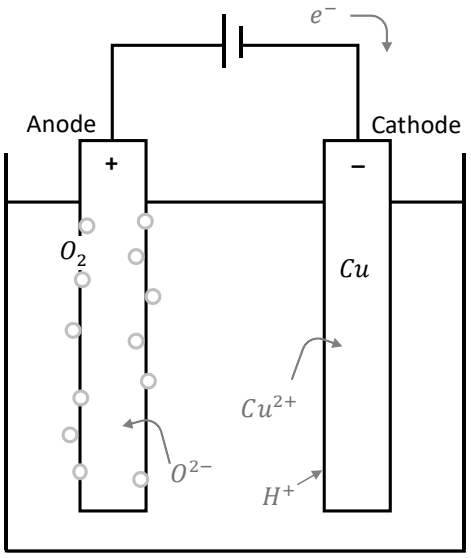

Figure 2.2: *Simplified electrochemical cell illustrating the reduction of Cu^{2+} into solid copper, and the decomposition of water to form bubbles of oxygen.*

When a voltage is applied to the cell, the resulting flow of current initiates the electrochemical reactions. Electrons flow towards the cathode, causing it to have a negative charge, which in turn attracts the cupric cations. The electrons in the cathode react with the cupric ions at the cathode-solution interface, where solid copper is formed and plates the cathode. The electrolyte is an ionic conductor, and just as cations move towards the negatively charged cathode, anions move towards the positively charged anode. Water becomes oxidised at the anode, forming hydrogen ions and oxygen gas, which bubbles out the top of the cell. The electrons produced in this oxidation reaction flow through the anode back towards the cathode, completing the electric circuit (Schlesinger *et al.*, 2011).

Equation 6 is the overall cell reaction, combining the reduction of cupric ions and oxidation of water. It is noted that the products of the reaction are the solid plated copper, oxygen gas and dissociated sulphuric acid (hydrogen ions and sulphate ions).

$$Cu^{2+}_{(aq)} + SO^{2-}_{4(aq)} + H_2O_{(l)} \rightarrow Cu_{(s)} + \frac{1}{2}O_{2(g)} + 2H^+_{(aq)} + SO^{2-}_{4(aq)} \qquad E^0 = -0.89\ V \qquad [6]$$

2.2.1.3 Subsidiary Reactions

In reality, the electrolyte in electrowinning contains additional species or impurities which also undergo electrochemical reactions at the electrodes. These subsidiary reactions influence the efficiency of the electrowinning process, as the current can be used up by undesired reactions instead of the copper plating reaction. Iron is a major impurity in copper ores, and while the solvent extraction circuit lowers iron levels for electrowinning, some remains in the electrolyte. Iron undergoes cyclic reduction and oxidation at the cathode and anode respectively, as per Equation 7.

$$Fe^{3+}_{(aq)} + e^- \leftrightarrow Fe^{2+}_{(aq)} \qquad E^0 = 0.77\ V \qquad [7]$$

The reduction of ferric (Fe^{3+}) to ferrous (Fe^{2+}) ions has a higher reduction potential than the reduction of cupric ions to solid copper, and therefore occurs more readily.

2.2.2 Non-Standard Conditions and the Nernst Equation

The standard reduction potential is only valid under standard conditions which assume that the activities of all species involved in the reaction are equal to one. Under non-standard conditions, reduction potentials need to be corrected using the Nernst equation, which takes into account the equilibrium thermodynamic energy requirement for the process (Aminian *et al.*, 2000). The Nernst equation is provided in Equation 8, where the actual reduction potential is a function of the standard reduction potential, species activities at the electrode surface, temperature and number of electrons involved the electrochemical half reaction $O^{n+} + ne^- \rightarrow R$ (Bard and Faulkner, 2001).

$$E = E^o - \frac{RT}{nF}\ln\left(\frac{a_R}{a_{O^{n+}}}\right) \qquad [8]$$

Where E = Reduction potential (V)

E^0 = Standard reduction potential (V)

a = Activity (dimensionless)

T = Temperature (K)

n = Number of electrons involved in reaction (dimensionless)

R = Universal gas constant (8.314 J/(mol·K))

F = Faraday's Constant (96485 C/equivalent mol)

2.2.3 Electrode Polarisation and Overpotential

As soon as current is passed through the electrolyte, the system is no longer at equilibrium. The difference in potential from the equilibrium condition, when zero current flows through the system, is known as polarisation. The magnitude of polarisation is the overpotential, which can be calculated as per Equation 9

(Newman and Thomas-Alyea, 2004). When the overpotential increases, the anode becomes more positive and the cathode becomes more negative.

$$\eta = U - E \quad [9]$$

Where U = Applied potential (V)

E = Reduction potential (V)

η = Overpotential (V)

Overpotential is considered the driving force that allows the electrochemical reactions to occur in an electrolytic cell (Scott *et al.*, 1987; Free *et al*., 2013). The total overpotential consists of both activation overpotential and concentration overpotential. Activation overpotential refers to the energy required to drive the charge transfer reaction, while concentration overpotential is the energy used to drive mass transfer of ions to or from the electrode surface (Bard and Faulkner, 2001).

2.2.4 Faraday's Law

Faraday's law of electrolysis states that the amount of species that reacts in a redox reaction is directly proportional to the quantity of charge that passes. The most useful form of Faraday's Law for application in electrowinning is provided in Equation 10, indicating the mass of a species that reacts as a function of the applied current, or charge passed per time (Newman and Thomas-Alyea, 2004).

$$m_i = \frac{M_i I t}{nF} \quad [10]$$

Where m_i = Mass of species i (g)

M_i = Molar mass of species i (g/mol)

I = Current (A)

t = Time (s)

2.3 Reaction Mechanism and Kinetics

2.3.1 Introduction to the Reaction Mechanism

According to Faraday's Law (Section *2.2.4 Faraday's Law*) the mass of copper that deposits through the reduction of cupric ions is a function of the applied current. Alternatively, it can be stated that the current utilised is proportional to the reaction rate (Beukes and Badenhorst, 2009). Not all the current that flows through the cell is used directly in the plating reaction, therefore it is important to delve further into the reaction mechanism in order to quantify the plating kinetics and relevant current.

The mechanism for an electrochemical reaction is discussed in detail in the subsequent sections. The steps involved consist of mass transfer of the respective ion to the electrode surface, the charge transfer reaction and either deposition of a solid or the mass transfer of the product away from the electrode back into the

bulk electrolyte. It is important to note that the slowest step in the reaction mechanism will determine the rate of the reaction, and that at steady state, the rates of each step will be equal as there is zero accumulation of species (Bard and Faulkner, 2001).

2.3.2 Mass Transfer

2.3.2.1 Mass Transfer Steps

The mass transfer mechanism consists of three steps: convection, diffusion and migration (Beukes and Badenhorst, 2009). *Figure 2.3* illustrates the reaction mechanism for the case of cupric ions that will undergo reduction at the cathode. The first step is the convection of the cupric ions from the bulk solution to the electrode surface region. This convective transfer can be by natural (through a density gradient) or forced means (through a pressure gradient or mechanical stirring). In static solutions or when the flowrate is low, natural convection is dominant (Beukes and Badenhorst, 2009).

Once the ions are located close to the electrode, diffusion occurs based on a concentration gradient. In the diffusion process, cupric ions are transferred from the bulk phase onto the electrode surface (Beukes and Badenhorst, 2009).

Migration occurs based on an electrical potential gradient (Bard and Faulkner, 2001). Migration is induced by the applied voltage, which creates a difference in charge between the electrode and electrode interface. The attractive and repulsive forces caused by the charge difference instigates the movement of ions known as migration (Chang, 2009).

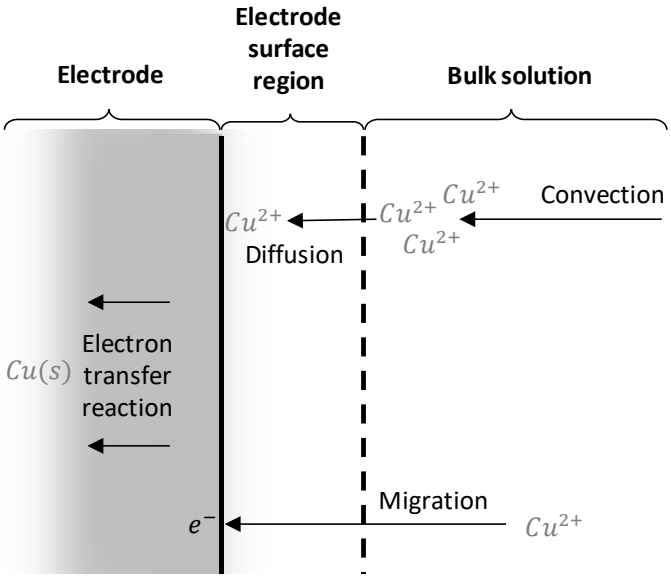

Figure 2.3: *Diagrammatic representation of the mass transfer and reaction steps pertaining to the plating of copper from a solution.*

Once the ions are located at the electrode surface, the charge transfer reaction occurs. If the product of the electrochemical reaction is a solid, such as in the copper reduction reaction, the solid atom should adhere to the electrode surface. Alternatively, if the product of the electrochemical reaction remains in the aqueous phase, such as a ferric or ferrous ion, the product ion diffuses back into the bulk solution.

2.3.2.2 Electrical Double Layer

The phenomena occurring at the electrode-solution interface affect both the mass transfer of ions to and from the electrode surface and the reaction kinetics. The region from the electrode surface to the bulk electrolyte can be modelled as an Electrical Double Layer (Bard and Faulkner, 2001), which is illustrated in *Figure 2.4* for a negatively charged cathode. The inner layer comprises of solvent molecules and specifically adsorbed molecules or ions (anions in *Figure 2.4*). The centre of the specifically adsorbed ions forms the Inner Helmholtz Plane (IHP). Any solvated ions can only get as close to the electrode surface as this inner layer will allow. The Outer Helmholtz Plane (OHP) exists at the distance from the electrode surface to the centre of the solvated ions. Ions undergo diffusion in the region from the OHP to the bulk solution, and in this layer the ions are referred to as being non-specifically adsorbed to the electrode.

The ions in the layer closest to the electrode surface form a barrier between the electrode and the solvated ions. A potential gradient therefore exists which affects the rate of the reaction (Bard and Faulkner, 2001).

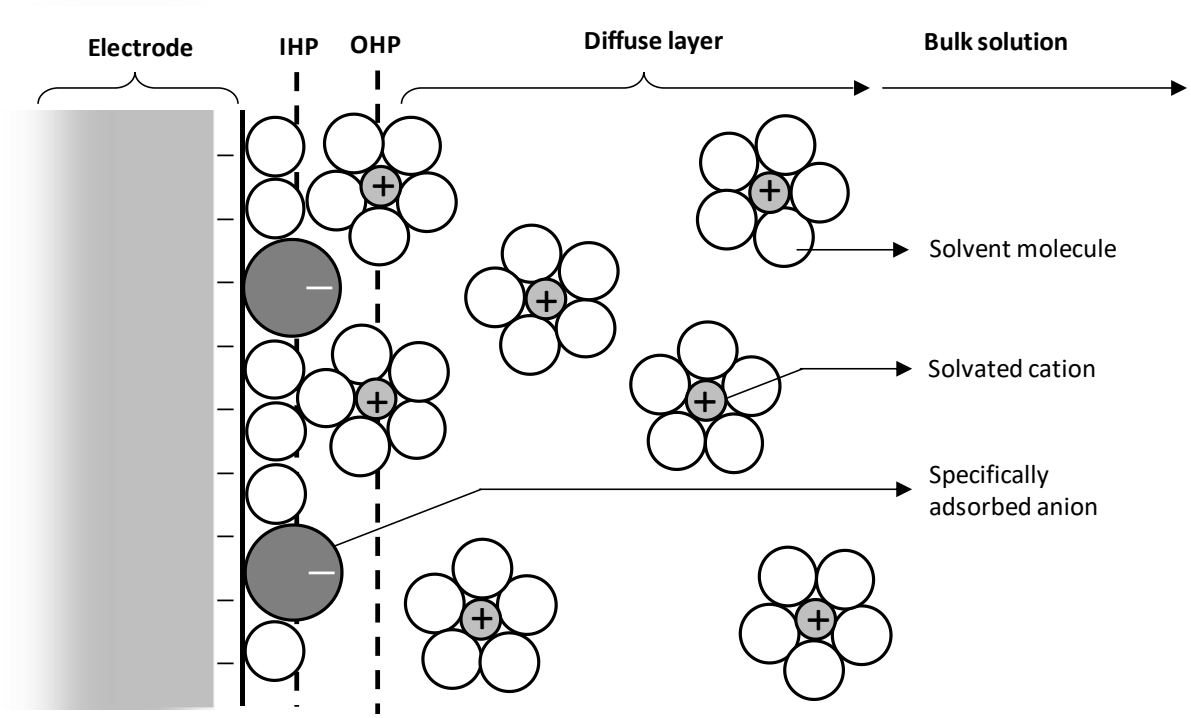

Figure 2.4: *Illustration of the electrical double layer at the electrode-solution interface of a negatively charged cathode , after Bard and Faulkner (2001).*

2.3.2.3 Rate of Mass Transfer

The mass transfer rate of ions in solution can be calculated using the Nernst-Planck equation for three-dimensional mass transfer (Equation 11). Each term in the Nernst-Planck equation represents the contributions of diffusion, migration and convection respectively to the overall flux (Beukes and Badenhorst, 2009).

$$\boldsymbol{J}_i = -D_i \boldsymbol{\nabla} C_i - \frac{n_i F}{RT} D_i C_i \boldsymbol{\nabla} \phi + C_i \boldsymbol{v} \qquad [11]$$

Where $\boldsymbol{J}_i$ = Flux of species i (mol/(s·cm^2))

D_i = Diffusion coefficient (cm^2/s)

$\boldsymbol{\nabla}$ = Gradient operator

C_i = Molar concentration of species i (mol/cm^3)

n_i = Number of electrons involved in reaction (dimensionless)

ϕ = Potential (V)

$\boldsymbol{v}$ = Velocity (cm/s)

The Nernst-Planck equation can be simplified for application in electrowinning models in which the determination of all constants and terms is not practical. According to Free *et al*. (2013) and Beukes and Badenhorst (2009), the effects of migration are minimised when the material of the electrode is chemically inert in the electrolyte. It could therefore be assumed that the migration term of the Nernst-Planck equation is negligible when considering mass transfer rates to the electrodes in electrowinning, which are inert in the electrolyte. Najim (2016) supports this claim by stating that the high conductivity of the sulphuric acid in the electrowinning electrolyte serves as the major current carrier, with insignificant contributions due to migration.

In industrial electrowinning applications, there is minimal movement of electrolyte in the electrode surface region, and it can therefore be assumed that convection can be eliminated from the Nernst-Planck equation for electrowinning applications (Beukes and Badenhorst, 2009). The Electrical Double Layer theory, in which the diffusion layer is stagnant, is based on the assumption of zero convection. In some electrowinning models and applications it is impractical to determine some of the variables associated with migration and convection, such as the gradient operator for potential over the electrode and species velocity in the electrode surface region. Therefore, the simplification of mass transfer is necessary in some electrowinning applications, especially in an industrial context (Moats and Khouraibchia, 2009).

When migration and convection are considered negligible, the flux of ions is equivalent to diffusion, or the concentration gradient between the bulk electrolyte and electrode surface. It can be assumed that in electrowinning, the concentration gradient is normal to the electrode surface (the x direction) because of the difference in electrolyte composition between the bulk phase and electrode interface where the reactions

occur. Diffusion over the parallel axes (y and z directions) can be neglected because electrochemical reactions remain similar over the electrode surface area and therefore electrolyte composition in these directions does not vary significantly. The Nernst-Planck equation for one dimensional flux excluding migration and convection is provided in Equation 12, which is synonymous with Fick's First Law of Diffusion (Beukes and Badenhorst, 2009).

$$J_i(x) = -D_i \frac{\partial C_i(x)}{\partial x} \quad [12]$$

Where $\frac{\partial C_i(x)}{\partial x}$ = Concentration gradient in the x direction

In certain electrochemical applications, the concentration gradient in the diffusion layer is approximated as linear. This linear approximation is known as the Nernst Diffusion Model, and is illustrated in *Figure 2.5* showing an actual versus linear concentration profile (Paunovic and Schlesinger, 2005). The resulting ionic flux equation is a function of the diffusion coefficient, diffusion layer thickness and change in concentration between the bulk solution and at the electrode surface. The boundary layer thickness and diffusion coefficient can be combined into a mass transfer coefficient, as shown in Equation 13 (Bard and Faulkner, 2001). When incorporated into an electrochemical model, the mass transfer coefficient for diffusion may be considered an effective mass transfer coefficient which incorporates all mass transfer effects into an effective diffusion term.

$$J_i(x) = -\frac{D_i}{\delta}\left(C_{i,bulk} - C_{i,surface}\right) = m_i\left(C_{i,bulk} - C_{i,surface}\right) \quad [13]$$

Where δ = Diffusion layer thickness (cm)

m_i = Mass transfer coefficient for species i (cm/s)

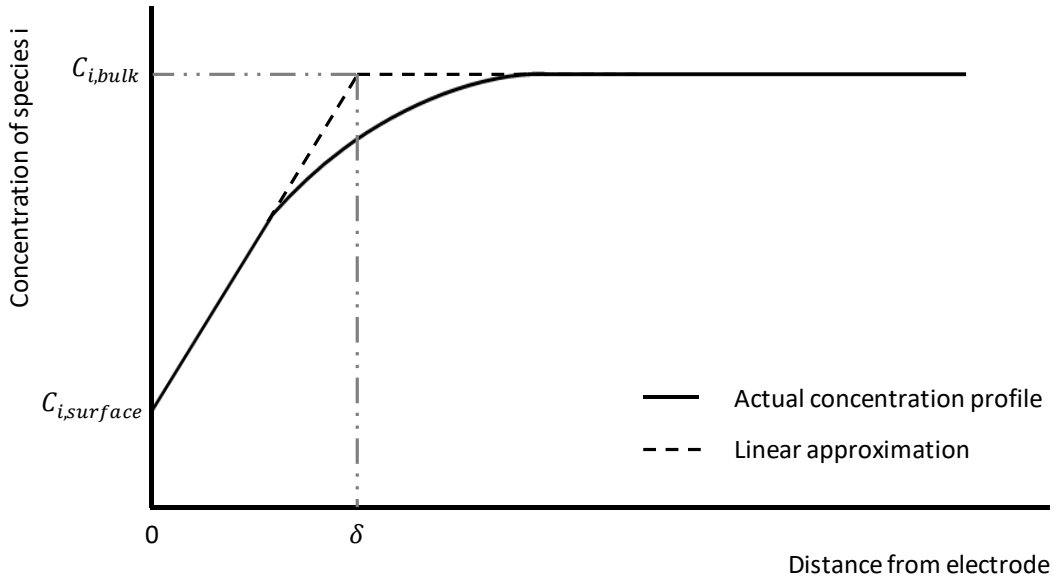

Figure 2.5: *Illustration of the actual vs. linear approximation of the concentration profile of an ion, i, in the diffusion layer.*

2.3.3 Reaction Rate

2.3.3.1 Electrodeposition Principle

An electrochemical reaction takes place when the relevant ion is situated at the electrode surface after mass transfer from the bulk electrolyte. If an ion gets reduced to a solid atom, as in the reduction of cupric ions, the solid will adhere to and plate the cathode. After the electron transfer reaction, the copper adatom that is formed adsorbs to the electrode surface and diffuses to a nucleation site. Nucleation sites can be any irregularities in the electrode surface (Free *et al.*, 2013). Grains of copper are formed over time, which plate the cathode (Pasa and Munford, 2006). The quality of the copper product is largely affected by its morphology and is desired to be smooth and adherent (Alfantazi and Valic, 2003).

2.3.3.2 Reaction Rate Calculation

The rate of an electrochemical reaction can be calculated using the Butler-Volmer equation, assuming the reaction is not mass transfer limited. The Butler-Volmer equation is given in Equation 14 and relates the current density used for the specific reaction to the overpotential at that electrode. Current density is the flux of charge, or the current per electrode surface area perpendicular to the flow of current (Newman and Thomas-Alyea, 2004). The reaction rate, or mass of species reacted per unit time, can be calculated directly from the current density using Faraday's Law.

$$i = i_0 \left[\exp\left(\frac{-\alpha n F}{RT}\eta\right) - \exp\left(\frac{(1^* - \alpha) n F}{RT}\eta\right) \right] \quad [14]$$

Where i = Current density (A/m^2)

i_0 = Exchange current density (A/m^2)

α = Charge transfer coefficient (dimensionless)

n = Number of electrons involved in reaction (dimensionless)

F = Faraday's Constant (96485 C/equivalent mol)

R = Universal Gas Constant (8.314 J/(mol·K))

T = Temperature (K)

η = Overpotential (V)

* For the copper reduction reaction, this value is 2 (for a 2 step reaction).

Due to the reversibility of electrochemical reactions, the Butler-Volmer equation is split into two terms: the first describing the rate of the cathodic component of the reaction, the second term describing the rate of the anodic component of the reaction. For the negative overpotential associated with a reduction reaction, the first term in the square bracket of Equation 14 dominates over the second term and the resulting current density is positive. On the other hand, for a positive overpotential associated with an oxidation reaction, the

resulting current density will be negative (Bard and Faulkner, 2001). *Figure 2.6* represents the Butler-Volmer equation for an arbitrary system, showing the current density as a function of overpotential. The solid line represents the net reaction, and dashed lines the anodic and cathodic components. It is observed that at large enough negative or positive overpotentials, the respective anodic or cathodic terms of the Butler-Volmer equation can be considered negligible.

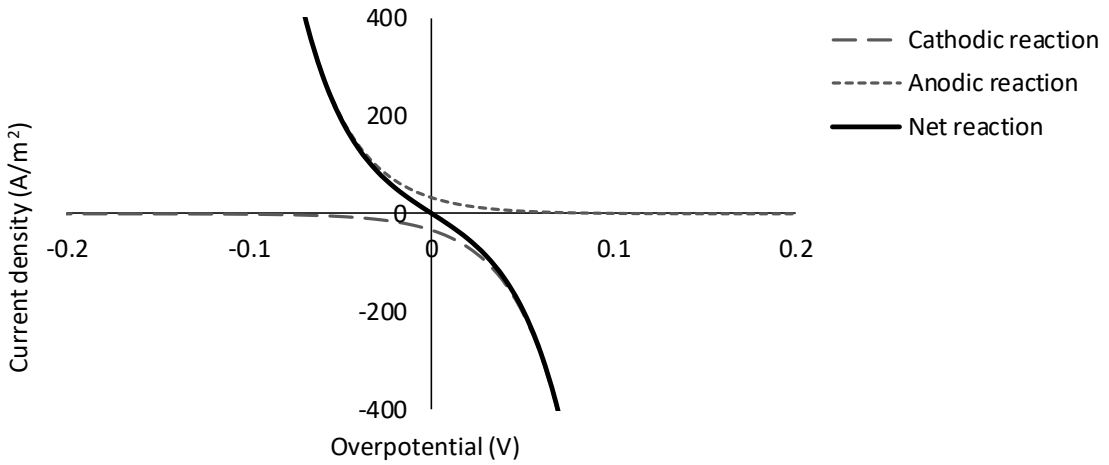

Figure 2.6: *Illustration of a current overpotential curve, showing the cathodic, anodic and net components of the Butler-Volmer equation, modified from Bard and Faulkner (2001).*

The exchange current density (i_0) is a parameter in the Butler-Volmer equation which depends on several factors including the concentration of products and reagents, temperature, any contaminating impurities and the nature of the electrode interface. Exchange current density therefore varies significantly between different electrowinning scenarios, anywhere from less than 10^{-7} mA/cm^2 to over 1 mA/cm^2, according to Newman and Thomas-Alyea (2004). Higher values of the exchange current density correspond to faster reactions at both the cathode and anode. At a higher value of exchange current density, a desired current density could be delivered by a lower overpotential (a less positive overpotential for a cathodic reaction or less negative overpotential for an anodic reaction). The effect of the exchange current density on the rate kinetics described by the Butler-Volmer equation is shown graphically in *Figure 2.7*. Lower values of the exchange current density correspond to a more horizontal curve, meaning that a higher overpotential is required to deliver a current density, and vice versa for higher exchange current densities.

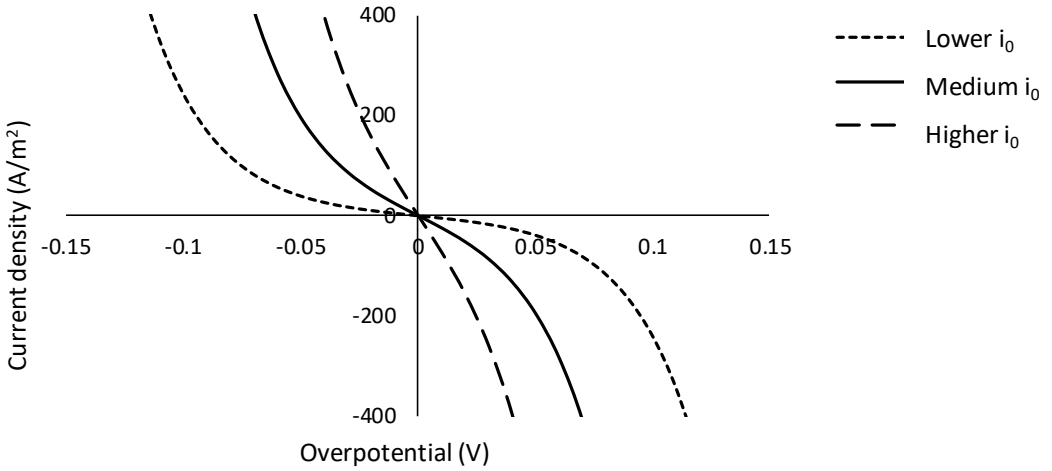

Figure 2.7: *Graphical representation of a change in exchange current density (i_0) on the Butler-Volmer equation, modified from Bard and Faulkner (2001).*

Overpotential at an electrode may favour one reaction direction over the other, and this non-symmetrical response is characterised by the charge transfer coefficient (α) in the Butler-Volmer equation. For copper reduction, alpha must lie between zero and two to ensure that the forward and reverse components of the Butler-Volmer equation are portrayed correctly (with the correct sign in the exponent of each term). Typical charge transfer coefficients for copper reduction range from 0.2 to 2 (Newman and Thomas-Alyea, 2004). A graphical representation of the effect of changing the alpha value on the current density calculated using the Butler-Volmer equation is presented in *Figure 2.8*. A higher charge transfer coefficient for cathodic reactions (top left hand quadrant of the figure) signifies faster kinetics, with a less negative overpotential translating into a higher current density and therefore plating rate. A higher charge transfer coefficient for anodic reactions (bottom right hand quadrant of the figure), however, displays the opposite effect with a more positive overpotential required to translate into a desired negative current density.

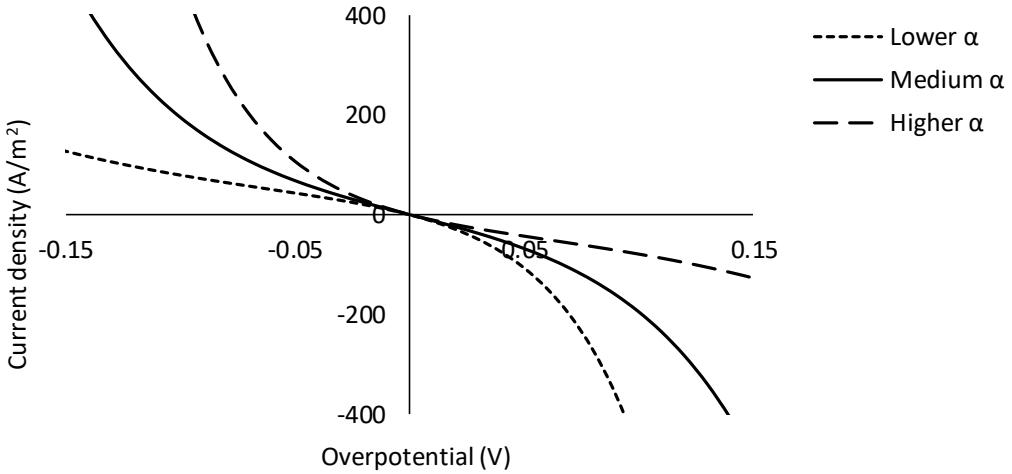

Figure 2.8: *Graphical representation of a change in charge transfer coefficient (α) on the Butler-Volmer equation, modified from Bard and Faulkner (2001).*

2.3.4 Combining Mass Transfer and Reaction Rate Kinetics

2.3.4.1 Limiting Current Density

The limiting current density is a maximum current density that can be applied, after which any increase in potential does not cause an increase in the reaction rate (Bard and Faulkner, 2001). The limiting current density comes about due to a mass transfer rate limiting step. If the diffusion of ions to the electrode surface is slower than the rate of reaction, any additional voltage supply will not influence the reaction. The influence of the limiting current density is seen in *Figure 2.9*, which presents the current density versus the overpotential for an arbitrary cathodic reaction. When the Butler-Volmer equation is used in isolation, the relationship between current density and overpotential remains exponential. A more realistic representation occurs, however, with mixed effects of reaction rate and mass transfer kinetics, shown by the levelling off of the reaction rate at the limiting current density (Free *et al.*, 2013). The limiting current density is a function of the hydrodynamics and physical properties of the system such as interelectrode distance.

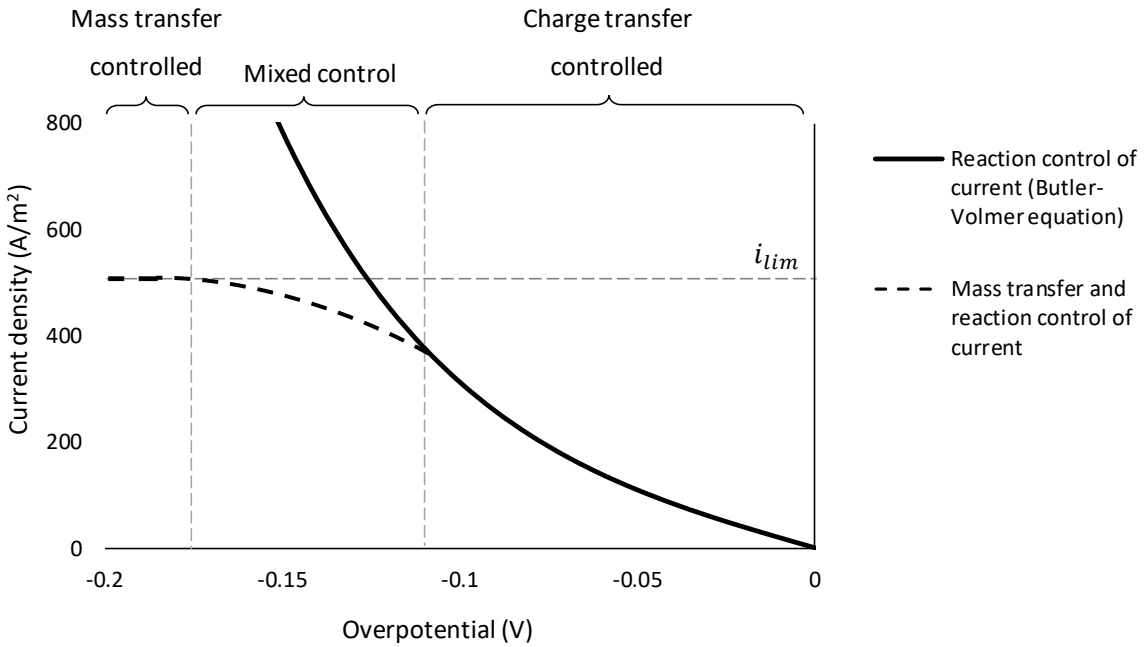

Figure 2.9: *Diagram of current density vs overpotential comparing the mixed effects of mass transport and reaction kinetics, and reaction kinetics (Butler-Volmer equation) only.*

Ferric ions, which are present as an impurity in the electrolyte from the ore, are reduced more readily than the cupric ions when a voltage is applied. The preferential reduction of ferric ions over cupric ions is due to their respective reduction potentials, with ferric reduction having a higher reduction potential of 0.77 V as opposed to the reduction potential for cupric ions of 0.34 V. The limiting current density is reached for the reduction and oxidation of iron (and therefore the maximum reaction rate), and thereafter any additional

current applied will reduce the cupric ions (Aminian *et al.*, 2000). The voltage that is applied to an electrowinning cell should be such that the desired copper reduction reaction rate is obtained, whilst remaining below the limiting current density for copper reduction. Generally, operating current density is at about 50% of the limiting current density, otherwise current becomes unevenly distributed and causes irregular copper deposits (Winand, 1992). Once the limiting current for copper reduction has been exceeded, not only is it electrically inefficient, but the very fast reaction means that insufficient crystal growth occurs and copper powder is deposited instead of the required adherent copper plating (Mishra and Cooper, 2016).

2.3.4.2 Incorporation of Mass Transfer Effects into Rate Kinetics Equations

According to Bard and Faulkner (2001), the standard Butler-Volmer equation (Equation 14) can be used should the electrowinning system be operating below the limiting current density, or when the ion concentration at the surface does not differ significantly from the bulk concentration. When the effects of mass transfer cannot be ignored, however, the Butler-Volmer equation can be modified to Equation 15, which incorporates mass transfer effects. In the mass transfer modified form of the Butler-Volmer equation, each term is multiplied by a mass transfer factor, which is the concentration of the respective ion at the electrode surface per the concentration in the bulk electrolyte. R refers to the reduced species and O refers to the oxidised species.

$$i = i_0 \left[\mathrm{C}_R \exp\left(\frac{-\alpha n F}{RT}\eta\right) - \mathrm{C}_\mathrm{O} \exp\left(\frac{(1^* - \alpha) n F}{RT}\eta\right)\right] \quad [15]$$

Where $C_R = \frac{C_{R,surface}}{C_{R,bulk}}$, $C_R = 1$ when the species is plated

$C_O = \frac{C_{O,surface}}{C_{O,bulk}}$

For $O^{n+} + ne^- \leftrightarrow R$

Industrial electrowinning operations operate far below the limiting current density for the reduction of copper (Bard and Faulkner, 2001). Therefore, it can be assumed that the copper reduction kinetics can be described using the standard Butler-Volmer equation (Equation 14) when operating under normal operating conditions (Section *2.4.4 Effect of Operating Conditions*). Ignoring mass transfer effects for copper reduction in electrowinning systems is supported by Moats and Khouraibchia (2009) and Beukes and Badenhorst (2009).

It is widely recognised that in industrial electrowinning, the cyclic reduction and oxidation between ferric and ferrous ions is limited by mass transfer, and therefore the mass transfer modified Butler-Volmer equation should be used for ferric and ferrous ion reaction rate kinetics (Aminian *et al.*, 2000; Moats and Khouraibchia, 2009).

2.4 Electrowinning in Practice

This section contains the practical aspects involved in industrial electrowinning of copper, which occur in a tankhouse. The rates of electrochemical reaction and efficiency of the electrowinning process are largely affected by the cell design and network of cells in the tankhouse, along with the operating conditions. The performance of the electrowinning operation is therefore not only determined by simple reaction rate kinetics, but on details surrounding the design and operation of electrowinning plants.

2.4.1 Physical Tankhouse Design

2.4.1.1 Single Cell Design

An industrial electrowinning cell is depicted in *Figure 2.10*, and is essentially a scaled up version of the electrolytic cell described in the previous sections. The cell consists of up to hundreds of suspended anodes and cathodes, which alternate (Wiechmann *et al.*, 2016). The cells themselves are made from acid resistant polymer concrete, often with a fiberglass lining (Davenport *et al.*, 2002; Beukes and Badenhorst, 2009). Typically in industry, the electrolyte flows continuously into each cell through a manifold at the bottom, and then overflows out of one of the sides. A side view representation of an electrowinning cell is depicted in *Figure 2.10*, indicating alternating anodes and cathodes and the flow of electrolyte through the cell (with full electrical connections depicted in Figure 2.11). Less common configurations exist in industry as well, such as the electrolyte entering on the left-hand side and overflowing on the right-hand side of the cell. Air sparging is also sometimes introduced to allow for more adequate mixing of the electrolyte within the cell (Davenport *et al.,* 2002).

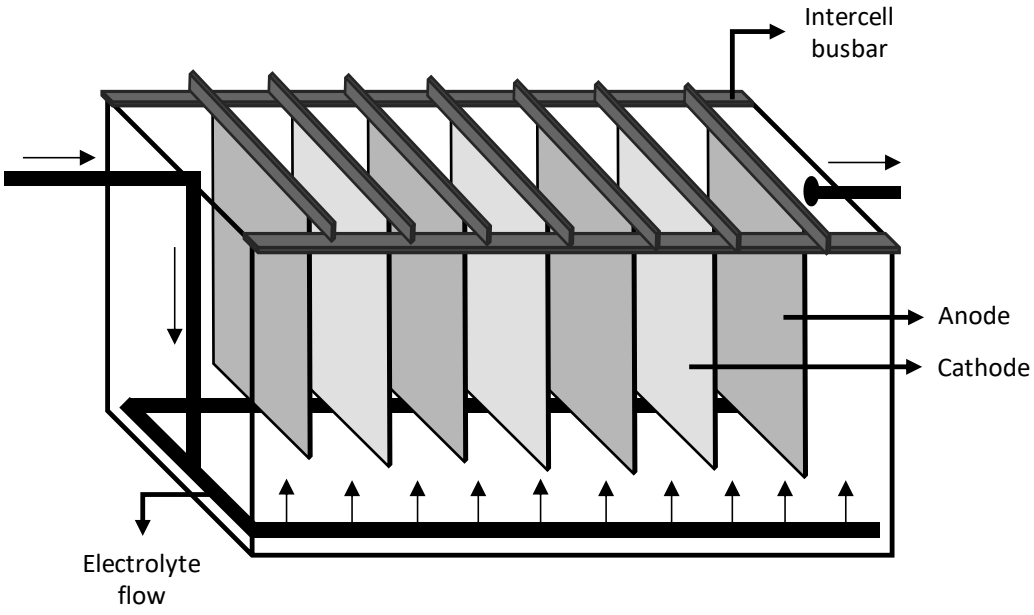

Figure 2.10: *Side view representation of a typical electrowinning cell.*

The anodic material used in electrowinning cells is usually a cold rolled lead alloy (Beukes and Badenhorst, 2009), but graphite is also sometimes used (Panda and Das, 2001). An advantage of using lead is that a regenerative oxide layer is formed during electrowinning which inhibits corrosion of the anode (Yuwono *et al.*, 2018). It is important that the anode material is chemically inert in the electrolyte (Brent Hiskey, 2009). Anodes are usually replaced every 7 – 9 years (Beukes and Badenhorst (2009). The cathodes used in most electrowinning tankhouses are 316L stainless steel blanks, but older plants sometimes use copper starter sheets instead (Davenport *et al.*, 2002). Cathode starter sheets are reusable and should not corrode in the acidic electrolyte (Aminian *et al.*, 2000; Pfalzgraff, 2009).

The electrodes are soldered onto hanger bars which allow them to be suspended in the cell. The hanger bars rest on intercell busbars which enable the electrical connection within the cell and between adjacent cells.

2.4.1.2 Intercell Connections

Adjacent cells are connected by busbars, which are highly conductive strips of metal used to transfer current between the cells (Scott *et al.*, 1987). Busbars are typically made of electrolytic-tough-pitch grade copper (Wiechmann *et al.*, 2016), which is resistant to corrosion and contact deterioration (Scott *et al.*, 1987). The most common configuration of intercellular connections is known as the Walker configuration, where all the anodes of one cell are connected to all the cathodes of the adjacent cell by insulating some of the contacts (Wiechmann *et al.*, 2014). The Walker configuration of intercellular connections is illustrated in *Figure 2.11*, showing the connections in a bank of six cells, each containing three cathodes and four anodes.

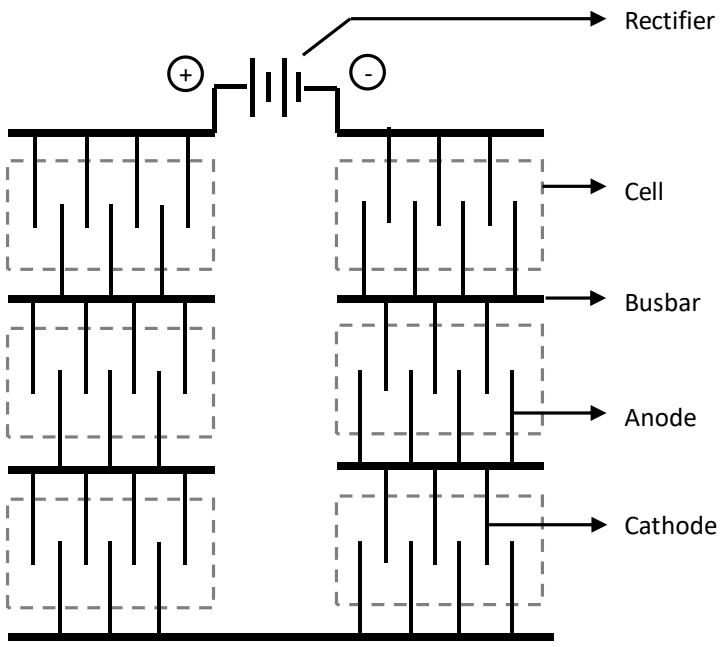

Figure 2.11: *Simplified illustration of the Walker configuration of intercellular connections.*

2.4.1.3 Tankhouse Design

Electrowinning cells are connected together to form a complete electric circuit, and a tankhouse consists of an average of four circuits, each powered by a rectifier which converts the current from AC to DC (Aqueveque *et al.*, 2015). Each circuit consists of about 120 cells, and each of these cells usually contain 40 to 60 electrode pairs (Aminian *et al.*, 2000; Aqueveque *et al.*, 2015). The top view of a typical tankhouse layout is illustrated in *Figure 2.12*.

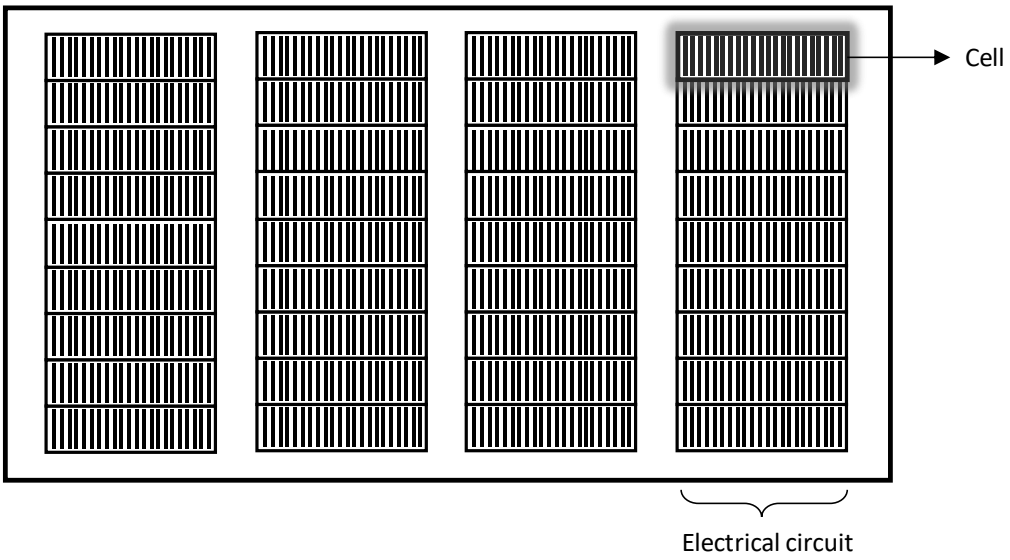

Figure 2.12: *Simplified representation of the top view of an electrowinning tankhouse (indicating the electrical circuits made up of electrowinning cells).*

The electrowinning section of a hydrometallurgical processing plant consists not only of the tankhouse itself, but the operations concerning the inlet, outlet, and recycling of electrolyte. A process flow diagram of a typical electrowinning operation is provided in *Figure 2.13*, from the inlet boundary as the advance electrolyte from solvent extraction (SX), to the final solid copper product and spent electrolyte that exits the system. The advance electrolyte (stream 1) is stored in an active storage tank (T-101), where it is combined with recycled spent electrolyte (stream 2). Stream 3 is called the recirculating electrolyte, which is pumped (using P-101) to the electrowinning cells. The heat exchanger (E-101) heats the recirculating advance electrolyte to the desired operating temperature using the recycled spent electrolyte which is heated up from the exothermic electrochemical reactions (Wiechmann *et al.*, 2016). The advance electrolyte is split equally to flow through each cell and combines again after the electrowinning cells (EW-101). The solid copper cathodes that are produced in the cells exit as a product (stream 4), where they are mechanically stripped, and the copper sold. The spent electrolyte (stream 5) splits into three streams: the recycle back to the storage tank (stream 2), recycle back to solvent extraction (stream 6) and a bleed stream which exits the process to control impurity levels (stream 7). According to Davenport *et al.* (2002), about 25 to 50% of the

spent electrolyte (stream 5) is recycled back to the solvent extraction circuit, or alternatively to the leaching operation, with the remainder recycled back to electrowinning or bled out of the system.

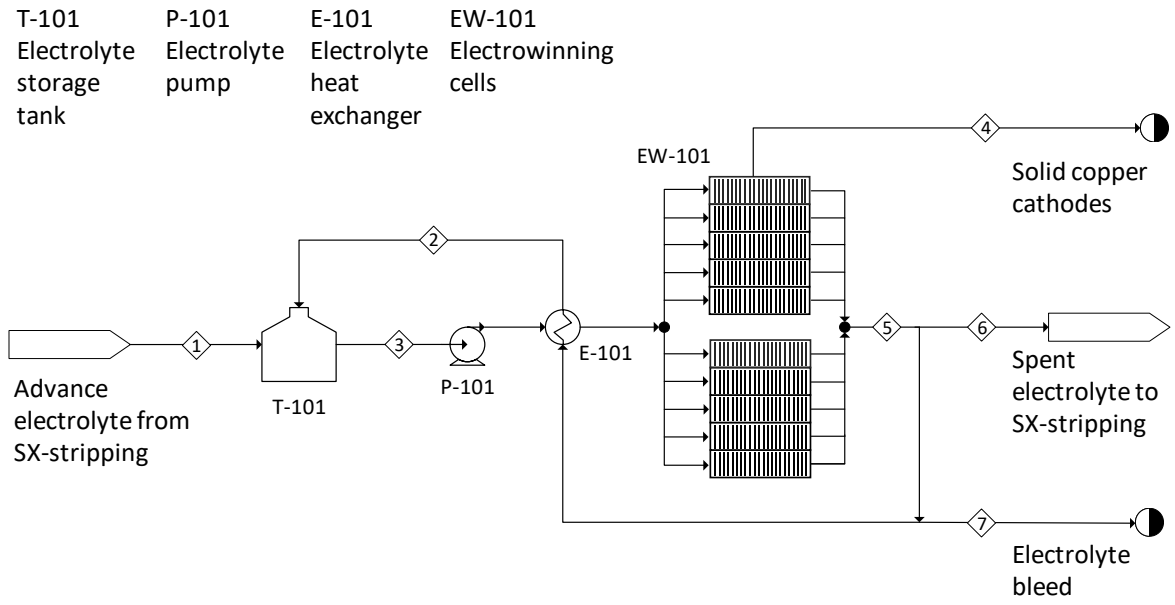

Figure 2.13: *Process Flow Diagram of the electrowinning section of a hydrometallurgical copper process.*

Note that the above process flow diagram represents a typical electrowinning operation, but each plant may differ slightly in its configuration.

2.4.2 Power Contribution

An electrolytic cell can be represented by a circuit diagram, which aids in distinguishing the constituents of voltage and current in the cell. A combination of Aminian *et al.* (2000) and Dao and McPhee's (2011) circuit diagrams for a single anode and cathode is provided in *Figure 2.14*. The total external voltage applied to the cell constitutes the anodic and cathodic voltage drops and voltage lost to ionic resistance (resistance of the electrolyte) and electronic resistance (resistance in hardware and contacts) (Loutfy and Leroy, 1978). The breakdown of total cell voltage into its constituent parts is provided in Equation 16 (Aminian *et al.*, 2000).

$$U_T = U_a + U_c + IR_{h,a} + IR_{h,c} + IR_s \qquad [16]$$

Where U_T = Total potential applied (V)

U_a = Anodic potential (V)

U_c = Cathodic potential (V)

I = Current (A)

$R_{h,a}$ = Hardware resistance associated with the anode (Ω)

$R_{h,c}$ = Hardware resistance associated with the cathode (Ω)

R_s = Resistance of the electrolyte (Ω)

The potential, current, and resistance are related by Ohm's Law, provided in Equation 17.

$$U = I \cdot R \quad [17]$$

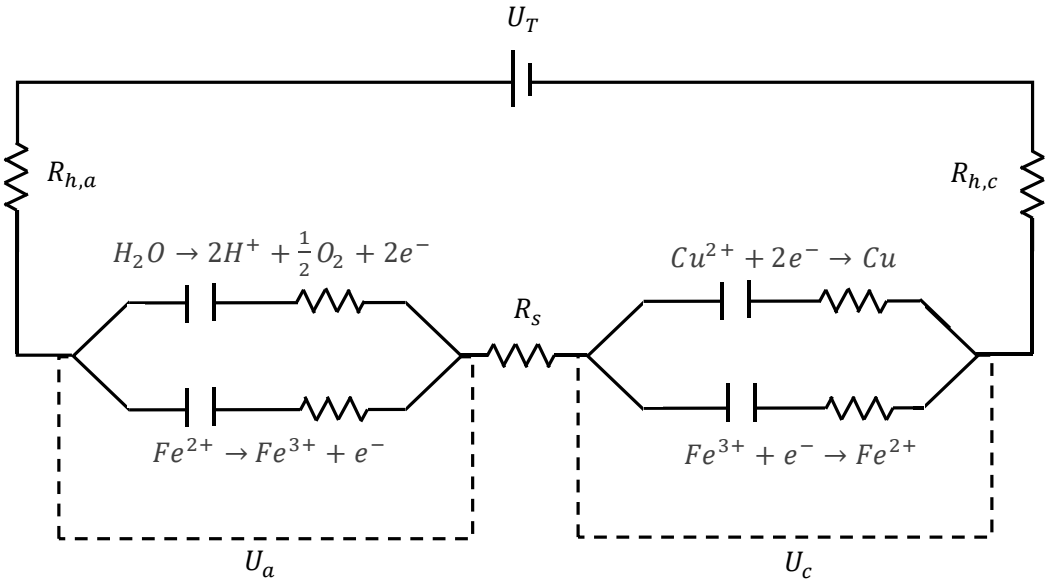

Figure 2.14: *Simplified electrical circuit representation of an anode-cathode pair, modified from* Aminian *et al.* (2000) *and* Dao and McPhee (2011).

In the circuit diagram, each electrochemical reaction is represented by a capacitor-resistor pair to represent the Butler-Volmer equation. The reactions at a particular electrode are connected in parallel (Dao and McPhee, 2011). Within each electrode, the total current splits into the current used for each reaction occurring there. In *Figure 2.14*, the reactions indicated are the main copper reduction and water evolution reactions, and the reduction and oxidation of the iron impurity. Additional reactions could be added to the circuit diagram in a similar parallel manner (Dao and McPhee, 2011).

The voltage at each electrode constitutes the reduction potential and overpotential associated with the electrochemical reactions. Equation 18 is an expansion of Equation 16 which represents the voltage of each electrode as its constituent parts of reduction potential and overpotential. The minimum potential that is required to be applied for the reactions to occur is provided by the difference in reduction potentials of the anode and cathode. The overpotentials at each electrode are incorporated to provide the driving force for the redox reactions (Davenport *et al.*, 2002; Schlesinger *et al.*, 2011).

$$U_T = E_a - E_c + \eta_a + |\eta_c| + IR_{h,a} + IR_{h,c} + IR_s \quad [18]$$

Where E = Reduction potential (V)

η = Overpotential (V)

I = Current (A)

R = Resistance (Ω)

Electricity is supplied to the electrowinning cell as a source of power, which is the product of voltage and current. *Figure 2.15,* redrawn from Schlesinger *et al.* (2011), shows the contributions to total power in the system by representing contributions to voltage on the x axis, and contributions to current on the y axis. The diagram can be viewed by isolating each axis individually to investigate the contributions of components to the total voltage or current, or combining the two axes to view power contribution as an area on the figure. The overall voltage applied to a cell is approximately 2 V (Aqueveque *et al.*, 2015; Davenport *et al.*, 2002; Schlesinger *et al.,* 2011). Total cell voltage constitutes the thermodynamic potential requirement of 0.89 V (for copper reduction and water oxidation), cathodic overpotential of 0.05 – 1 V, anodic overpotential of approximately 0.5 V, potential drop over the electrolyte of about 0.25 – 0.3 V, and potential drop due to any hardware resistance of about 0.3 V. Also indicated in the power contribution diagram of *Figure 2.15* is that the total current constitutes the current used in the copper reduction and water oxidation reactions, current wasted to side reactions and short circuits, and lost as stray currents.

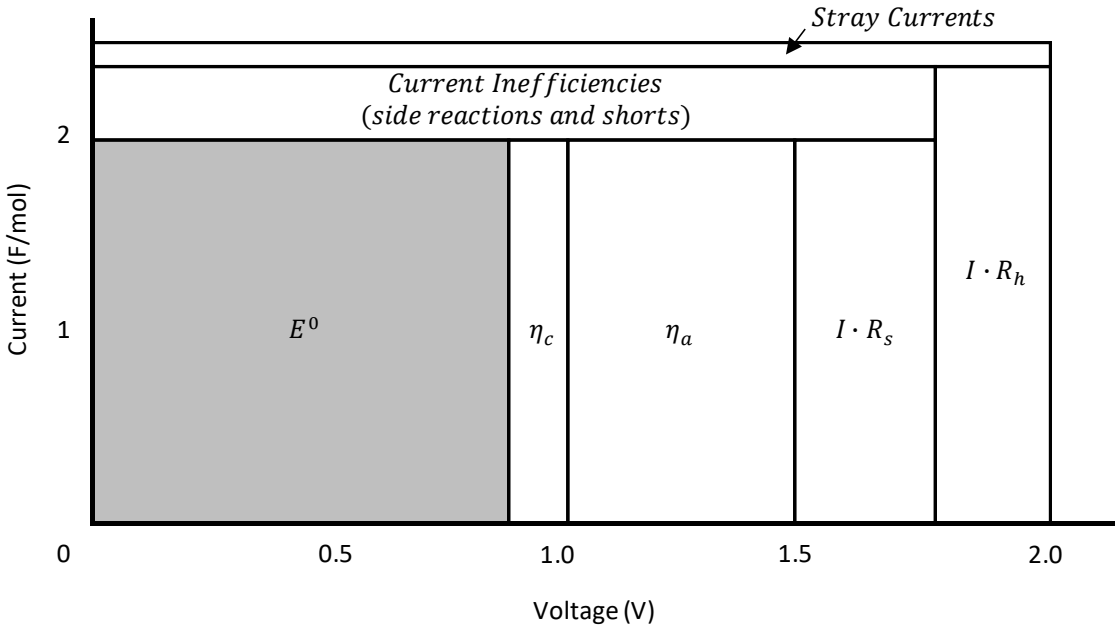

Figure 2.15: *Contributions of the current and voltage to the power requirement of an electrowinning cell, after Schlesinger et al. (2011)*

Inefficiencies in the power utilisation make the electrowinning process highly energy intensive and costly, with only a fraction of the power being used for the deposition of copper (shaded on the diagram). According to Schlesinger *et al.* (2011), the copper reduction reaction without overpotential accounts for only 30% of the electrowinning energy requirement. This power requirement for copper reduction is about 750 kWh/t, of the total 2000 kWh/t applied to the cell (Davenport *et al.*, 2002).

2.4.3 Tankhouse Performance Indicators

Key performance indicators for the electrowinning process are provided in this section, including the quantity and standard of copper production and efficiency of the electrowinning process. Determination of electrowinning performance is paramount to operations in industry, as the plant efficiency and yield and quality of the product drive revenue. Performance indicators should therefore make up the major outputs of any predictive model or tool which aids in the improvement of the electrowinning operation efficiency.

2.4.3.1 Yield

The yield of copper sheets produced is required to meet the demand of the buyer. Yield is simply measured as the mass of copper produced after going through the electrowinning cycle from the blank cathode to the stripped copper sheets. The electrowinning cycle occurs in industry for anywhere between 4 and 14 days (Robinson *et al.*, 2013b). Plating is generally deemed sufficient when the sheet thickness is between 5 – 8 mm (Schlesinger *et al.*, 2011). The rate of plating per cathode surface area lies between 0.01 – 0.10 g/(s.m^2), with an average of 0.06 g/(s.m^2), calculated from an average of global electrowinning data compiled by Robinson *et al.* (2013b).

2.4.3.2 Current Efficiency

Current efficiency is one of the most important criteria in determining optimum tankhouse operation. It is defined as the proportion of the total cell current that is actually used to produce solid copper. The current efficiency calculation is provided in Equation 19, as the actual current used divided by the theoretical current. A more practical means of calculating the current efficiency is shown in Equation 20, as the actual mass of copper produced divided by the theoretical mass calculated from Faraday's Law (Beukes and Badenhorst, 2009).

$$\beta = \frac{I_{actual}}{I_{theoretical}} \quad [19]$$

$$\beta = \frac{m_{Cu,measured}}{m_{Cu,theoretical}} \quad [20]$$

Where β = Current efficiency (fraction)

I = Current (A)

m = Mass (kg)

Industrial tankhouse current efficiencies range from 78 to 95%, with an average of 89% as indicated in a survey of global electrowinning tankhouses (Robinson *et al.*, 2013b).

2.4.3.3 Specific Energy Consumption

A measure of the power utilised during electrowinning is the Specific Energy Consumption (SEC), in megawatt hours per tonne of copper produced as calculated per Equation 21. According to Schlesinger *et al.* (2011), the total energy requirement is on average approximately 2 MWh/t, which is confirmed by Robinson *et al.* (2013b) in a global operating survey of electrowinning tankhouses. SEC ranges from 1.7 – 2.6 MWh/t in plants worldwide.

$$SEC = \frac{IU_T t}{m_{Cu}} \quad [21]$$

Where t = Plating time (s)

m_{Cu} = Mass of copper produced (tonne)

U_T = Total voltage (V)

2.4.3.4 Quality

The first major indicator of copper quality is the grade. Generally in electrowinning, high purity cathodes are produced that are 99.99% copper (Aqueveque *et al.*, 2015), and the remainder consists of impurity particles which are physically entrapped (Schlesinger *et al.*, 2011). Some of the entrapped impurities are iron, lead, sulphur, cobalt, nickel, selenium and tellurium among others. The inclusion of the solvent extraction step in the hydrometallurgical process removes most of these impurities from the electrolyte, however some may still be carried through to electrowinning by physical or chemical means.

The second major indicator of quality is the morphology of the deposit. The grain size and roughness of the plated copper needs to uphold a certain standard to conform with downstream processing, physical handling and appearance of the copper plates (Alfantazi and Valic, 2003). Morphological characteristics of the copper sheets can be measured using electrochemical impedance spectroscopy, x-ray photoelectron spectroscopy, and scanning electron microscopy (Aqueveque *et al.*, 2015). These quality indicators are affected by a number of factors including the current density, system hydrodynamics, cell temperature, presence of chloride and other electrowinning additives (Fabian, 2005; Moats *et al.*, 2016).

2.4.4 Effect of Operating Conditions

2.4.4.1 Electrical Input

The quantity of power supplied to an electrowinning cell is selected to achieve the required current density that is associated with it. The current density is one of the most important operating variables as it directly correlates to the yield of pure copper produced and impacts the current efficiency of the tankhouse and quality of the deposit. According to the analysis of world copper processing plant data by Robinson *et al.*

(2013b), typical currents densities range anywhere between 100 to 450 A/m^2, but most plants operate between 200 and 375 A/m^2 (Beukes and Badenhorst, 2009).

Current efficiency increases with increasing current density (Su *et al.*, 2017). Panda and Das (2001) add that the current efficiency decreases when the current density exceeds the limiting current density for copper plating, as the deposit does not effectively adhere to the surface. Winand (1992) supports this claim that the copper deposit becomes powdery above the limiting current density. The current density affects the quality of the metal deposit by influencing the size of the deposited grains. The higher the current density, the faster the reaction kinetics and the less time for the formation of large crystals. Therefore, at higher current densities, finer grains are deposited and the smoother the electrode surface is than at lower current densities (Murray *et al.*, 2016). However, extensively high current densities, above the limiting current density for copper, cause a rough and nodular deposit which may become powdery due to insufficient crystal growth from fast kinetics (Davenport *et al.*, 2002). In addition, the adhesion of the solid copper to the cathode is also affected by the current density. If the adhesion is poor, the copper will detach from the stainless-steel cathode prematurely. Conversely, if there is too much adhesion, the stripping of copper from the cathode will be difficult.

2.4.4.2 Electrolyte Resistance

The electrolyte, or ionic resistance is that of the ions in the electrolyte and causes a loss in the total voltage of the electrowinning cell. Ionic resistance is a function of the conductivity of the solution, cross sectional area and length on which it acts, as shown in Equation 22 (Aqueveque *et al.*, 2015). The lower the resistance of the electrolyte, the more voltage can be used in the plating reaction, which is favourable. As per Equation 22, the closer the electrodes are to one another, the lower the electrolyte resistance and therefore the higher the rate of electrochemical reactions including copper plating.

$$R_s = \frac{1}{\kappa}\frac{L}{A} \qquad [22]$$

Where R_s = Ionic resistance (Ω)

κ = Conductivity (S/m)

L = Length (m)

A = Cross sectional area (m^2)

A higher electrolyte conductivity is favourable for increased ion mobility within the solution (Kalliomäki *et al.*, 2016). As ionic resistance is inversely proportional to the conductivity, the resistance will decrease, and become more favourable, with increasing temperature. The conductivity of a strong electrolyte is in the order of tens of S/m, and increases with increasing temperature (Reade *et al.*, 1992).

2.4.4.3 Hardware Resistance

Hardware, or electronic resistance is that of the metal equipment present in the electrowinning circuit, which includes resistance in the electrodes, hanger bars, busbars, the rectifier itself and in the contacts between these materials. Hardware resistance therefore depends on the type and size of material and its age and may vary significantly between plants. The hardware resistance remains relatively constant within the electrowinning process, as it is a function of the cell design rather than the operating conditions. For this reason, hardware resistance is represented as a fixed resistor on the circuit diagram of the electrowinning cell, depicted in *Figure 2.14* of Section *2.4.2 Power Contributions*.

2.4.4.4 Copper Concentration

The concentration of copper in the advance electrolyte is dependent on the ore grade and upstream processing steps. Copper concentration is commonly about 45 g/l (Davenport *et al.,* 2002) but can range anywhere from 25 to 70 g/l (Robinson *et al.*, 2013b). With each single pass through an electrowinning cell, about 5 g/l of copper is used up in the plating reaction (Davenport *et al.*, 2002).

Dini and Snyder (2011) suggest that should the copper concentration exist within the standard operating range, it will not be very critical to the performance of the electrowinning process, besides decreasing the conductivity and increasing the ionic resistance slightly. If, however, the copper concentration is too high and exceeds the saturation limit, crystallisation will occur (Schlesinger *et al.*, 2011). If the copper concentration is too low, it is possible that insufficient natural convection occurs to deliver enough cupric ions to the electrode boundary layer and therefore the rate of plating will decrease.

Copper concentration has a marginal impact on current efficiency, with a higher efficiency reached for higher copper concentrations (Das and Gopala Krishna, 1996; Aminian *et al.*, 2000; Moats and Khouraibchia, 2009).

2.4.4.5 Sulphuric Acid Concentration

The concentration of sulphuric acid in the advance electrolyte largely depends on whether a solvent-extraction step is included upstream of electrowinning. In industrial processes excluding solvent extraction, the concentration of sulphuric acid is typically between 20 and 30 g/l, while in plants that include solvent-extraction the range is between 160 and 200 g/l (Robinson *et al.*, 2013b). Electrowinning plants most commonly operate at about 170 g/l (Davenport *et al.*, 2002). A drawback to the high acidity is that it causes extensive corrosion and unfavourable labour conditions in the tankhouse.

There are opposing physical effects of sulphuric acid concentration on current efficiency. Su *et al.* (2017) and Panda and Das (2001) suggest that higher acid concentrations decrease the anodic overpotential which decreases the current efficiency. Conversely, the direct result of the sulphuric acid concentration on the pH

of the system means that the more acidic the solution, the more conductive the electrolyte becomes and hence the higher the energy efficiency (Davenport *et al.*, 2002). Although the effect of sulphuric acid concentration on current efficiencies can vary, results by Kalliomäki *et al.* (2016) indicate that the effect is only marginal with a 1% increase in current efficiency when sulphuric acid concentration increased from 160 to 220 g/l.

The higher the concentration of sulphuric acid, the more likely the quality of the copper deposit is compromised (Dini and Snyder, 2011). The sulphate anion specifically adsorbs to the cathode surface which inhibits the nucleation of new copper crystals and causes the existing crystals to increase in size, which explains why nodular copper deposits are produced in higher sulphuric acid concentrations (Panda and Das, 2001).

2.4.4.6 Electrolyte Flowrate

Electrowinning cell flowrate is adjusted to provide an optimal interfacial velocity, which influences the boundary layer at the electrode surface and thus the mass transfer rates of ions (Beukes and Badenhorst, 2009; Najminoori *et al.*, 2015). The interfacial velocity can be determined from the flowrate according to Equation 23.

$$u = \frac{Q}{A\,N} \qquad [23]$$

Where u = Interfacial velocity (m/s)

Q = Volumetric flowrate (m^3/s)

A = Surface area (m^2)

N = Number of cathodes per cell

Interfacial velocities range from 0.08 to 0.14 m/s industrially, according to Kafumbila (2017), with 0.12 m/s being the most common. The associated volumetric flowrate per cell is, on average, approximately 15 m^3/h (Davenport *et al.*, 2002).

2.4.4.7 Temperature

For optimum rate of copper production and deposit quality, the temperature in the electrowinning cells is required to be maintained between 45°C and 55°C (Beukes and Badenhorst, 2009; Schlesinger *et al.*, 2011). Temperature affects the rate of ion diffusion, with an increase in temperature causing higher mass transfer rates due to higher solution conductivity and lower viscosity (Paunovic and Schlesinger, 2005; Su *et al.*, 2017). A higher cell temperature causes higher solution conductivity and therefore lower electrolyte resistance, meaning the power can be used instead in the electrochemical reactions and therefore that the rate of copper plating will be higher (Alfantazi and Valic, 2003; Najim, 2016). According to Alfantazi and Valic (2003)

and Panda and Das (2001), the quality of the copper deposit improves as the temperature increases, which can be attributed to the higher rate of mass transfer enabling constant smooth growth of copper crystals. However, should the temperature be too high it may have an adverse effect on deposit quality, because faster reaction kinetics cause insufficient time for a smooth crytal structure to be formed, creating a rougher deposit (Pradhan *et al.*, 1996; Ehsani *et al.*, 2016). In addition, excessive heat will degrade the organic phase taking part in solvent extraction when contacted with the recycled spent electrolyte.

Under electrowinning operating conditions which fell within industrial norms, Alfantazi and Valic (2003) and Zhang *et al.* (2018) found that an increase in temperature caused a decrease in current efficiency, which could be attributed to an increase in mass transfer coefficient with temperature due to higher solution conductivity and lower viscosity. These changes in physicochemical properties of the electrolyte also indicate that the limiting current density will increase with an increase in cell temperature (Cifuentes and Simpson, 2005).

2.4.4.8 Impurities and Trace Elements

The electrolyte consists of several elements in low concentrations that do not form part of the major electrochemical equations for the plating of copper. Some of these elements are impurities carried through from the ore, and others are trace elements which may be added to the system for their beneficial effects.

Iron is the first major impurity to be discussed and is present in the solution in both ferric (Fe^{3+}) and ferrous (Fe^{2+}) form. The total iron concentration ranges between 0.7 and 5 g/l in industry, with an average of 1.9 g/l (Robinson *et al.*, 2013b), and is usually higher when no solvent-extraction stage is present upstream. Iron undergoes cyclic reduction and oxidation at the electrodes, and consequently uses up current and reduces current efficiency. Davenport *et al.* (2002) and Das and Gopala Krishna (1996) indicate that each 1 g/l of iron present reduces the current efficiency by approximately 2.5%. If the ratio of ferric to ferrous ions is less than or equal to one, the current efficiency should be higher than 90% (Das and Gopala Krishna, 1996). Other elements present in the electrolyte also undergo electrochemical reactions, such as Nickel, Cobalt, Lead and Manganese. Moats and Khouraibchia (2009) suggest, however, that these elements do not have a significant effect on the current efficiency, as their reduction potentials fall out of the range of copper electrowinning.

Manganese can be present in the electrolyte. It is deposited at the anode as manganese dioxide where it passivates the anode and causes corrosion. Deposition of manganese dioxide can cause chips of lead to peel off the anode and contaminate the copper cathode (Pfalzgraff, 2009). Furthermore, the oxidation of manganese to permanganate can be detrimental to the organic phase in the solvent-extraction circuit. The presence of iron in Fe:Mn ratios of between 5 and 10 helps to reduce the negative effects of manganese on the anode (Mirza *et al.*, 2016).

Cobalt is an impurity that can exist naturally or is often physically added to the electrolyte due its positive impact on the electrowinning process. It is necessary to maintain cobalt levels at approximately 80 to 250 mg/l (Robinson *et al.*, 2013a) in order to stabilise the lead oxide layer that forms on the anode so that it does not detach and contaminate the copper deposit (Pfalzgraff, 2009).

Chlorine is also present in the electrolyte in trace amounts (20 – 30 mg/l) (Robinson *et al.*, 2013a). Chlorine mostly exists naturally, but is also sometimes added to increase the quality of the copper deposit by acting as a brightening and smoothing agent. Chlorine brightens and smooths the deposit by aiding in the binding of copper crystals (Dini and Snyder, 2011; Murray *et al.*, 2016). The level of chlorine needs to be maintained carefully as too much can cause a nodular deposit to be formed by adsorbing to the cathode surface and inhibiting the growth of copper crystals (Dini and Snyder, 2011). A high level of chloride can also corrode the cathode and other tankhouse equipment and is toxic to plant operators (Pfalzgraff, 2009).

2.4.4.9 Electrowinning Additives

In order to plate copper smoothly onto the cathodes, electrowinning additives or smoothing agents can be added to the electrolyte in the order of parts per million. Guar gum, polysaccharides and polyacrylamides are commonly used as smoothing agents in industrial electrowinning. Smoothing agents influence the properties of the electrolyte through their thickening ability and influence the nucleation of copper in order to form a bright, uniform deposit (Fabian, 2005; Murray *et al.*, 2016).

2.4.5 Processing Challenges

Certain conditions or events occur within electrowinning cells in industrial tankhouses that negatively impact the running of the electrowinning plant in terms of operator safety, tankhouse corrosion, and inefficient or ineffective operation. Good housekeeping and maintenance, process optimisation and fault detection can help to reduce the effects of these process challenges to maximise the electrowinning performance.

2.4.5.1 Acid Mist

Acid mist is inevitably produced in electrowinning tankhouses when sulphuric acid particles are trapped in the ascending bubbles of oxygen formed at the anode (Wiechmann *et al.*, 2016). The acid mist creates an extremely harsh environment in the tankhouse – equipment easily corrodes and working conditions are highly toxic (Aminian *et al.*, 2000; Aqueveque *et al.*, 2015).

One method to control acid mist levels is to float a layer of balls or beads on top of the electrolyte, which creates a more convoluted path for acid mist bubbles so they burst less violently (Al Shakarji *et al.*, 2013; Aqueveque *et al.*, 2015). Another physical method of controlling acid mist is to cover the cells and ventilate the mist elsewhere (Pfalzgraff, 2009). Chemical suppressants can also be added to the electrolyte (Al Shakarji

et al., 2013), or alternatively surfactants or foaming agents can be used which stabilise the oxygen bubbles into a foam layer (Pfalzgraff, 2009; Aqueveque *et al.*, 2015).

2.4.5.2 Short Circuits

Short circuits, or low resistance connections through which all the current will flow, are detrimental to the electrowinning process as they disrupt the flow of current within and between cells. When plating does not occur smoothly, especially when the nucleation rate is too high, nodular growths called dendrites are formed. The peaks of the dendrites receive a larger ion flux than the valleys on the electrode surface, and continue to grow larger (Free *et al.*, 2013). Not only do dendrites form a rough copper surface, but a short circuit could occur if consequent contact between the electrodes is made (Aqueveque *et al.*, 2015). Short circuits which occur in the electrowinning system use up current which could otherwise have been used for the copper plating reaction and therefore decrease the current efficiency extensively. Measures are put into place to eliminate short circuits such as optimising the plating rate and time and adding smoothing agents to the electrolyte. Some plants use infrared technology and voltage measurements on cells in order to detect faults caused by short circuiting.

2.4.5.3 Insufficient Electrode Contact

If the electrodes do not make proper contact at the connections between materials, blank cathodes will be produced. Insufficient electrode contact causes high electrical resistance and therefore current cannot flow through to initiate the copper plating reaction. Insufficient electrode contact therefore has a large negative impact on the yield of pure copper produced, current efficiency and specific energy consumption (Aqueveque *et al.*, 2015).

2.4.5.4 Stray Currents

Stray currents to ground are one of the main contributors to losses in current efficiency (Khouraibchia and Moats, 2010; Wiechmann *et al.*, 2010; Shukla, 2013). Stray currents are simply deviations of current from the standard electrowinning circuit to ground.

2.4.5.5 Entrainment

Entrainment is the dispersion of droplets of one liquid phase or material within another phase, due to ineffective phase disengagement during solvent extraction or stripping. Any entrained material that ends up in the electrolyte detriments electrolytic quality and the electrowinning process. Entrainment of the aqueous pregnant leach solution in the organic phase carries undesired impurities into electrowinning. Entrainment of the organic phase into the advance electrolyte causes poor copper nucleation (Pfalzgraff, 2009),

discoloured cathodes, and is a fire hazard (Schlesinger *et al.*, 2011). Solid material that becomes entrained and ends up in the electrolyte creates sites for nucleation on the cathodes and causes the formation of dendrites (Pfalzgraff, 2009).

2.5 Electrowinning Modelling

There are several existing electrochemical models in the literature, from which key aspects will be used as the basis for this research. This section is presented in terms of major advances in modelling of the electrowinning process. Noteworthy key features and limitations of the existing models are highlighted, and the gaps in the literature for a full-scale electrowinning model to predict process performance are illustrated.

2.5.1 Modelling of an Electrochemical Cell

Models exist in the literature that develop the reaction kinetics of both electrolytic and galvanic electrochemical cells. Chang (2009) created a dynamic electrochemical model from first principles, basing the electrochemical cell as a capacitor at constant temperature and solving through finite element software. The first principles included combining the Nernst equation, Butler-Volmer equation, ionic flux and Faraday's Law to determine rate kinetics. Dao and McPhee (2011) used the same first principles approach but went one step further and used linear graph theory to represent the cell. Dao and McPhee (2011) also represented the electrochemical equations as circuit diagram equivalents, with the Nernst equation signified by a nonlinear capacitor, and the Butler-Volmer equation signified as a nonlinear resistor.

A limitation of these electrochemical kinetics models is that they only consider isolated reactions on a single pair of electrodes under theoretical circumstances and could be considered too approximate for a full-scale electrowinning model. The reaction kinetics equations are an important tool which can be taken forward into the model development of this research.

2.5.2 Computational Fluid Dynamics Models

The equations used in the first principles approach to modelling an electrolytic cell have been used in a variety of Computational Fluid Dynamics (CFD) models, using Multiphysics software. These CFD models incorporate the geometry of a single electrode pair together with the reaction kinetics and are therefore more useful in their application to an electrowinning cell.

The hydrodynamics in the interelectrode gap were investigated by Kim *et al.* (2013) and Leahy and Schwarz (2014). Kawai and Miyazawa (2014) modelled the hydrodynamics and concentration profiles for electrorefining and noted that there was little change in mass transfer for different configurations of fluid flow in the cell. It was determined that there was an upward electrolyte flow at the anode due to oxygen bubbles ascending, and an upward flow at the cathode due to the consumption of cupric ions, causing a

downward flow towards the centre of the interelectrode space (Najminoori *et al.*, 2015). Current density distributions have also been modelled extensively by Georgiadou (2003) and Werner *et al.* (2018) for a single electrode pair, and Laitinen and Tanttu (2008) extended this to a tankhouse. A zinc electrowinning cell has also been optimised for current distribution (Choi *et al.*, 2014).

Najminoori *et al.* (2015) were one of the only sources to investigate the performance of a copper electrowinning tankhouse. They also take a CFD modelling approach, and determine the effects of current density, electrolyte flowrate, and the distance between electrodes on the three-dimensional distribution of copper and velocity in the cell. It is noted that the copper concentration only changed by about 0.02 g/l from the bulk phase to the surface of the cathode. A limitation of this model is that it did not include any impurities or other losses in current, and therefore would not be able to accurately predict energy usage or efficiency in an electrowinning cell. However, the work of Zhang *et al.* (2018) may be more useful in the circumstances as the current efficiency is predicted for a single electrode pair by taking the iron redox reactions into account. This model compared well to experimental data but was not considered useful for a wide range of operating conditions or parameters, because the current efficiency prediction was limited to a comparative equation of iron and copper diffusion.

The influence of impurities on electrorefining was studied by Zeng *et al.* (2015), who use the modified Butler-Volmer equation to estimate particle trajectories and velocity fields in copper electrorefining. It was concluded that the flowrate, current and cell temperature all influence the quality of copper cathode produced in terms of the amount of impurities on the cathode surface.

CFD models have been used to determine profiles of velocity, concentrations, current density and the hydrodynamics in the interelectrode space and sometimes the entire cell, and thereby clarify differences in mass transfer and plating rates throughout cells and help to optimise processes. However, the objectives of these models differ from this research, and thus the existing literature does not adequately predict key efficiency indicators for full scale electrowinning processes.

2.5.3 Circuit Diagram Approach to Modelling

In predicting the performance of an electrowinning tankhouse it is important not only to consider electrode kinetics in isolation, but to combine the effects of all electrochemical reactions and cell geometry (Armstrong, 1972). All effects can be combined using the circuit analysis approach to modelling the electrowinning process, where electric principles are used to calculate the split of current or potentials between circuit elements. Blackett and Nicol (2010) used circuit simulation software to model current distribution within an electrochemical cell. Reaction rates for the main copper redox reactions were modelled as diodes, and fixed resistances of the busbar contacts and electrolyte were incorporated. The effects of poor electrode alignment, short circuits and the cathode harvesting were modelled by altering the circuit resistances. This

circuit diagram research can be considered a noteworthy contribution to electrowinning modelling, but once again the objective was only to look at current density distributions, leaving scope for the development of a model to predict tankhouse efficiencies and performance.

2.5.4 Modelling of an Electrowinning Cell

In order to effectively model electrowinning performance in a cell, the electrochemical rate and mass transfer kinetics, cell geometries and effects of impurities and other current losses need to be combined. This can be done by using a first principles approach to modelling and using the circuit diagram analysis to constrain the problem. According to Scott *et al.* (1987), the fundamental equations required in an electrowinning model are mass balances, energy balances and electrochemical equations (thermodynamics and kinetics).

Aminian *et al.* (2000) simulated an electrowinning operation using the principles discussed in the above paragraph. They predicted the current in the system as well as spent electrolyte composition, with iron as a major impurity. Inputs to their model included the potential applied, feed composition as well as flowrate and hardware resistance. The model contains many noteworthy modelling approaches, but it is limited to predicting the output for only a single pair of electrodes, with a very approximate approach to fitting parameters to rate equations. A similar approach was taken by Free *et al.* (2006) in their model of electrowinning performance. They considered similar input variables to Aminian *et al.* (2000), but went further to predict the current efficiency, power consumption and morphology of the copper deposit as well. Their outputs were compared to experiments performed on an idealistic rotating disc electrode and the model performed relatively well. Their predicted current efficiencies were approximately 0.4% higher than the experimental values, due to current losses other than to iron redox reactions that were not included in the simulation. The model by Free *et al.* (2006) did not incorporate parameter fitting, and used idealised parameters from literature. These two simulations of copper electrowinning provide a solid backbone to further electrowinning models that could be developed and highlight the need for a proper parameter fitting approach, the inclusion of additional current losses and the further scale up from a single electrode pair to an electrowinning cell.

Also, in the literature are models of the reactive dialysis of copper (a system is which the electrodes are separated by a membrane). Similar fundamental principles were used as in the electrowinning models, whereby an iterative approach was used to solve mass balances, activity equations, ion transport through the membrane, overpotentials and equilibrium potentials and the mass of copper produced (Cifuentes *et al.*, 2007). Simulations of the electrowinning process for Nickel (Lie and Hauge, 2008), Zinc (Scott *et al.*, 1987; Mahon, 2016) and Manganese (Rodrigues, 1983) have also been conducted using the electrowinning fundamentals, but still a gap in the literature exists for a predictive model together with parameter fitting

approach that will model the performance of an entire electrowinning cell that can be readily applied to industrial processes.

2.6 Summary of the Literature

The electrowinning model that was developed in this research was based on first principles, and therefore required an in-depth understanding of the fundamentals of the electrowinning process. Copper electrowinning is an application of an electrolytic cell, where a potential is applied and the subsequent reduction of copper occurs at the cathode and evolution of water occurs at the anode. Iron is a major impurity in copper electrowinning processes, and undergoes cyclic oxidation and reduction, using up current. The kinetics of the electrochemical reactions can be calculated using the Butler-Volmer equation, together with mass transfer kinetics depending on whether the reaction is rate or mass transfer limiting. There are several parameters included in the rate equations, which are dependent on the specific system, and largely influence the kinetics. The development of an approach for plant parameter fitting in conjunction with the model is therefore made evident.

Key performance indicators in electrowinning are the yield of copper produced, current efficiency, specific energy consumption and quality of the copper deposit. Although the process fundamentals are key to predicting electrowinning performance, these needed to be extended to a full-scale electrowinning cell, which consists of up to hundreds of electrode pairs and several non-idealities that contribute to loss in current. Some additional phenomena that occur in full scale tankhouses which may affect operation include the formation of acid mist, short circuits, insufficient electrode contact, stray current and entrainment from solvent extraction or stripping. A circuit diagram approach could be used to monitor the contributions to total current and potential in the system.

The effects of operating conditions formed an integral part of this research, from the model assumptions and limitations to logical consistency checking. The direct effect of the variables discussed on the key performance indicators is therefore summarised in *Table 2.1.* The table indicates the effect of an increase in specific operating condition on the yield, current efficiency, specific energy consumption and quality (in terms of an increase, decrease, a negligible effect, or not applicable to the performance).

Table 2.1: *Summary of the effect of electrowinning operating conditions on key performance indicators.*

Effect of an increase in operating condition	**Effect on key performance indicators**			
	Copper yield	**Current efficiency**	**Specific energy consumption**	**Deposit Quality**
Current density	Increase	Increase	Decrease	Decrease
Electronic resistance	Decrease	Decrease	Increase	n/a
Copper concentration	Negligible	Slight increase	Slight decrease	Increase
Sulphuric acid concentration	Negligible	Conflicting	Conflicting	Decrease
Electrolyte flowrate	Negligible	n/a	n/a	Increase
Temperature	Increase	Decrease	Unknown	Conflicting
Iron concentration	Decrease	Decrease	Increase	Decrease

The overall electrochemical reaction rate in an electrowinning setup can be affected by many factors including the mass transfer mode and surface adsorption, voltage and current in the system, the material and geometry of the electrode, composition of the electrolyte and external factors such as time and temperature (Bard and Faulkner, 2001). The rate of reaction can therefore differ substantially between systems, highlighting the need to incorporate as many of these factors into an electrowinning model as possible.

There are several models that exist in the literature which were analysed and will form the backbone to this research. Models of electrochemical cells provided details on the kinetics, and CFD models investigated distributions of current, concentration, and flow in the interelectrode space and through cells. Although these models provided insight into the electrowinning process, the objective of this research to evaluate overall performance requires further knowledge on the scaled up cell and other current losses in the system. The circuit diagram approach to modelling is key in that it encompasses the overall process instead of looking at components in isolation. The models by Aminian *et al.* (2000) and Free *et al.* (2006) provided many useful insights, but their parameter fit is limited, as is their application to a full size electrowinning cell. Therefore, there is scope for an electrowinning model to accurately predict process performance in any full-scale electrowinning tankhouse to which it is applied, by the provision of a basic model together with parameter fitting approach. It is also highly necessary to model not only a single electrode pair, but an entire cell, and the effects of iron and other factors which contribute to current loss, in order to accurately determine process efficiency.

3

MODEL DEVELOPMENT

3.1 Introduction

The first objective of this research was to develop a semi-empirical electrowinning model that could predict process performance. The model development was based on a first principles approach and is discussed in detail in the succeeding sections of this chapter. An overview of the modelling approach is shown in *Figure 3.1*, indicating the steps in formulating the computerised model from physical phenomena of the electrowinning system (Martis, 2006). The first step in the modelling procedure was to analyse the electrowinning process to develop a conceptual model through a series of relationships and assumptions, majority of which were obtained from the literature. Once the applicable conceptual model had been defined using an electric circuit diagram which was scaled up from a single electrode pair to represent a cell, the governing relationships and equations were programmed into MATLAB. In *Chapter 4 Parameter Fitting Approach*, the approach to fitting model parameters is outlined in order to calibrate the programmed model to the physical electrowinning system.

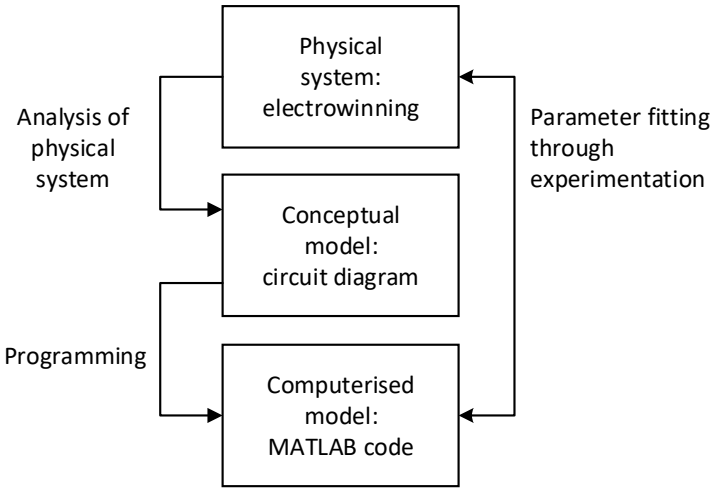

Figure 3.1: *Overview of the model development approach, from the physical system to the computerised model.*

3.2 Model Function

The electrowinning model was required to predict key performance indicators based on a set of input variables. The model needed to be applicable to an entire electrowinning tankhouse, which consists of circuits of electrowinning cells. Therefore, if electrowinning operation and performance in an average cell

could be simulated, the model could be expanded and applied to the entire tankhouse. The system boundary, and major focus of the model development, was therefore a single electrowinning cell.

The key performance indicators of an electrowinning plant are provided in *Table 3.1* together with the model output variables required for their calculation. The performance indicators that could be predicted through modelling were the yield, current efficiency and specific energy consumption. It was therefore imperative that the model predicted the mass of copper plated and associated current utilised in the copper plating reaction. The total current also needed to be calculated for use in the energy efficiency performance indicators, which meant that the current used in iron side reactions and other current losses also need to be included in the model.

Table 3.1: *Electrowinning key performance indicators and the model outputs required in their calculation.*

Key performance indicator	Model output variables required
Yield	Mass of copper plated
Current Efficiency	Current used in plating reaction Total current (including current losses)
Specific Energy Consumption	Total current (including current losses) Mass of copper plated
Quality	n/a

All input variables are available or measured in industrial tankhouses before the electrolyte enters the electrowinning cell and the plating process begins, while output variables are measured once the electrowinning process is complete. The input variables to the model were independent from the output variables, which was critical for the model to be entirely predictive.

The input variables were split into two categories: operational variables and fixed variables due to cell design. *Table 3.2* lists and describes the input variables for the model, and the reasons they may change during operation due to controlled or uncontrolled disturbances. The input variables are currently measured on majority of the electrowinning plants that exist globally, or could easily be measured if desired (Beukes and Badenhorst, 2009; Robinson *et al.*, 2013b). The practicality of measuring input variables was important for the model to be readily applicable to industrial electrowinning plants.

Table 3.2: *Input variables to the model and the reason they may vary within the running of the tankhouse.*

Category	Input variable	Changes in input variable
Operational variables	Electrolyte composition: Copper concentration Sulphuric acid concentration Iron concentration	Changes in composition of the ore, or controlled to a certain extent in upstream operation
	Electrolyte flowrate	Flowrate controlled by operator
	Voltage applied	Rectifier voltage controlled by operator
	Cell temperature	Heat exchanger controlled by operator
Fixed cell design	Hardware resistance	Degradation of equipment material, or defective contact between pieces of hardware
	Interelectrode spacing	Constant
	Electrode surface area	Constant
	Number of cathodes	Constant

3.3 Electrowinning Conceptual Model

3.3.1 Model Basis: Circuit Diagram Representation

A circuit diagram approach to electrowinning modelling was decided upon as this was able to encapsulate all the individual electrochemical reactions and equipment considerations and combine them together in a steady state model. This is a top-down modelling approach and was used by a few researchers in the modelling of the electrowinning system, as discussed in *Chapter 2 Literature Review*.

Aminian *et al.* (2000) used a circuit diagram to conceptualise the electrowinning process occurring between a single anode and cathode. Their research was limited, however, to predicting only a few output variables for a single anode-cathode pair, with a rudimentary parameter fitting approach. The circuit diagram modelling approach by Aminian *et al.* (2000) formed the foundation for the model development of this research, and would be expanded to predict the electrowinning performance in a cell.

3.3.2 Scaled Up Circuit Diagram

In order to predict electrowinning performance in a tankhouse, the circuit diagram for a single electrode pair needed to be scaled up to represent an entire cell. An analysis of the current flow in a typical industrial electrowinning cell with Walker configuration was conducted, and *Figure 3.2* illustrates the start to the formation of an electric circuit on the top view of a cell. The cell in the figure is simplified to contain only a few electrodes, but in reality, up to hundreds of electrodes may exist in the same pattern. The circuit for a

single pair of electrodes is highlighted: electrons will flow from the power source to the first cathode connected to the right hand side busbar, where the reduction reactions occur on the surface and copper is plated. Charge is carried between the cathode and anode via the ions in the electrolyte. At the anode surface which faces the cathode, the oxidation reactions will occur on and oxygen gas will bubble up through the electrolyte. Electrons then flow through the busbar on the opposite (left hand) side of the cell and back to the power source, completing the circuit. Current flows in the opposite direction to the electrons in the circuit.

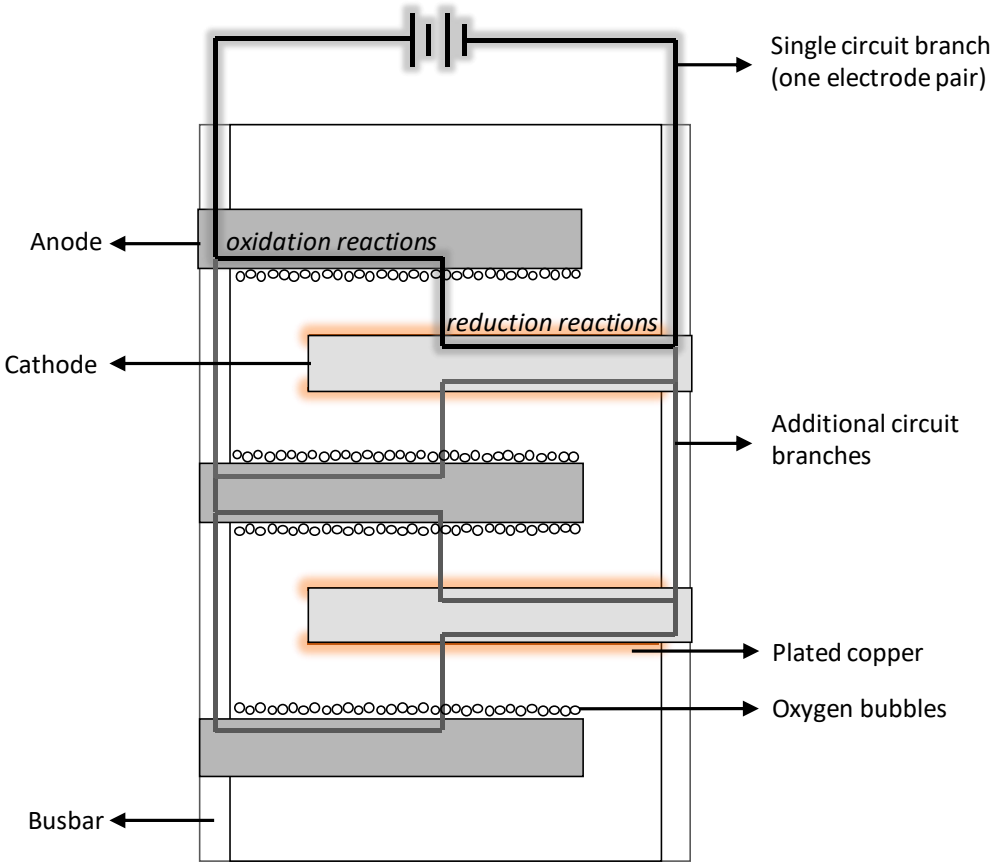

Figure 3.2: *Illustration of the top view of an electrowinning cell with electrical connections for use in the circuit diagram.*

Also illustrated in *Figure 3.2* is that additional electrodes pairs can be incorporated into the circuit diagram by adding more branches in parallel. Each of these branches contains an anodic and cathodic reaction occurring on electrode surfaces that face each other. In an electrowinning cell, there is always one more anode than cathode, ensuring that every cathode is plated on both faces. *Figure 3.2* contains three anodes and two cathodes which means that four cathode faces will be plated, or that there are four main branches in the circuit diagram.

The circuit diagram equivalent of the electrowinning cell is provided in *Figure 3.3* representing four branches, or two cathodes plated on both faces. Iron was included as a major impurity in the electrolyte and its cyclic

reduction and oxidation are included together with the copper reduction and water oxidation reactions respectively. The scaled up version of the circuit diagram not only includes additional branches representing more electrode pairs, but a fixed resistance in parallel representing additional current losses. In a full-scale plant, there are several non-idealities which draw current from the system and affect the energy efficiency. This current loss is associated with additional side reactions (other than iron which is already incorporated), short circuits, insufficient equipment contact and stray currents. The current loss factor differs in every electrowinning tankhouse due to variations in operation and design. Current loss is essential in the prediction of performance and will become an important parameter to fit as part of the parameter fitting approach (*Chapter 4: Parameter Fitting Approach*).

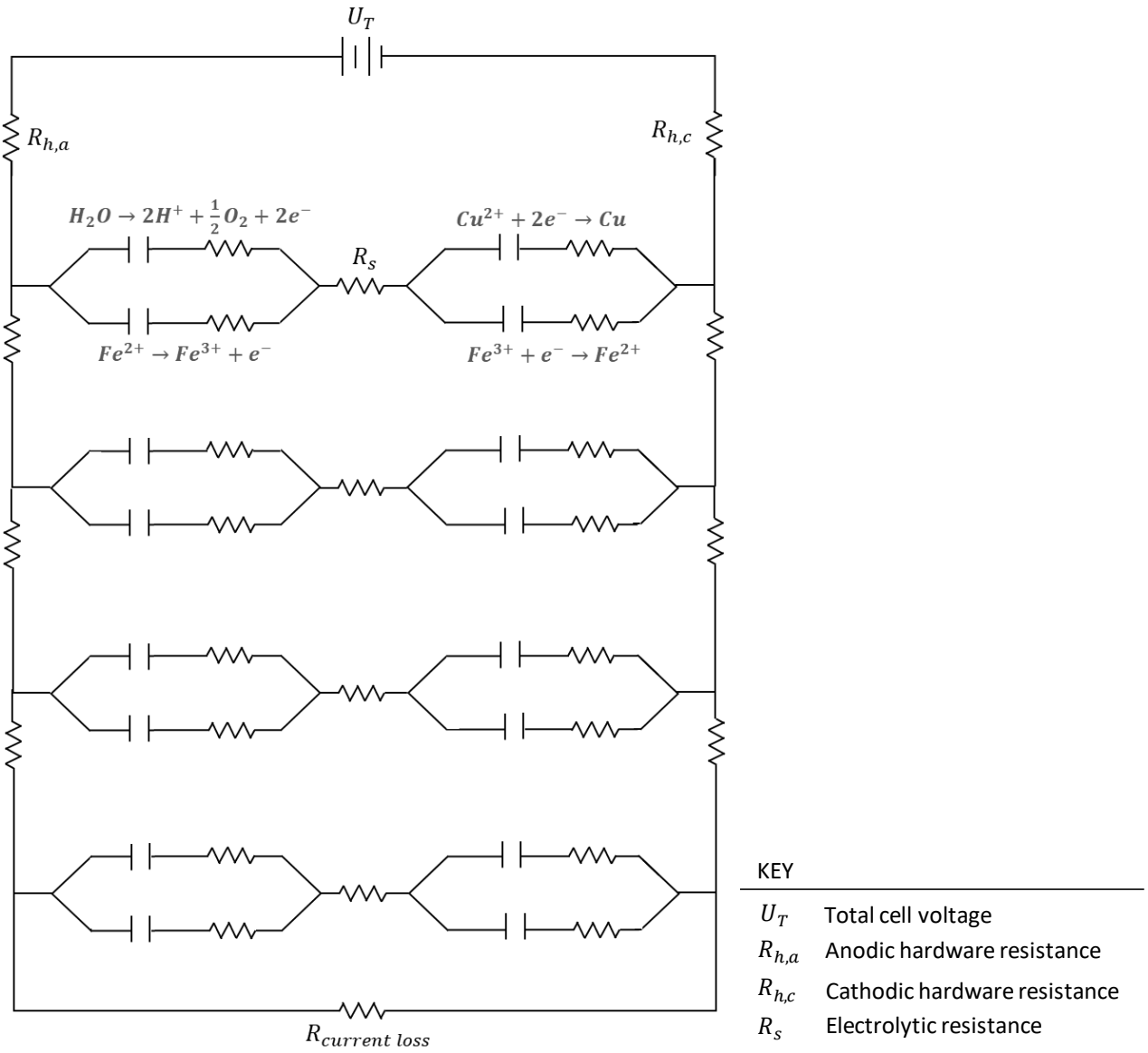

Figure 3.3: *Circuit diagram of an electrowinning cell, consisting of a number of electrode pairs and additional current loss resistance.*

The circuit diagram of the electrowinning cell (*Figure 3.3*) formed the backbone to the model, and could be expanded to represent the number of electrode pairs occurring in any cell. The modelled cell represented an average cell in an electrowinning tankhouse with standard Walker intercellular connections (anodes of one cell connected to cathodes of next cell). The performance of the entire tankhouse was based on the performance of this average cell. Should any other electrical configuration between or within cells occur in a given plant, the circuit diagram could easily be altered.

3.4 Major Assumptions

The major assumptions used in the development of the electrowinning model are provided in *Table 3.3* with an explanation of their implication on the model. Other minor assumptions required for the model programming are provided within the relevant section (Section *3.5 Programming*).

Table 3.3: *Major assumptions used in electrowinning model development and the implications thereof.*

Assumption	**Implication**
Steady state	The steady state approximation meant that time was not to be incorporated into the model: all reaction rates remained constant, and the rate of reaction was equal to the rate of mass transfer.
Perfectly mixed	The composition of the electrolyte within the cell is equal to the composition of the spent electrolyte. This was proven to be an accurate approximation through electrowinning tracer tests conducted by Aminian *et al.* (1998).
Identical electrode pairs	From an electrical standpoint, it was assumed that every electrode pair and associated hardware and electrolyte resistance was identical. This meant that the average operation of the electrowinning cell was modelled.
Electrolyte constituents are copper, sulphuric acid and iron	The effects of iron reduction and oxidation were included in the model, but the effects of other impurities were considered negligible as they only occur in trace amounts and would only use up minor amounts of total current. This assumption was based on findings from Moats and Khouraibchia (2009) and Aminian *et al.* (2000). The effects of impurities other than iron were lumped together within the current loss parameter.
Model valid under standard operating conditions	The range of operation was based on a survey of global electrowinning plants (Robinson *et al.*, 2013b), which was assumed to be representative of standard operating conditions.

3.5 Programming

3.5.1 Model Overview

The general approach to the electrowinning modelling was to predict the output variables for a single electrode pair based on Aminian *et al.'s* (2000) model, repeat for the additional electrode pairs that make up the cell and then incorporate the additional current losses and calculate the performance indicators. An overview of the modelling algorithm is provided in *Figure 3.4*, and the succeeding sections within the programming breakdown go into further detail as to how the electrowinning concept was captured in the model.

The modelling process was initiated with the definition of input variables, parameters and constants and some preliminary calculations (Section *3.5.2 Initial Definitions and Calculations* and *Section 3.5.4 Property Correlations*). For the first iteration, the spent electrolyte composition was approximated as the advance electrolyte composition and an initial voltage drop over the cathode was an estimated guess. This cathodic voltage drop was used to calculate the rates of reduction of copper and ferric ions and associated cathodic current for one electrode pair (Section *3.5.7 Kinetics*), which included the determination of component activities (Section *3.5.5 Activity Calculations*). Thereafter, the anodic voltage drop was determined from the contributions to total voltage in the circuit diagram (Section *3.5.6 Voltage Contributions*) and correlation for electrolytic resistance (Section *3.5.4 Property Correlations*). The anodic voltage drop was used to calculate the rates of oxidation of water and ferrous ions and associated anodic current. If the current in the cathode was equal to the current at the anode, the next step in the modelling algorithm could be taken, but if not, the cathodic voltage drop was altered and the process of determining the electrode currents repeated. Once the model had converged to a solution where the difference in current at the anode and cathode was lower than the prescribed tolerance (Section *3.5.8 Model Convergence and Tolerance*), mass balances were utilised to determine the spent electrolyte composition (Section *3.5.3 Mass Balances*). The calculated spent electrolyte composition was input into the start of the respective iteration (after the preliminary calculations) and the procedure was repeated until the compositions had converged to within the desired tolerance.

After the modelling of one electrode pair had been completed, scale-up calculations were performed to account for the number of electrode pairs in the cell (Section *3.5.9 Scale Up*). Final calculations were carried out to calculate the performance of the electrowinning cell in terms of yield, current efficiency and specific energy consumption (Section *3.5.10 Final Performance* Calculations). Finally, hardcoded limits and warnings were programmed in so that the model remained within operational boundaries (Section *3.5.11 Hardcoded Limits and Warnings*).

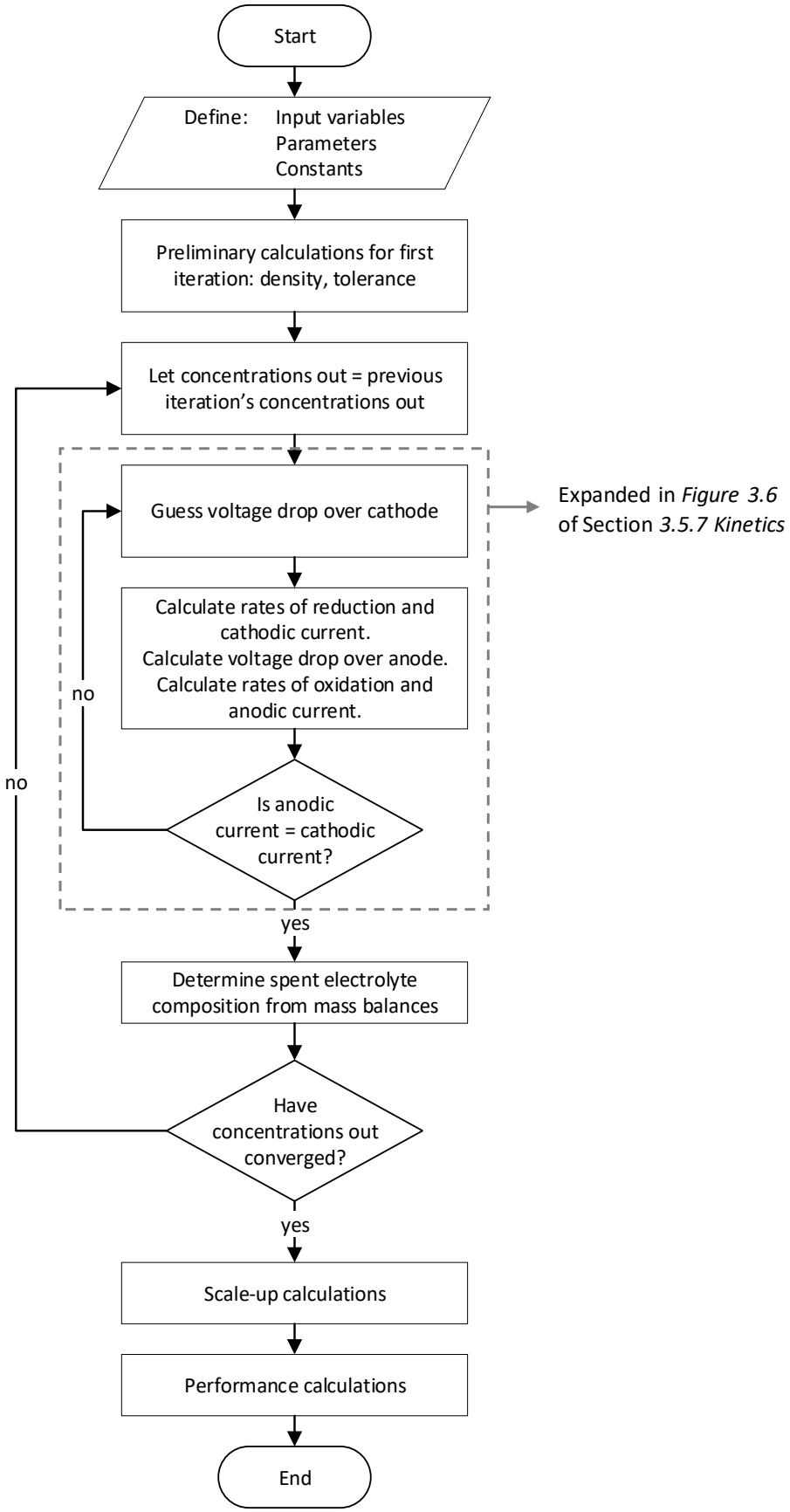

Figure 3.4: *Overview of the modelling algorithm for performance determination of the electrowinning cell.*

3.5.2 Initial Definitions and Calculations

The first step in the electrowinning modelling process was to define the initial variables and perform some basic preliminary calculations. Variable definitions entailed input variables, parameters and constants. The values of the input variables should be based on the specific plant to which the model will be applied to and would be entered in by the model user. These variables were introduced in Section *3.2 Model Function*. For the first generation of the electrowinning model, the input variables were based on industry averages from a global electrowinning survey (Robinson *et al.*, 2013b). These average input variables are provided in *Table 3.4*, including the ranges of typical industry operation (Robinson *et al.*, 2013b). The hardware resistance, or associated voltage loss due to hardware is often not physically measured in current electrowinning operations. This being said, the hardware resistance could easily be measured should a plant decide to utilise this electrowinning model (Wiechmann *et al.*, 2009). According to Aqueveque *et al.* (2015), Davenport *et al.* (2002) and Schlesinger *et al.* (2011), the average voltage lost to hardware is approximately 0.3 V, and this value was used in the initial model calculations (the hardware resistance will be an input into the model upon application in a plant scenario). In reality, the hardware resistance would increase the further away the electrodes were from the voltage source (Loutfy and Leroy, 1978), but it was assumed that the resistance was constant and represented an average hardware resistance The input variables were used to calculate the electrolyte density, as a preliminary calculation (see Section *3.5.4 Property Correlations*).

Table 3.4: *Average industry values used as initial inputs into the electrowinning model, with typical industry ranges* (Robinson *et al.*, 2013b).

Input variable	Description	Initial value	Typical industry range
$x_{Cu,in}$	Initial concentration of copper	44 g/l	30 – 70 g/l
$x_{Fe\ ,in}$	Initial concentration of iron	2.0 g/l	0.23 – 5.75 g/l
$x_{H_2SO_4,in}$	Initial concentration of sulphuric acid	175 g/l	27.5 – 200 g/l
U_T	Total voltage applied to cell	1.98 V	1.8 – 2.3 V
Q_{in}	Electrolyte flowrate into cell	14 m^3/h	0.78 – 36 m^3/h
T	Cell temperature	45°C	33 – 65°C
d	Distance between anode and cathode	50 mm	45 – 65 mm
A	Surface area of side of the cathode	1.2 m^2	0.69 – 1.32 m^2
N	Number of cathodes in the cell	60	21 - 228
U_h	Voltage lost to hardware resistance	0.3 V	-

The next initial model definitions were the parameters. Parameters included the exchange current densities and charge transfer coefficients used in the reaction rate (Butler-Volmer) equations, mass transfer coefficients used in the mass transfer rate calculations, and the current loss parameter including losses in current to additional side reactions, ineffective electrode contacts, short circuits and stray currents. It was assumed that the parameters remained constant over time – an implication of the steady state assumption. The parameter values could be determined for a specific plant setup using the parameter fitting approach (Section *Chapter 4 Parameter Fitting Approach*). For the initial iteration of the model, the rate parameters generated by Aminian *et al.* (2000) were used, and these are provided in *Table 3.5*.

Table 3.5: *Parameters incorporated into the electrowinning model and their initial values (Aminian et al., 2000).*

Parameter Type	Specific Parameter	Initial value
i_0	$i_{0,Cu}$	2.3E-03 A/cm^2
Exchange current density used in the Butler-Volmer equations for reaction kinetics	$i_{0,Fe,red}$	1.2E-07 A/cm^2
	$i_{0,Fe,ox}$	3.1E-06 A/cm^2
	i_{0,H_2O}	2.06E-08 A/cm^2
α	α_{Cu}	0.62
Charge transfer coefficients used in the Butler-Volmer equations for reaction kinetics	$\alpha_{Fe,red}$	0.1
	$\alpha_{Fe,ox}$	0.1
	α_{H_2O}	0.2
m	m_{Cu}	0.122 cm/s
Mass transfer coefficients used in mass transfer equations	m_{Fe3^+}	0.0301 cm/s
	m_{Fe2^+}	0.0403 cm/s
	m_{H_2O}	0.0201 cm/s
Current loss parameter	I_{loss}	0

The final definitions that were incorporated into the model were the constants (fixed variables), which were built into the model and cannot be altered by operators. These constants include the relevant species molar masses and standard reduction potentials, number of electrons involved in the electrochemical equations, Faraday's Constant and the Universal Gas Constant. Relevant constants are provided in *Table 3.6*.

Table 3.6: *Constant inputs into the electrowinning model.*

Constant	Description	Value
F	Faraday's Constant	96487 C/equivalent mol
R	Universal Gas Constant	8.314 J/(mol·K)
E^0_{Cu}	Standard reduction potential: $Cu^{2+} + 2\,e^- \rightarrow Cu$	0.34 V
E^0_{Fe}	Standard reduction potential: $Fe^{3+} + \ e^- \rightarrow Fe^{2+}$	0.77 V
E^0_H	Standard reduction potential: $H_2O \rightarrow 2H^+ + \frac{1}{2}O_2 + 2\,e^-$	1.23 V
n_{Cu}	Number of electrons involved in the copper reduction reaction	2
n_{Fe}	Number of electrons involved in the iron reduction and oxidation reactions	1
n_H	Number of electrons involved in the acid evolution reaction	1

After the definition of variables, the composition of the spent electrolyte was set equal to the composition of the advance electrolyte, and an initial guess of the voltage drop across the cathode was made (these guesses were part of the initial iteration only). The density was calculated using a property correlation (Section *3.5.4.1 Density*) and the initial concentration of ferric and ferrous ions was approximated using a ferrous to ferric ratio of 6.4:1 which is an average ratio from industrial tankhouses (Robinson *et al.*, 2013b). The tolerances for the differences in outlet concentration between iterations, and the differences between anodic and cathodic current were defined as part of the initial definitions as well.

3.5.3 Mass Balances

Mass balances were used in the calculation of the electrolyte composition, which was required to converge from the initial guess to the actual outlet composition values. The model demonstrates a single pass through the electrowinning cell, and relevant inlet and outlet streams used in the mass balances are illustrated in *Figure 3.5*. The composition of the electrolyte flowing directly into the cell was defined as part of the input variables, and that of the stream directly out of the cell was estimated from the model. The plated copper product was also treated as an outlet 'stream', with the plating rate acting as the stream flowrate. It was assumed that there were no losses of electrolyte due to evaporation or acid mist generation.

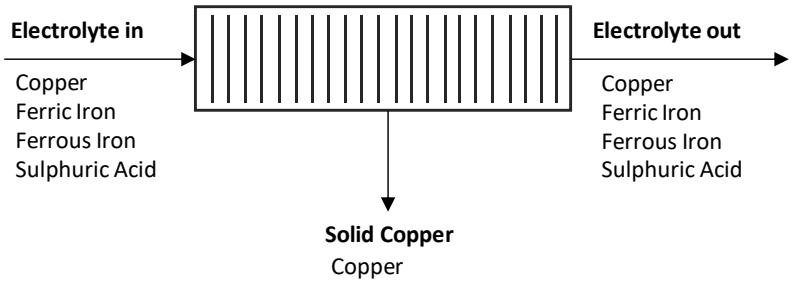

Figure 3.5: *Illustration of the streams surrounding an electrowinning cell, for use in the model mass balances.*

The general equation that was used in the species mass balances is provided in Equation 24, where the accumulation term is equal to zero because of the steady state assumption.

$$\{accumulation\} = \{electrolyte\ in\} + \{generation\} - \{consumption\} - \{electrolyte\ out\} - \{cathode\ out\} = 0 \quad [24]$$

Mass balances for copper, sulphuric acid, ferric ions and total mass were performed in order for the system to be fully defined with zero degrees of freedom. The mass balance equations are provided in Equations 25 to 28, where the subscript 'in' refers to the initial advance electrolyte and 'out' refers to the spent outlet electrolyte. It is assumed that the rate of generation of ferric ions equals the rate of consumption of ferrous ions, and likewise, the rate of consumption of ferric ions is equal to the rate of generation of ferrous ions.

Overall balance: $$Q_{in} \cdot \rho_{in} = Q_{out} \cdot \rho_{out} + P_{Cu} \quad [25]$$

Copper balance: $$Q_{in} \cdot x_{Cu,in} = Q_{out} \cdot x_{Cu,out} + P_{Cu} \quad [26]$$

Sulphuric acid balance: $$Q_{in} \cdot x_{H_2SO_4,in} + P_{H_2SO_4} = Q_{out} \cdot x_{H_2SO_4,out} \quad [27]$$

Ferric ion balance: $$Q_{in} \cdot x_{Fe^{3+},in} + P_{Fe^{3+}} = Q_{out} \cdot x_{Fe^{3+},out} + P_{Fe^{2+}} \quad [28]$$

Where Q = Volumetric flowrate (m^3/s)

ρ = Density (kg/m^3)

x = Concentration (g/l)

P = Plating rate (for copper) or rate of species generation (kg/s)

The volumetric flowrate and initial electrolyte concentrations were all input variables into the model, which were used in model calculations of the rates of reaction (plating and generation or consumption) of the species. It was assumed that the volumetric flowrate remained constant, as the steady state assumption meant no accumulation could occur and the density differences (which would be the only other differentiating factor between inlet and outlet volumetric flowrate) could be assumed negligible. The mass balances were rearranged to calculate the concentrations of species in the outlet electrolyte and solved in an iterative manner: converging closer to a solution with every model iteration until the outlet concentrations had converged to within the desired tolerance.

3.5.4 Property Correlations

The electrowinning model contained correlations for two electrolyte properties (density and conductivity) based on studies found in the literature.

3.5.4.1. Density

A density correlation was proposed by Price and Davenport (1980) for copper sulphate-sulphuric acid electrolytes pertaining to electrowinning and electrorefining. The electrolyte density is a function of copper concentration, sulphuric acid concentration and temperature, and is provided in Equation 29. This density correlation was also used by Werner *et al.* (2018) and Aminian *et al.* (2000) in their electrowinning models. It is noted that standard electrowinning operation would fall within the provided ranges of copper concentration and temperature. The concentration of sulphuric acid in electrowinning systems may slightly exceed the 180 g/l upper limit that was tested by Price and Davenport (1980), however it was assumed that the correlation still remained accurate above this upper limit as the range tested was wide and could therefore be extended slightly to include higher concentrations with relatively similar accuracy.

$$\rho = 1018.56 + 2.38\, x_{Cu} + 0.54\, x_{H_2SO_4} - 0.59\, T(°C) \quad [29]$$

Where ρ = Density (g/l)

x_{Cu} = Copper concentration (g/l), for $10\frac{g}{l} \leq x_{Cu} \leq 60\frac{g}{l}$

$x_{H_2SO_4}$ = Sulphuric acid concentration (g/l), for $10\frac{g}{l} \leq x_{H_2SO_4} \leq 180\frac{g}{l}$

T = Temperature (°C), for $20°C \leq T \leq 70°C$

3.5.4.2. Conductivity

A correlation for the electrolyte conductivity was incorporated in the model, from a study by Mathew (2012). The conductivity correlation is provided in Equation 30, and is a function of the copper concentration, sulphuric acid concentration and temperature (in Kelvin). The results of the correlation correspond to the conductivities experimentally determined by Price and Davenport (1980).

$$\kappa = \left(3200 + 7.3\, x_{Cu} - 5.6\, x_{H_2SO_4} - 14.6\, T\right)^{-1} \times 10^5 \quad [30]$$

Where κ = Conductivity (S/m)

The conductivity was used further to calculate the resistance of the electrolyte, as per Equation 31, which takes the cell geometry (plating area and distance between electrodes) into account.

$$R_S = \frac{1}{\kappa}\frac{d}{A} \quad [31]$$

Where d = Interelectrode distance (m)

A = Surface area used in plating (m^2)

3.5.5 Activity Calculations

The Nernst equation (which was used to calculate reduction potentials for the rate kinetics) required activities (or effective concentrations) for all species reacting in and produced by the electrochemical equations. It was assumed that the solid copper and water behaved ideally (with activities equal to one), but the activities of the ions needed to be calculated so that they took the interactions between other ions into account. Activities for the ions in the solution (simplified to Cu^{2+}, H^{+}, HSO_4^{-}, Fe^{2+} and Fe^{3+}) were calculated using the method proposed by Samson *et al.* (1999) for calculating activity coefficients of ions in concentrated electrolytes. In order to simplify the system for practical application purposes, it was assumed that the copper sulphate and sulphuric acid dissociated fully and the sulphate from the copper sulphate became bisulphate, which is supported by Werner *et al.* (2018) in their electrowinning model. The method used in the calculation of species activity is outlined as follows:

Equation 32 is a modification of the Davies equation by Samson *et al.* (1999) for the calculation of activity coefficients.

$$\ln(\gamma_i) = -\frac{\mathrm{A}\cdot z_i^2\sqrt{IS}}{1+\boldsymbol{B}\cdot r_i\sqrt{IS}} + \frac{\left(0.2-\left(4.17\times10^{-15}\right)IS\right)\mathrm{A}z_i IS}{\sqrt{1000}} \qquad [32]$$

Where γ_i = Activity coefficient of species i (dimensionless)

A = A parameter in the Debye-Hückel model (dimensionless)

B = B parameter in the extended Debye-Hückel model (dimensionless)

z_i = Charge number of ion (dimensionless)

IS = Ionic strength (mol/m^3)

r_i = species radius (m)

The ionic strength is a function of the concentrations and charges for all species in the electrolyte, and is calculated using Equation 33 to be input into the calculation of the activity coefficients.

$$IS = 0.5\sum z_i^2 C_i \qquad [33]$$

Where C_i = Molar concentration of species i (g/m^3)

The A and B parameters from the extended Debye-Hückel activity model were calculated using Equations 34 and 35 and were inputs into the activity coefficient equation. These parameters are a function of the species permittivity and temperature.

$$\mathrm{A} = \frac{\sqrt{2}F^2 e_0}{8\pi(\epsilon_i RT)^{\frac{3}{2}}} \quad \& \quad \mathrm{B} = \sqrt{\frac{2F^2}{\epsilon RT}} \qquad [34] \ \& \ [35]$$

Where F = Faraday's Constant (96485 C/equivalent mol)

e_0 = Charge of one electron (1.602 x 10^{-19} C)

ϵ_i = Permittivity of species (F/m)

$$\epsilon_i = \epsilon_0 \epsilon_r \quad [36]$$

ϵ_0 is the permittivity of a vacuum (8.85 x 10^{-12} F/m)

ϵ_r is the species dielectric constant (dimensionless)

R = Universal Gas Constant (8.314 J/(mol·K))

T = Temperature (K)

Once the activity coefficient for each ion had been obtained, the relevant activity could be calculated as a function of its concentration in the electrolyte, according to Equation 37.

$$a_i = \gamma_i C_i \quad [37]$$

Where a_i = Activity of species i (dimensionless)

γ_i = Activity coefficient of species i (dimensionless)

C_i = Molar concentration of species i (mol/l)

3.5.6 Voltage Contributions

The contributions to the total voltage by each constituent part (as per the circuit diagram) are used in the model as constraints for the anodic and cathodic voltages. The contributions towards the total applied voltage are the anodic potential, cathodic potential, anodic and cathodic hardware resistance and electrolytic resistance, with the relevant equation provided in Equation 16 from Section *2.4.2 Power Contributions* of *Chapter 2 Literature Review*. The anodic and cathodic voltages were expanded to incorporate the reduction potentials and overpotentials at the anode and cathode according to Equation 18.

$$U_T = U_a + U_c + IR_{h,a} + IR_{h,c} + IR_s \quad [16]$$

$$U_T = E_a - E_c + \eta_a + |\eta_c| + IR_{h,a} + IR_{h,c} + IR_s \quad [18]$$

Where U = Potential (V)

I = Current (A)

R = Resistance of the hardware or electrolyte (V)

E = Reduction potential (V)

η = Overpotential (V)

Equations 16 and 18 were combined and rearranged to form Equation 38 which was used in the model to calculate the anodic potential. The total voltage and hardware resistance were provided as input variables, the standard reduction potential and overpotential for copper were calculated using the initial guess of cathodic potential (Section *3.5.7 Kinetics*), and the electrolytic resistance was determined from the conductivity correlation (Section *3.5.4.2 Conductivity*).

$$U_a = U_T + E_c - |\eta_c| - IR_h - IR_s \quad [38]$$

3.5.7 Kinetics

The rate kinetics formed an integral part of the electrowinning model as they directly corresponded to the process performance indicators. The rate of each electrochemical reaction was calculated separately and used to calculate the current in the circuit using the steps illustrated in the modelling algorithm of the overall kinetics in *Figure 3.6* (see *Figure 3.4* for context within overall model). The circuit diagram representation indicates that the total current in the anode is equal to the total current in the cathode. Within each electrode, the current splits between the reactions that occur there. Therefore, the approach to calculating the current in the system was to determine the current used in each reaction at each electrode, sum together the current for reactions within an electrode, and determine whether total current was equal in each electrode. The kinetics were based on an initial guess of the cathodic voltage, therefore if the current the electrodes was not equal, the initial guess was altered until the currents converged to an equal value.

The rates of reaction and associated current were calculated for the reduction of cupric and ferric ions and oxidation of water and ferrous ions, as highlighted (shaded) in the schematic of overall kinetics algorithm in *Figure 3.6*. A similar general procedure was followed for the determination of current in each of these electrochemical reactions, and the relevant steps are provided in *Figure 3.7* for a reaction $O^{n+} + ne^{-} \leftrightarrow R$ (Equation 1).

As detailed in the modelling algorithm in *Figure 3.*7, the rate kinetics modelling began with the determination of reduction potential by the Nernst equation and determination of overpotential for use in the Butler-Volmer equation for the reaction kinetics. It was assumed that both mass transfer and reaction rates were relevant, as it was unknown at this stage whether the reactions were rate limited or mass transfer limited, but this would be tested in the experimental procedure. Therefore, the extended Butler-Volmer equation incorporating mass transfer was used for reaction rate kinetics. Note that the reaction kinetics were calculated as equivalent current densities. The steady state assumption meant that the reaction rate and mass transfer rates were equal, which allowed for the surface concentration of the species to be calculated as detailed in the modelling algorithm.

The mass transfer equation was based on the assumption that the Nernst Diffusion Layer model applied, which was supported by Free *et al.'s* (2006) electrowinning model and meant that mass transfer effects could be encompassed by one mass transfer coefficient parameter. Additional parameters used in more complex mass transfer models would not be able to be specifically quantified and therefore would not necessarily increase the model accuracy. The major assumption that the model is valid under standard operating conditions implies that the process operates below the limiting current density for copper reduction and water oxidation. After the current density associated with the electrochemical reaction was determined using the rate kinetics equations, it was multiplied by the surface area of the relevant electrode to calculate the current.

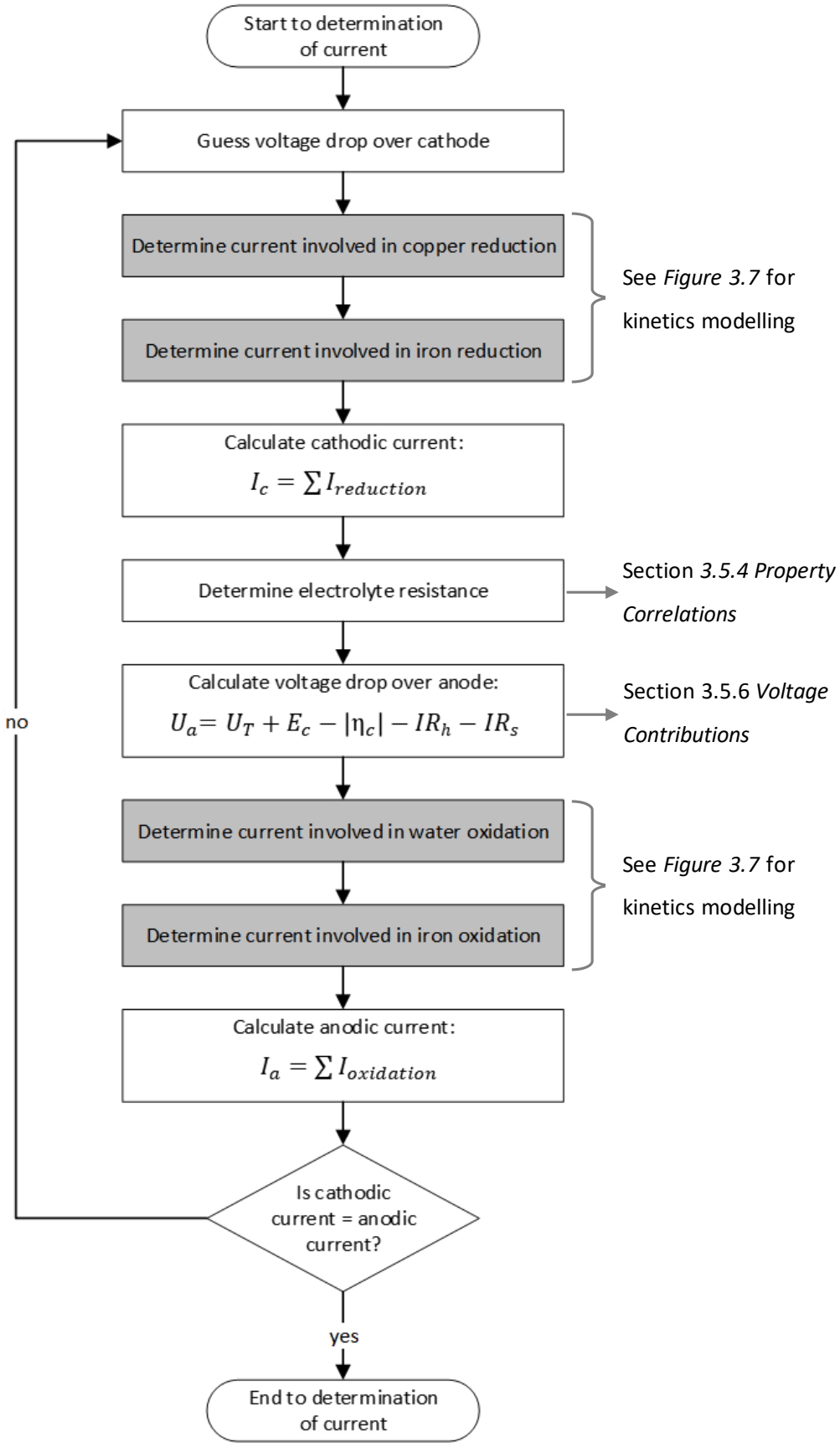

Figure 3.6: *Diagram showing the algorithmic calculation of the anodic and cathodic currents, by combining the kinetics at each electrode.*

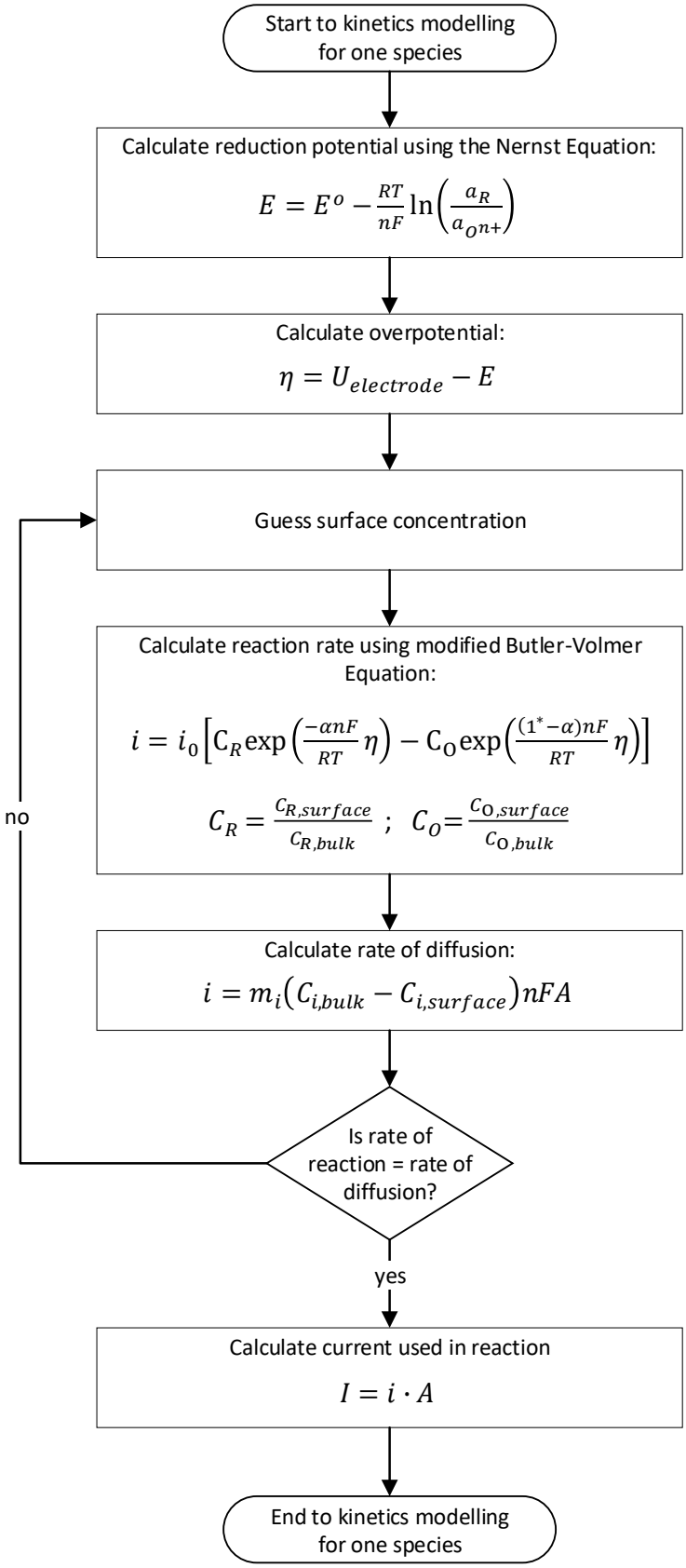

Figure 3.7: *Diagram indicating the modelling algorithm for the kinetics of the electrochemical reaction of a specific species at one electrode.*

3.5.8 Model Convergence and Tolerance

The coding of the model required a series of initial guesses and iterations based on constraints by the circuit diagram (equal electrode currents), mass balances (outlet concentrations that had converged) and steady state assumption (equal mass transfer and reaction rates). All iterations ran until the desired tolerance of 0.1% of the relevant variable was obtained (i.e. until the difference in a variable's value between two iterations was within the desired tolerance). The variables that were required to converge are provided in *Table 3.7* with an explanation of the iteration or constraint to which they conform. A maximum of 100 model iterations was hardcoded into the model to ensure termination of the iterative loop, with a warning generated if this was the case. It is noted that the warning for termination of the iteration was used in the model development phase only, so that troubleshooting could be performed. It was ensured that the final model always converged to a solution.

Table 3.7: *Model variables and associated constraints used in model iterations and convergence.*

Variable	Associated model iteration or constraint
Current	Alteration of the cathodic voltage drop until cathodic and anodic currents are equal.
Copper concentration out Sulphuric acid concentration out Ferrous ion concentration out	Convergence of the outlet concentrations of sulphuric acid, cupric and ferrous ions calculated from the mass balances.
Current density for copper reduction Current density for ferric ion reduction Current density for water oxidation Current density for ferrous ion oxidation	Alteration of the relevant species surface concentration until the current density associated with the reaction was equal to the current density associated with the diffusion of species to the electrode surface.

3.5.9 Scale Up

Once the model iterations had been completed to simulate electrowinning between two adjacent electrodes, this needed to be scaled up to represent the entire cell. Firstly, the simulation for the single electrode pair was expanded by assuming that the cell was made up of a number of identical pairs of electrodes connected in parallel, as per the scaled up version of the circuit diagram. The typical flow of electrolyte through the cell by upwards dispersion through a manifold at the bottom means that the concentration profile over the cell is not pronounced and therefore the assumption of identical electrode pairs and associated electrolyte composition is valid.

A scale up factor was defined as twice the number of cathodes in the cell (Equation 39), because each cathode is plated on both faces, and a single plated side is represented as a single branch of the circuit diagram. The total voltage applied to the cell remains the same for each circuit diagram branch (Equation 40) because the branches are connected in parallel. The total effective current, however, is multiplied by the scale up factor (Equation 41) because current is divided between parallel branches of the circuit.

$$scale\ up\ factor = 2N \quad [39]$$

Where N = Number of cathodes

$$U_{scale\ up} = U_{single\ branch} \quad [40]$$

$$I_{effective} = I_{single\ branch} \cdot scale\ up\ factor \quad [41]$$

The total mass of copper produced in cell was also determined using the scale up factor (Equation 42), and the corresponding current associated with the plating of total copper was calculated in Equation 43 using Faraday's Law.

$$m_{Cu,scale\ up} = P_{Cu}t \cdot scale\ up\ factor \quad [42]$$

$$I_{Cu,scale\ up} = \frac{m_{Cu,scale\ up}nF}{Mt} \quad [43]$$

The final calculation to be included in the model scale up was the incorporation of the current loss parameter which would be estimated during parameter fitting through calibration of the model with experimental data. The current loss parameter was added to the total effective current calculated within the model, to create the scaled up current that flows through the cell, and this is shown in Equation 44. The current loss parameter represents an average loss in current within the operation of an electrowinning cell and is specific to every plant or experimental scenario.

$$I_{scale\ up} = I_{effective} + I_{loss} \quad [44]$$

3.5.10 Final Performance Calculations

The determination of electrowinning performance was the ultimate objective of the model, and could be calculated using the final scaled up output variables listed in Section *3.5.9 Scale Up*. The yield of copper produced was determined directly using Equation 42, while the current efficiency was calculated from the scaled up current used in the plating of copper and total current as shown in Equation 45. Finally, the specific energy consumption in MWh/t was determined from the scaled up current, voltage, mass of copper plated and plating time as per Equation 46, and concluded the calculations pertaining to the model development.

$$\beta = \frac{I_{Cu,scale\ up}}{I_{scale\ up}} \cdot 100 \quad [45]$$

$$SEC = \frac{I_{scale\ up} U_{scale\ up} t}{m_{Cu,scale\ up}} \quad [46]$$

3.5.11 Hardcoded Limits and Warnings

Several process limits were hardcoded into the electrowinning model to ensure viability. If any of the concentrations or flowrates decreased to below zero, the value was set equal to zero with a warning text generated. In addition, if any of the cathodic overpotentials were positive or any of the anodic overpotentials were negative, the overpotential was set to zero to ensure no reaction occurred. Finally, a charge balance was conducted from the ionic species concentrations to ensure that electrical neutrality was maintained in the operation. The hardcoded limits and warnings formed part of the model development of this research for troubleshooting purposes, and no warnings were generated as part of the completed model, proving its validity.

3.6 Summary

An electrowinning model was developed to predict the performance indicators of copper yield, current efficiency and specific energy consumption from specified input variables, which achieved the first objective of this research. A circuit diagram formed the conceptual model of the electrowinning process, which was scaled up to include multiple parallel branches representing the many electrodes in a cell, and a current loss parameter. A steady state computerised model was created to simulate electrowinning between a single anode and cathode, and then extended to represent the scaled up circuit diagram. The model was based on a first-principles approach using a set of iterative loops constrained by electrolyte constituent mass balances and voltage and current contributions. Calculations performed in the model included species activity, property correlations for density and conductivity, the contributions to total voltage and current within the cell, and rate kinetics for each electrochemical reaction. The reaction rate kinetics incorporated reaction and mass transfer rates and were determined using the extended Butler-Volmer and diffusion equations. The parameters required in the reaction kinetics equations were taken from literature as an initial approximation but would be fitted later using the parameter fitting approach which enabled the model to represent a specific electrowinning operation.

4

PARAMETER FITTING APPROACH

4.1 Introduction

This chapter describes the methodology used in fitting the parameters contained in the electrowinning model that was developed, and comprises the design of a bench-scale experimental procedure to generate data which would be used to fit the model parameters. The parameter fitting approach is divided into two sections, the first section (forming the second objective of this research) which is to generate bench-scale electrowinning data (Section *4.2 Experimental Procedure*). The second section of the parameter fitting approach forms the third objective which is to calibrate the experimental data to the model through a parameter fitting approach (Section *4.3 Fitting Parameters to Experimental Data*). Details on the experimental design, laboratory scale equipment setup, experimental methodology and analysis are provided in the experimental procedure. The parameter fitting section describes the modelling procedure and calculations associated with fitting the current loss parameter and rate kinetics parameters to the relevant oxidation and reduction reactions.

4.2 Experimental Procedure

4.2.1 Experimental Design

4.2.1.1 Parameter Fitting Experiments

The experiments that were conducted in the laboratory scale electrowinning cell were specifically designed so that parameters could be fit to the model. The input and output variables pertaining to the model were either set or measured in the electrowinning experiments. *Table 4.1* provides details on the implementation of the model input variables in the bench-scale experiments.

Table 4.1: *Electrowinning model input variables with details on their application in the laboratory scale experiments.*

Model input variable	Description of mode input variable	Details for experiment
$x_{Cu,in}$	Initial concentration of copper	Varied as part of factorial design
$x_{Fe,in}$	Initial concentration of iron	Varied as part of factorial design
$x_{H_2SO_4,in}$	Initial concentration of sulphuric acid	Varied as part of factorial design
U_T	Total voltage applied to cell	Industrial voltages are set to maintain a desired current density, therefore current densities were varied as part of factorial design and additional experiments.
Q_{in}	Electrolyte flowrate into cell	Constant at 3.5 l/h. See Section *4.2.3.5 Flowrate Setting and Measurements* for details
T	Cell temperature	Constant at 45°C
d	Interelectrode distance	Constant at 20 mm
A	Electrode surface area	Constant at 320 cm^2
N	Number of cathodes	Constant at 1 cathode plated on both faces
R_h	Hardware resistance	Measured during experiments

A full factorial design approach was used in the experimental design, testing two levels each of current density, initial copper concentration and initial sulphuric acid concentration, and three levels of iron concentration. A low and high level of each of these variables were tested based on worldwide electrowinning operating ranges (Robinson *et al.*, 2013b), and the values thereof are indicated in *Table 4.2*. A control makes up the third level of iron concentration, at 0 g/l. The parasitic iron reactions are a significant contributor to losses in electrowinning current efficiency, while any remaining current loss could be caused by stray currents and insufficient electrode contact. The inclusion of the control in the full factorial design enabled the current loss parameter to be fit by measuring differences in current efficiency in the presence or absence of iron. The input variables tested in the full factorial design were chosen for their direct effect on the rate kinetics given by the Butler-Volmer and diffusion equations. The factorial design allowed for the independent effect of each variable on the electrowinning performance to be quantified.

It was found that the current density had the largest impact on the Butler-Volmer equation, and therefore a set of additional experiments were carried out at current densities lower and higher than the industry range in order for a more accurate model fit. These additional experiments were carried out at average copper, sulphuric acid and iron concentrations (45 g/l, 175 g/l, 2 g/l respectively). The variables altered in each of the 24 full factorial design experiments and additional 6 current density experiments are provided in *Table 4.2*, with the complete design of each experiment in *Appendix B Experimental Procedure*.

Table 4.2: *Levels and values of input variables tested during the full factorial design of electrowinning experiments, and additional current density experiments used in the fitting of model parameters.*

Experimental input variable	**Number of levels**	**Values tested**			**Details**
Initial copper concentration	2	35 g/l		55 g/l	Full factorial design
Initial sulphuric acid concentration	2	165 g/l		185 g/l	
Initial iron concentration	3	0 g/l	1 g/l	4 g/l	
Current density	2	200 A/m^2		300 A/m^2	
Current density		100 A/m^2		400 A/m^2	Additional experiments at average copper, sulphuric acid and iron concentrations.
		500 A/m^2		600 A/m^2	

The fitting of parameters to the rate kinetics equations and determination of the current loss parameter required the measurement of experimentally dependent variables, as described in *Table 4.3*. These variables were either measured after each electrowinning experiment and corresponded to the predicted model output variables, or were measured during the execution of each experiment as inputs into the model.

Table 4.3: *Variables that were measured during or after the bench-scale electrowinning experiments.*

Measured variable	Description of measured variable	Details for measurement in electrowinning experiments	Application in model
m_{Cu}	Mass of copper plated	Weigh cathode before and after plating.	Output variables
$x_{Cu,out}$	Outlet concentration of copper	Analyse spent electrolyte using Atomic Absorption Spectroscopy (AAS).	
$x_{H_2SO_4,out}$	Outlet concentration of sulphuric acid	Analyse spent electrolyte through conductivity measurements.	
R_h	Hardware resistance	Measure using multimeter during experiments.	Input variables
U_T	Voltage applied to cell	Read off power source and multimeter during experiments.	

4.2.1.2 Plating Rate Experiments

An additional set of experiments was conducted to investigate whether the plating rate of copper would vary over time, to ensure that the steady state assumption of the model was valid. Two 24 hour experiments were conducted with a randomly chosen (out of the possible factorial design combinations) copper concentration of 55 g/l, sulphuric acid concentration of 185 g/l, iron concentration of 4 g/l and current density of 200 A/m^2. Every hour, the cathode plate was removed and weighed to determine the plating rate over time.

4.2.1.3 Validation Experiments

Four experiments were conducted on the bench-scale electrowinning cell that were not included in the fitting of parameters to the model. The input values tested lay within the range of the full factorial design input values, and details can be found in *Appendix B Experimental Procedure*. The results of these extra experiments were used to compare to the predicted results in order to validate the model and evaluate its accuracy.

4.2.2 Equipment Setup

The bench-scale electrowinning cell was designed as part of another study to simulate industrial electrowinning operation (Coetzee *et al.,* 2018). The 5 litre cell was made of PVC for its resistance to acid corrosion at electrowinning operating temperatures, and restored as part of this research so that all pipes and connections were PVC as well. *Figure 4.1* is an illustration of the electrowinning cell with the direct inlet

and outlet pipes used to transfer the electrolyte to and from the cell. The electrolyte enters the cell from the bottom, where it is dispersed through a perforated horizontal plate, and leaves the cell by overflowing over weirs in two opposite side walls near the top of the cell. The design of the electrolyte inlet and outlets facilitates the even distribution of advance and spent electrolyte throughout the cell. Electrodes can be inserted into grooves cut into the top of the cell, ensuring they remain in a fixed position with constant interelectrode spacing throughout the electrowinning experiments.

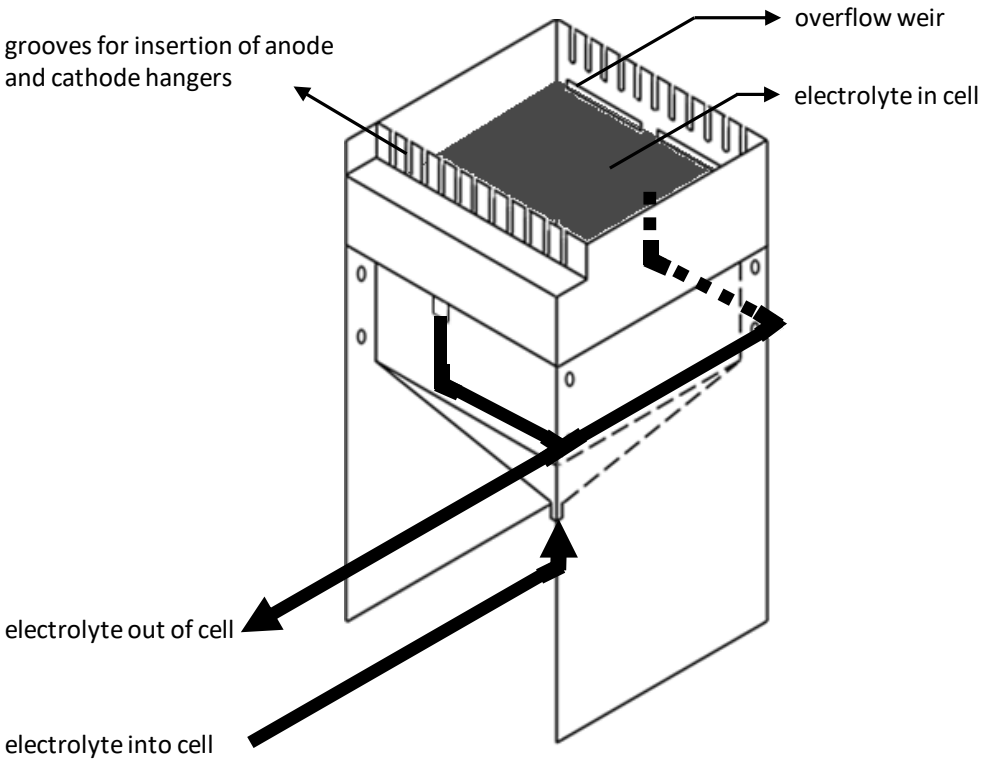

Figure 4.1: *Isometric projection of the bench-scale electrowinning cell with inlet outlet piping.*

One cathode was used for each experiment with an anode on either side to facilitate plating on both cathode faces. A new stainless steel blank cathode was used in every experiment with the same cold-rolled lead alloy anodes, both electrodes with dimensions of 15 x 12 cm. The electrodes were riveted to copper hanger bars which fit into the grooves on the cell. The wires connecting the power source to the electrodes were fixed to the hanger bars using lugs to ensure fixed contact resistance. The positive terminal of the power source (a Manson Switching Mode Power Supply, 1-16VDC, 60A) was connected to each of the anodes, and the negative terminal was connected to the cathode, as shown in *Figure 4.2* to replicate standard industrial cellular connections.

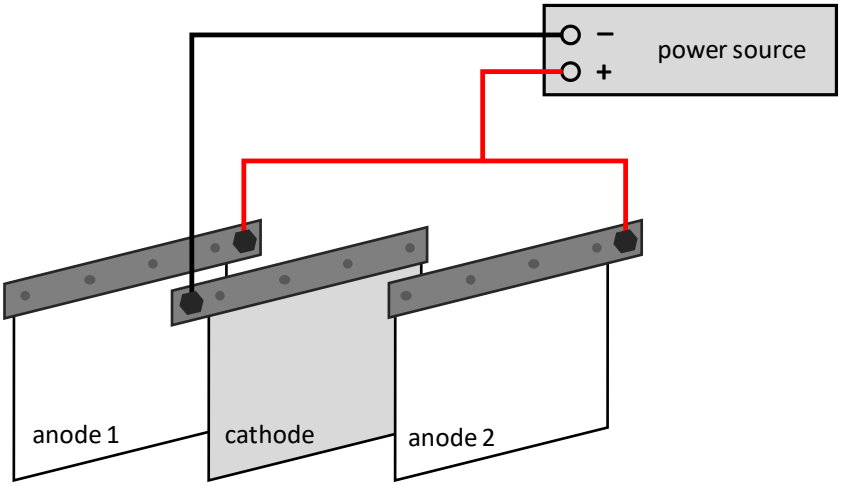

Figure 4.2: *Electrodes used in bench-scale electrowinning experiments and the electrical connections between them and the power source.*

All constituent equipment of the entire electrowinning operation including flow of electrolyte through adjoining pipes is depicted in *Figure 4.3*. The stock solution bottle containing the advance electrolyte was situated in a water bath, which was heated and maintained using a thermostat to the desired temperature value. The electrolyte was pumped using a peristaltic pump into the bottom of the electrowinning cell and overflowed over the weirs into connected pipes and back into the stock solution container by gravity. After completion of each experiment, the spent electrolyte was collected as waste.

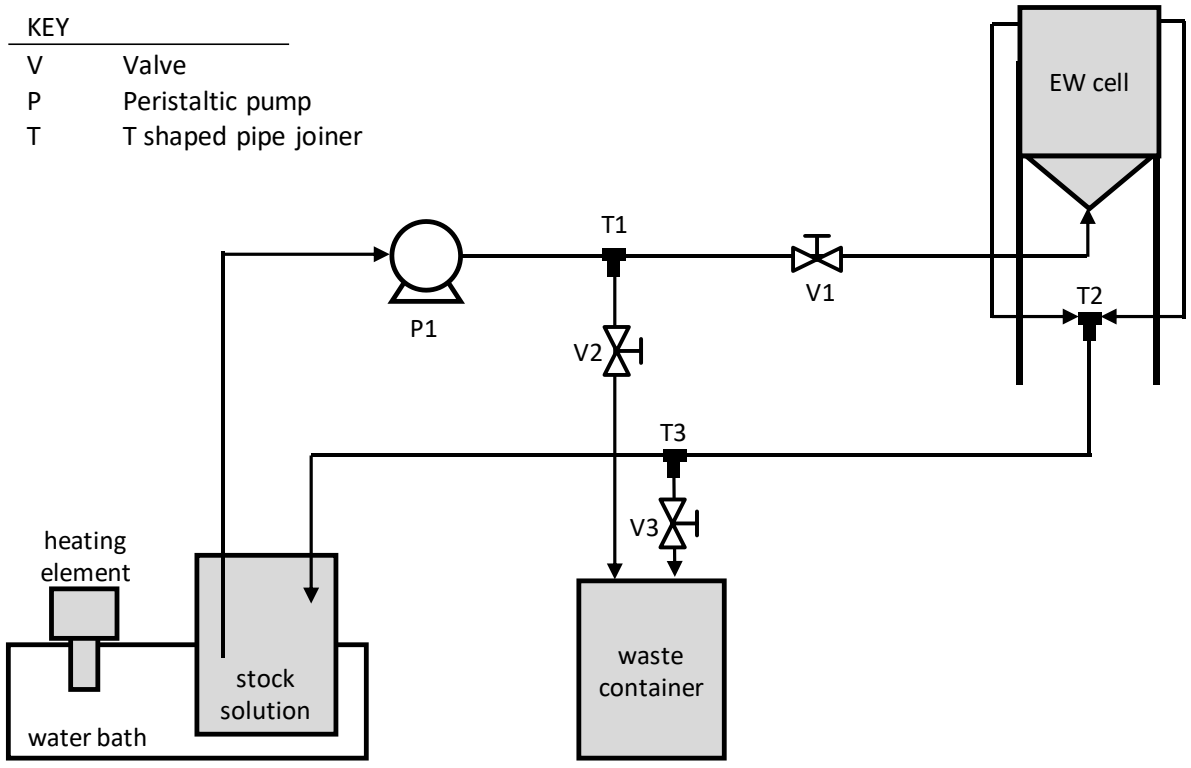

Figure 4.3: *Diagram illustrating the constituent equipment of the bench-scale electrowinning setup and adjoining pipes.*

An isometric projection of the electrowinning setup is provided in *Figure 4.4*. The cell itself was raised using a platform so that the electrolyte out of the cell could flow down into the stock solution container by gravity. A removable portion (by a threaded attachment) of PVC piping was included in the setup so that the stock solution container could be lifted out of the water bath, and the water bath was fitted with polystyrene insulation.

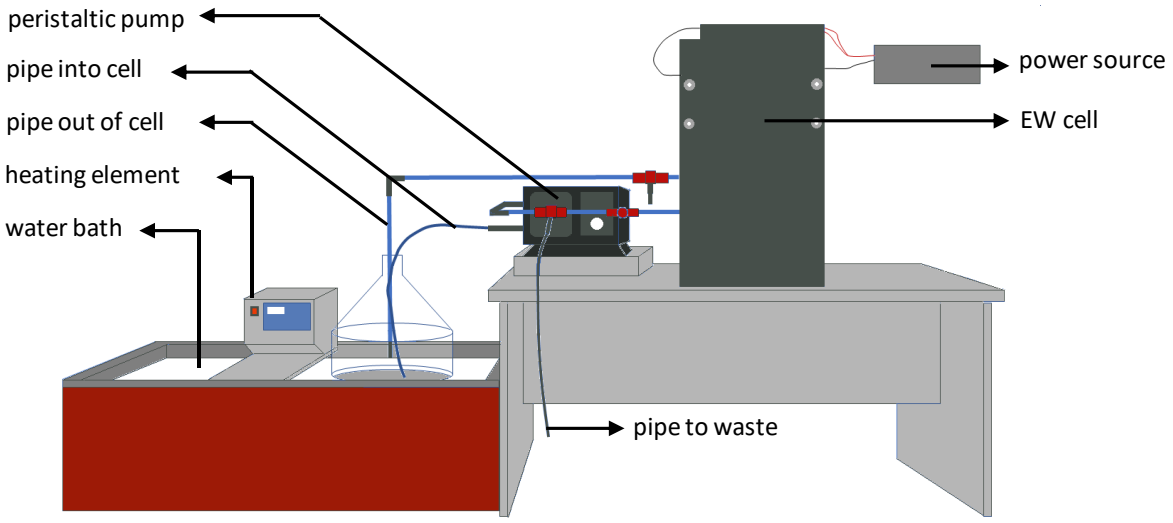

Figure 4.4: *Isometric projection of the entire bench-scale electrowinning setup.*

4.2.3 Methodology

4.2.3.1 Electrolyte Preparation

Each electrowinning experiment required the preparation of a synthetic electrolyte, containing the desired concentration of copper, sulphuric acid and iron. The electrolyte was prepared by weighing out the 98% sulphuric acid and adding it to tap water. Thereafter, the required mass of copper sulphate and ferric sulphate crystals were added to the acidic solution and water was added to make up 9.5 l of electrolyte. 500 ml of the synthetic solution was used for analysis of the initial electrolyte, leaving 9 l to circulate in the electrowinning system. Sample calculations regarding the amount of each reagent required to create the desired electrolyte composition are given in *Appendix B Experimental Procedure*.

4.2.3.2 Experimental Procedure

Before each electrowinning experiment was commenced, the equipment was set up by bolting the wire from the negative terminal on the power source to a new blank cathode and inserting the cathode into the cell between the two anodes. The stock solution bottle containing the prepared synthetic electrolyte was placed into the heated water bath, and inlet and outlet pipes inserted through the bottle neck. Thereafter, the pump

was switched on and set to the desired pump speed, and the electrolyte was circulated through the system until the temperature in the cell was maintained at 45°C. Once this steady state was reached, the power supply set to the required current was switched on to initiate the plating reaction, and the experiment was left to run for 4 hours. Thereafter, the power source and pump were switched off and the cathode was removed, rinsed with distilled water, air dried and then weighed to determine the mass of copper plated with reference to the mass of the blank cathode. A sample of the spent electrolyte was taken for analysis of its composition, and the spent electrolyte was drained out of the system and disposed of before flushing the system with water. A detailed step-by-step procedure is provided in *Appendix B Experimental Procedure.*

The plating rate experiments were run in a similar manner, except the cathode was removed and weighed (after rinsing and drying) every hour before placing back into the cell and switching the power source back on.

4.2.3.3 Voltage Measurements

At the start, end, and every hour of each electrowinning experiment, voltage measurements were conducted using a multimeter. In each instance, the total voltage was measured between the inlet and outlet of the power source, between the cathode and first anode, between the cathode and second anode, and over each wire. These voltage measurements were used to calculate the average loss in voltage over the respective parts of the circuit, which was used to determine the hardware resistance which was an input into the model. Furthermore, the voltage and current readings on the display of the power source were also recorded every hour and used to find average values of these two variables which were key to the model parameter fitting.

4.2.3.4 Sample Analysis

The samples of advance and spent electrolyte from before and after electrowinning were analysed to determine changes in the copper and sulphuric acid concentrations. The concentration of copper in the solution was determined by Atomic Absorption Spectroscopy (AAS), which was also used as an analysis method for copper in an electrolyte by Cifuentes *et al.* (2007). The sulphuric acid concentration in the electrolyte was determined by taking conductivity readings of the sample at the cell temperature and using a conductivity curve to find the associated acid concentration at the relevant copper and iron concentrations. The calibration curves were generated as part of this research based on the methodology by Thermo Fischer Scientific (2012). A detailed approach to the determination of copper concentration by AAS and sulphuric acid concentration by conductivity analysis with appropriate calibration curves are given in *Appendix B Experimental Procedure.*

4.2.3.5 Flowrate Setting and Measurements

The flowrate of electrolyte through the cell was set to simulate industrial interfacial velocity, which influences the electrode boundary layer and mass transfer kinetics. Typically in industry, the interfacial velocity is approximately 0.1 $m^3/(h \cdot m^2)$ (Beukes and Badenhorst, 2009; Robinson *et al.*, 2013b; Kafumbila, 2017). This translated to 3.5 l/h in the bench-scale cell (detailed in *Appendix B Experimental Procedure)* which was achieved at a pump speed setting of 20% of the maximum. The flowrate was measured by recording the volume of electrolyte that filled up a container in a given time.

4.3 Fitting Parameters to Experimental Data

4.3.1 Approach to Parameter Fitting

A new MATLAB code was generated to fit parameters to the predictive model, and the coding algorithm used in the parameter fitting is outlined in *Figure 4.5*. A more detailed explanation of each modelling step is provided in the succeeding sections.

The coding process was initiated with the definition of variables associated with the experiments and some preliminary calculations (Section *4.3.2 Definition of Variables and Preliminary Calculations*). Thereafter, the current loss parameter was calculated from the experiments that excluded iron (Section *4.3.3 Current Loss Parameter*), and a ratio of cathodic to anodic overpotential was guessed and used to calculate the voltage drop at the cathode. The approach to fitting the rate associated parameters was to isolate the rate equations that formed part of the model such that a nonlinear regression could be applied. Once the parameters for copper and iron reduction were determined (Section *4.3.4 Parameters Associated with Copper Reduction* and Section *4.3.6 Parameters Associated with Iron Reduction and Oxidation*), the anodic voltage drop was calculated and used to fit the water and iron oxidation equations (Section *4.3.5 Parameters Associated with Water Oxidation* and Section *4.3.6 Parameters Associated with Iron Reduction and Oxidation*). Finally, the anodic overpotential at an average current density in an electrowinning plant at 258 A/m^2 (Robinson *et al.*, 2013b) was calculated from the Butler-Volmer equation for water oxidation (incorporating the parameters fit during that iteration). If this anodic overpotential was equal to the approximate industry overpotential of 0.5 V (Davenport *et al.*, 2002), the parameter fitting iteration was terminated, however, if not the ratio of cathodic to anodic overpotential was altered.

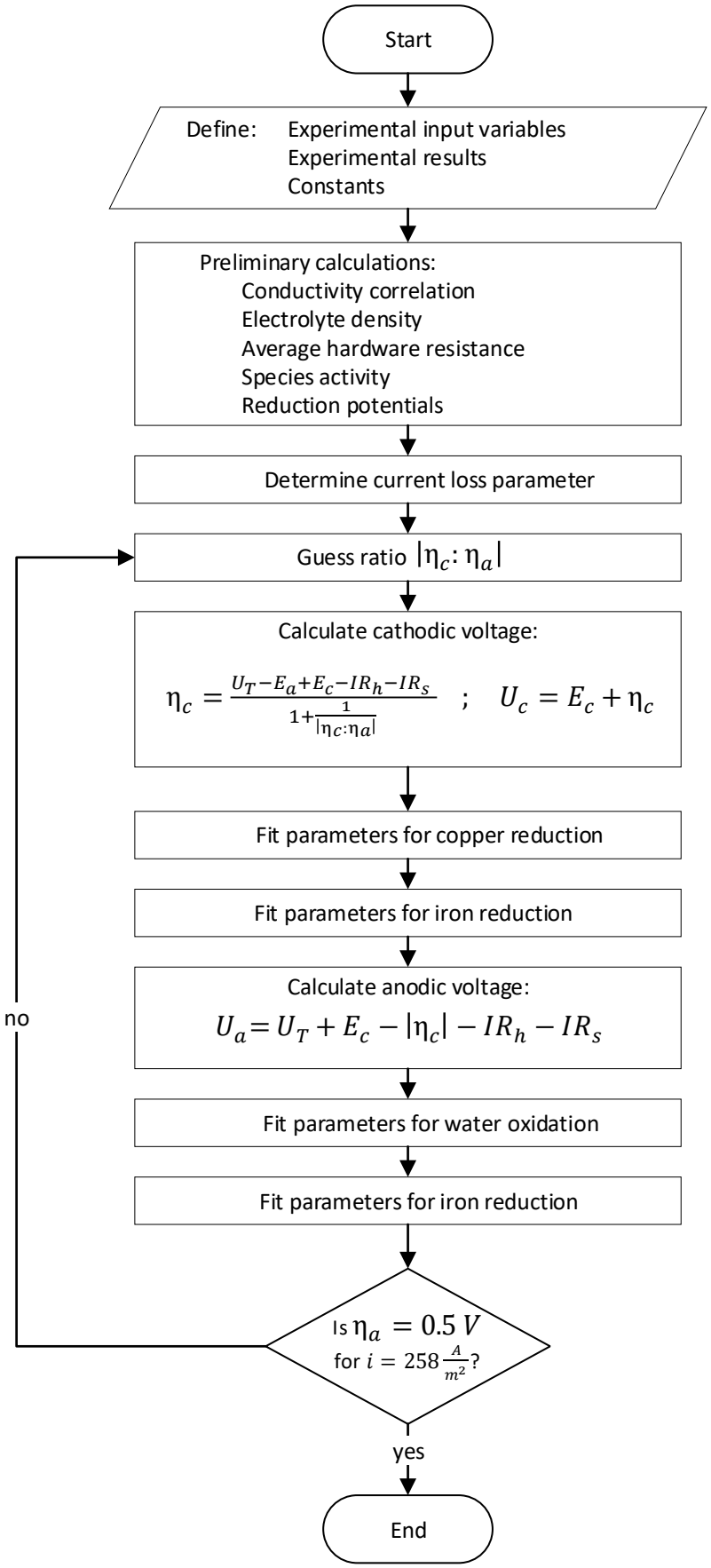

Figure 4.5: *Modelling algorithm for the fitting of parameters to the bench-scale electrowinning data.*

4.3.2 Definition of Variables and Preliminary Calculations

The parameter fitting code required the definition of a number of variables, including the experimental input and output variables and other constants, and these are given in *Table 4.4*. The experimental results and input information that varied across the experiments were defined as vectors in the MATLAB code. Constants that were required in the subsequent calculations were also defined and were the same as the constants defined in the electrowinning model.

Table 4.4: *Variables that are required to be defined in the MATLAB code for parameter fitting.*

Input variables required in predictive model	**Experimental results related to model output variables**	**Constants**
Copper concentration in	Copper concentration out	Faraday's Constant
Sulphuric acid concentration in	Sulphuric acid concentration out	Universal Gas Constant
Iron concentration	Mass plated	Standard reduction potentials of all species
Total cell voltage	Current	
Hardware resistance		Number of electrons involved in each electrochemical reaction
Number of cathodes		
Electrolyte flowrate		
Electrode surface area		Molar masses of all species
Cell temperature		
Interelectrode spacing		
Plating time		

Some preliminary calculations were conducted as in the predictive model (see *Chapter 3 Model Development*), including density and conductivity correlations, electrolytic resistances, species activities and reduction potentials using the Nernst equation. In addition, the hardware resistance of the bench-scale electrowinning cell was calculated as the average resistance of the hardware across all experiments.

4.3.3 Current Loss Parameter

The first parameter that was fit was the current loss parameter, which would account for any side reactions due to impurities in the water, ineffective electrode contact and stray currents. The current loss parameter

was calculated as the average loss in current for any reasons other than that of the iron reactions, by considering the current efficiencies pertaining to the experiments containing no iron (control experiments).

Specifically, the current used in the copper plating reaction was calculated from the mass of copper that was plated in the given time using Faraday's Law. This copper plating current was subtracted from the total current in the 8 control experiments to find the current loss, and the average current loss across all control experiments made up the current loss parameter. This calculation of the current loss parameter is provided in Equation 47.

$$I_{loss} = \frac{\sum_{j=1}^{n}\left(I_{total,j} - I_{Cu,j}\right)_{Fe=0}}{n} \quad [47]$$

Where j = Arbitrary experiment j

n = Sample size

4.3.4 Parameters Associated with Copper Reduction

In the original electrowinning model, both reaction kinetics (by the extended Butler-Volmer equation) and diffusion equations were present in the determination of copper reduction rate, as an initial premise based on the model by Aminian *et al.* (2000). However, other sources in the literature attest that copper reduction in electrowinning systems is primarily governed by reaction kinetics and that mass transfer effects could be neglected (Beukes and Badenhorst, 2009; Moats and Khouraibchia, 2009). One of the model assumptions was that operation was below the limiting current density for copper, and therefore the standard Butler-Volmer equation could be used for modelling without considering mass transfer effects (Bard and Faulkner, 2001). The assumption of operation under limiting current density was verified from the experimental results and it was found that the copper concentration did not have a significant effect on the mass plated (see *Chapter 5 Results and Discussion*). Therefore, the parameters that were fit were the exchange current density (i_0) and charge transfer coefficient (α) that form part of the standard Butler-Volmer equation.

After the initial variables had been defined, preliminary calculations performed and cathodic voltage drop and overpotentials determined for each electrowinning experiment, the parameters could be fit to a modified version of the Butler-Volmer equation. Equation 48 shows the Butler-Volmer equation modified using Faraday's Law to calculate the mass of copper plated, based off the general form provided in Equation 14. The measured mass of copper plated during each experiment was compared to the mass predicted at each overpotential using Equation 48, and the parameters fitted through a nonlinear regression (performed using MATLAB's 'fitnlm' function). The absolute value is used, as the convention for cathodic current density is negative, but this is not practical when calculating mass.

$$m_{Cu} = \left|\frac{M_{Cu}t}{n_{Cu}F} A\, i_{0,Cu}\left[\exp\left(\frac{-\alpha_{Cu}nF}{RT}\eta_c\right) - \exp\left(\frac{(1^*-\alpha_{Cu})nF}{RT}\eta_c\right)\right]\right| \quad [48]$$

Where m_{Cu} = Mass of copper plated per cathode side (g)

After the best fitting parameters had been determined, checks were conducted to ensure that the exchange current density was positive, and charge transfer coefficient was between 0 and 2. The experimental results were plotted on the model graph, and model fit statistics generated.

4.3.5 Parameters Associated with Water Oxidation

The parameters associated with the oxidation of water were the exchange current density and charge transfer coefficients in the standard Butler-Volmer equation. Similar to the argument for copper reduction, it was assumed that the water oxidation reaction operated below the limiting current density, and was found that the concentration of sulphuric acid had an insignificant effect on the reaction rate. Therefore, the mass transfer reaction was excluded from parameter fitting.

The mass of water that reacted per anode side was calculated from the difference in concentration in sulphuric acid from before and after each electrowinning experiment, and the stoichiometry of the water oxidation equation (Equation 49).

$$m_{H_2O,j} = \frac{\left[\left(\Delta x_{H_2SO_4,j}\right)V\frac{M_{H_2O}}{M_{H_2SO_4}}\right]}{number\ of\ anode\ faces} \quad [49]$$

Where $m_{H_2O,j}$ = Mass of water that was oxidised per anode side, for arbitrary experiment j (g)

$\Delta x_{H_2SO_4}$ = Change in sulphuric acid concentration (g/l)

V = Electrolyte volume (g/l)

M = Molar mass (g/mol)

After the anodic voltage drop had been calculated, the mass of water that had reacted in each experiment was calibrated to the mass predicted from the Butler-Volmer equation modified using Faraday's Law (Equation 50). The parameters were determined using a nonlinear regression (MATLAB's 'fitnlm' function), after which the results were plotted and parameter fit statistics generated. Checks were conducted to ensure that the exchange current density was positive, and charge transfer coefficient fell between 0 and 1.

$$m_{H_2O} = \frac{M_{H_2O}\,t}{n_H F} A\, i_{0,H_2O}\left[\exp\left(\frac{-\alpha_{H_2O}nF}{RT}\eta_a\right) - \exp\left(\frac{(1^*-\alpha_{H_2O})nF}{RT}\eta_a\right)\right] \quad [50]$$

4.3.6 Parameters Associated with Iron Reduction and Oxidation

The iron reduction and oxidation reactions occur above the respective limiting current density, therefore mass transfer effects limit the rate kinetics (Aminian *et al.*, 2000; Beukes and Badenhorst, 2009; Moats and Khouraibchia, 2009). From the electrowinning experiments, it was observed that the concentration of iron

had a significant impact on the reaction rate (it would not have done so if the kinetics were reaction rate limited). A similar approach to parameter fitting was employed for both the reduction and oxidation of iron, though these were investigated separately.

The mass transfer and rate kinetics parameters for iron reduction and oxidation comprised only the experiments in which iron was present. The currents associated with the iron reduction and oxidation for an arbitrary experiment, *j*, were calculated using Equations 51 and 52 respectively, by subtracting the current utilised in the major redox reaction and current loss parameter.

$$I_{Fe,red,j} = I_{total,j} - I_{Cu,j} - I_{loss} \quad [51]$$

$$I_{Fe,ox,j} = I_{total,j} - I_{H_2O,j} - I_{loss} \quad [52]$$

Thereafter, the current associated with the relevant experimental iron redox reaction was translated into a current density. The parameter fitting included finding, for reduction and oxidation scenarios, the exchange current density and charge transfer coefficients which were fit to the extended Butler-Volmer equation from Equation 15 of *Chapter 2 Literature Review*. Mass transfer coefficients were fit to the diffusion equations for the relevant species to and from each electrode. Equations 53 to 55 indicate the equations used in the fitting of parameters for iron reduction, and Equations 56 to 58 relate to iron oxidation. The parameter fitting was performed by rearranging the diffusion equations to solve for the surface concentrations, and subsequently substituting the surface concentration into the extended Butler-Volmer equation. The 'fitnlm' MATLAB function was applied to fit the parameters using a nonlinear regression.

Reduction: $i_{Fe^{3+},red} = i_{0,Fe^{3+},red}\left[\frac{C_{Fe^{2+},s}}{C_{Fe^{2+}}}\exp\left(\frac{-\alpha_{Fe^{3+},red}nF}{RT}\eta_a\right) - \frac{C_{Fe^{3+},s}}{C_{Fe^{3+}}}\exp\left(\frac{(1^*-\alpha_{Fe^{3+},red})nF}{RT}\eta_a\right)\right]$ [53]

Diffusion to cathode: $i_{Fe^{3+},red} = m_{Fe^{3+},red}(C_{Fe^{3+}} - C_{Fe^{3+},cathode\ surface})$ [54]

Diffusion away from cathode: $i_{Fe^{2+},red} = m_{Fe^{2+},red}(C_{Fe^{2+},cathode\ surface} - C_{Fe^{2+}})$ [55]

Oxidation: $i_{Fe^{2+},ox} = i_{0,Fe^{2+},ox}\left[\frac{C_{Fe^{2+},s}}{C_{Fe^{2+}}}\exp\left(\frac{-\alpha_{Fe^{2+},ox}nF}{RT}\eta_a\right) - \frac{C_{Fe^{3+},s}}{C_{Fe^{3+}}}\exp\left(\frac{(1^*-\alpha_{Fe^{2+},ox})nF}{RT}\eta_a\right)\right]$ [56]

Diffusion to anode: $i_{Fe^{2+},ox} = m_{Fe^{2+},ox}(C_{Fe^{2+}} - C_{Fe^{2+},anode\ surface})$ [57]

Diffusion away from anode: $i_{Fe^{3+},ox} = m_{Fe^{3+},ox}(C_{Fe^{3+},anode\ surface} - C_{Fe^{3+}})$ [58]

4.4 Summary

The fitting of parameters for reaction rates and current loss in the electrowinning model was completed by devising a set of bench-scale experiments and creating a parameter fitting code in MATLAB, accomplishing the second and third objectives of this research. Variables tested in the laboratory electrowinning cell were the copper concentration, sulphuric acid concentration, iron concentration and current density. Measurements taken as part of the electrowinning experiments were the mass of copper plated, changes in

copper and sulphuric acid concentration, hardware resistance and average cell voltage. These measured results were used in the parameter fitting code to calibrate to the predictive model. *Table 4.5* provides an overview of the approach to fitting each parameter. Once the best fitting parameters had been determined, they were input back into the electrowinning model to predict electrowinning performance for the laboratory scale electrowinning system. Model validation was performed by comparing the predicted performance and actual performance of the model for bench-scale experiments and data obtained from industrial tankhouses, which is discussed in *Chapter 5 Results and Discussion*.

Table 4.5: *Details on the approach to fitting each model parameter to electrowinning bench-scale data.*

Parameter	Constraint	Parameter fitting details
I_{loss}	n/a	Average difference between total current and current used to plate copper for experiments containing no iron.
$i_{0,Cu}$ α_{Cu}	$i_{0,Cu} > 0$ $0 < \alpha_{Cu} < 2$	Nonlinear regression used to calibrate measured mass of copper plated to that calculated with the Butler-Volmer equation combined with Faraday's Law.
i_{0,H_2O} α_{H_2O}	$i_{0,H_2O} > 0$ $0 < \alpha_{H_2O} < 1$	Nonlinear regression used to calibrate mass of water oxidised (calculated from difference in acid concentration) to that calculated with the Butler-Volmer equation combined with Faraday's Law.
$i_{0,Fe,red}$ $\alpha_{Fe,red}$ $m_{Fe^{3+},red}$ $m_{Fe^{2+},red}$	$i_{0,Fe,red} > 0$ $0 < \alpha_{Fe,red} < 1$ $m_{Fe^{3+},red} > 0$ $m_{Fe^{2+},red} > 0$	Nonlinear regression used to fit mass transfer coefficients for diffusion of ferric ions to the cathode and ferrous ions away from the cathode, and rate parameters associated with the extended Butler-Volmer equation.
$i_{0,Fe,ox}$ $\alpha_{Fe,ox}$ $m_{Fe^{2+},ox}$ $m_{Fe^{3+},ox}$	$i_{0,Fe,ox} > 0$ $0 < \alpha_{Fe,ox} < 1$ $m_{Fe^{2+},ox} > 0$ $m_{Fe^{3+},ox} > 0$	Nonlinear regression used to fit mass transfer coefficients for diffusion of ferrous ions to the anode and ferric ions away from the anode, and rate parameters associated with the extended Butler-Volmer equation.

5

RESULTS AND DISCUSSION

5.1 Introduction

The aim of this research, to develop an electrowinning model to predict process performance, was achieved through the development of a semi-empirical electrowinning model by first principles and a parameter fitting approach. The parameter fitting approach incorporated bench-scale electrowinning experiments and nonlinear regressions. This section evaluates the degree of accuracy of the model and parameter fitting, through comparisons to the bench-scale electrowinning experiments and data obtained from industrial tankhouses (which completes the fourth objective of this research). The development of the electrowinning model required the validation of the conceptual and computerised models, as illustrated in *Figure 5.1* and discussed in the succeeding sections. The parameter fitting approach was validated through comparisons between experimental data and model outputs. The application and limitations of the electrowinning model and parameter fitting approach in an industrial tankhouse are discussed. All experimental and parameter fitting data, statistical analyses thereof and plots of residuals are provided in *Appendix C Experimental and Model Results.*

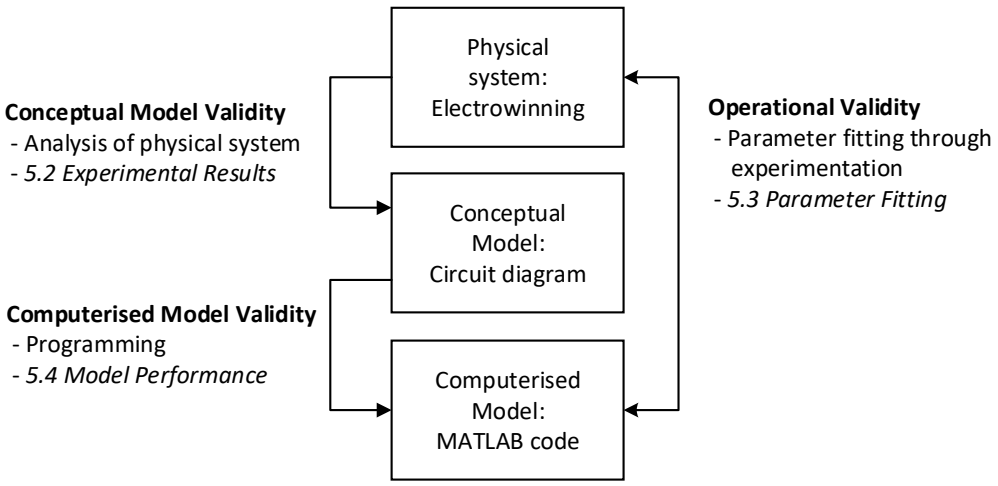

Figure 5.1: *Overview of the electrowinning model development process and validity criteria which will be evaluated.*

5.2 Experimental Results

5.2.1 Hardware Resistance

The physical electrowinning bench-scale system and experimental data was analysed to validate assumptions used in the model and determine input variables such as the hardware resistance, and output performance

variables. Hardware resistance affects the energy utilisation and performance of the model and differs between electrowinning setups. The hardware resistance across the anodic connections, cathodic connections and other losses for each bench-scale electrowinning experiment are shown in *Figure 5.2*. 'Other' resistance refers to additional differences between the reading on the power source and electrode plates and could be explained by internal rectifier resistance or contact between the hanger bars and electrodes. Hardware resistance should remain constant throughout all experiments, and the average value of 0.042 Ω was used as the model input value for the bench-scale experiments. Slight fluctuations in the cathodic resistance may be due to changes due to the bolted connection between the wire and hanger bar with each experiment, and fluctuations in the other resistance due to the sensitivity of the power source reading (especially at the low current densities of 100 A/m^2). Overall, however, the resistance remained relatively constant, as noted from the plots of residuals which are provided in *Appendix C Experimental and Model Results*.

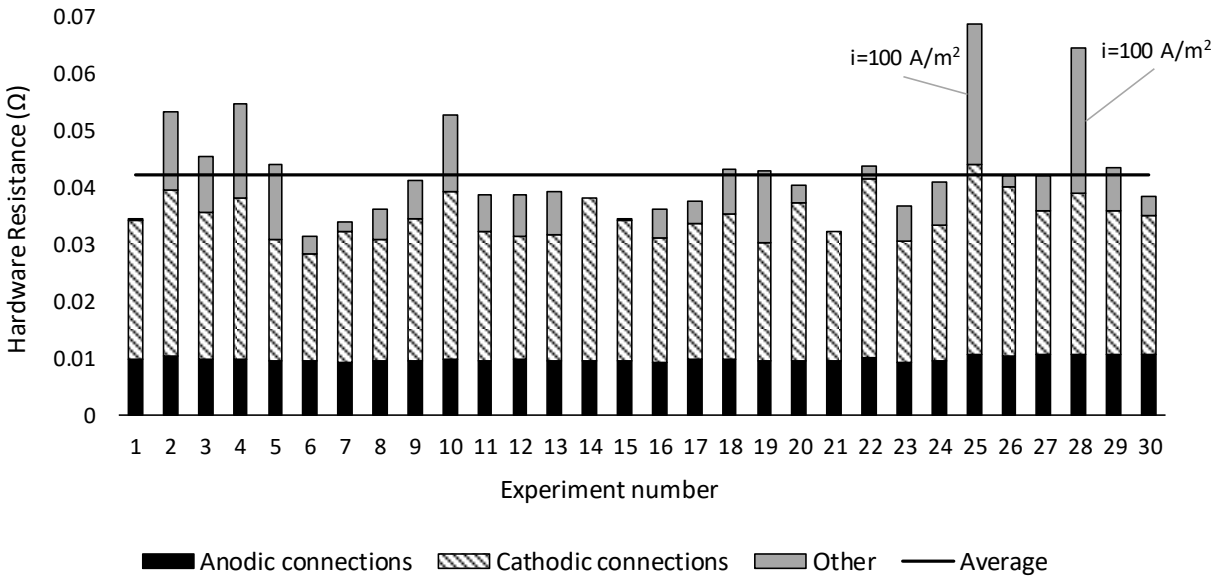

Figure 5.2: *Anodic, cathodic and other hardware resistances measured for each bench-scale electrowinning experiment.*

5.2.2 Plating Rate Experiments

A major assumption used in the electrowinning model was that the system was at steady state, and therefore that the rate of copper plating did not change with time. The steady state assumption was validated by measuring the cumulative mass of copper that had plated over time for two separate experiments to ensure repeatability, the averages of which are displayed in *Figure 5.3*. The mass of copper plated is linear over time, with a linear fit of R^2 equal to 0.999 confirming a constant plating rate. A hypothesis test at a 95% confidence level indicated that one cannot reject the null hypothesis that the plating rate did not change over time.

Therefore, the steady state assumption can be considered valid, as can the treatment of the copper plating as a 'stream' in the mass balances. This assumption of constant copper plating rate was extended to constant rates of reactions for the other reduction and oxidation reactions as well. The mass of copper plated in each plating rate experiment, comparison between the two plating rates, residual plots and statistical analysis are provided in *Appendix C Experimental and Model Results.*

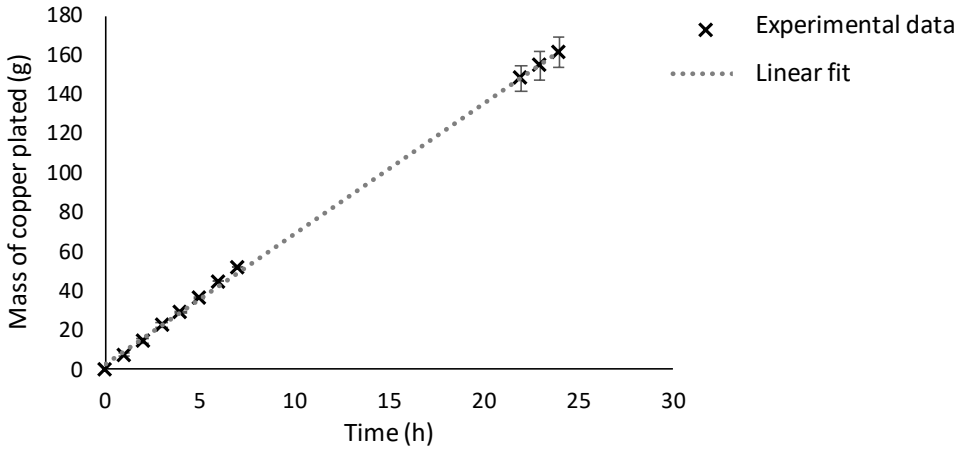

Figure 5.3: *Cumulative mass of copper plated on a cathode over time indicating a constant current density. (Operating conditions included a current density of 200 A/m^2, initial copper concentration of 55 g/l, initial sulphuric acid concentration of 185 g/l and iron concentration of 4 g/l.)*

5.2.3 Effect of Electrolyte Composition

5.2.3.1 Effect of Copper Concentration

The effect of copper concentration on the mass of copper that had plated after 4 hours was considered during the bench-scale electrowinning experiments, and shown in *Figure 5.4*. The mass of copper plated as a function of the copper concentration is provided in *Figure 5.4 (a)* for current densities of ~200 and ~300 A/m^2. It is apparent that for each current density considered, the mass of copper plated had no correlation to the concentration of copper in the electrolyte. The percentage deviation between the copper mass plated and the average copper mass plated at each current density is indicated in *Figure 5.4 (b).* The scatter in percentage deviation values highlight the independence of copper mass plated from the copper concentration. It is noted that the scatter within each of the four groups of data at each specific level of copper concentration and current density would be due to differences in iron and sulphuric acid concentrations and experimental variance. It not important to note any trends within each group of data, but between the groups of ~35 g/l and ~55 g/l copper concentrations at the specific current densities. The independence of copper mass plated from the copper concentration indicated that the copper reduction reaction was strongly reaction rate limited. Therefore, the mass transfer effects of cupric ions could be

ignored in the electrowinning model to eliminate the requirement for a mass transfer coefficient, which is supported by Moats and Khouraibchia (2009) and Beukes and Badenhorst (2009).

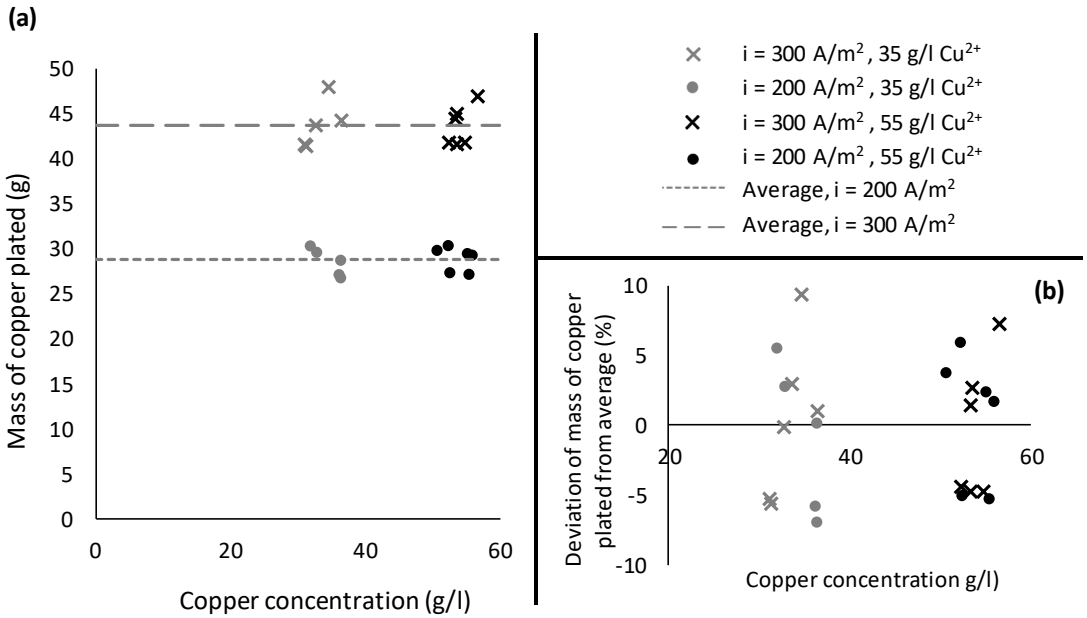

Figure 5.4: *Mass of copper plated as a function of the copper concentration (35 & 55g/l) of the bench-scale experiments at two levels of current density (200 & 300 A/m²)* ***(a)****, and percentage deviations from the average mass* ***(b)****.*

5.2.3.2 Effect of Sulphuric Acid Concentration

The effect of the sulphuric acid concentration on the kinetics of the anodic reaction was investigated at two levels of current density (~200 and ~300 A/m²) and provided in *Figure 5.5*. Water and sulphuric acid are related through the anodic reaction where water is oxidised into oxygen bubbles and hydrogen ions which associate with sulphate ions to become sulphuric acid. The mass of water that was oxidised was calculated from the difference in sulphuric acid concentration in the initial and spent electrolyte, as shown in *Appendix A Sample Calculations*. Following a similar argument to the effect of copper concentration on copper reduction kinetics, the sulphuric acid concentration did not appear to influence the mass of water oxidised either. *Figure 5.5 (a)* indicates that the mass of water oxidised was independent on the sulphuric acid concentration at each current density tested. The independence of the mass of water oxidised to the sulphuric acid concentration was observed from *Figure 5.5 (b)* indicating scattered percentage deviations from the average masses plated. Therefore, the reaction was rate limited and mass transfer effects could be ignored, which is supported by Moats and Khouraibchia (2009) and Beukes and Badenhorst (2009).

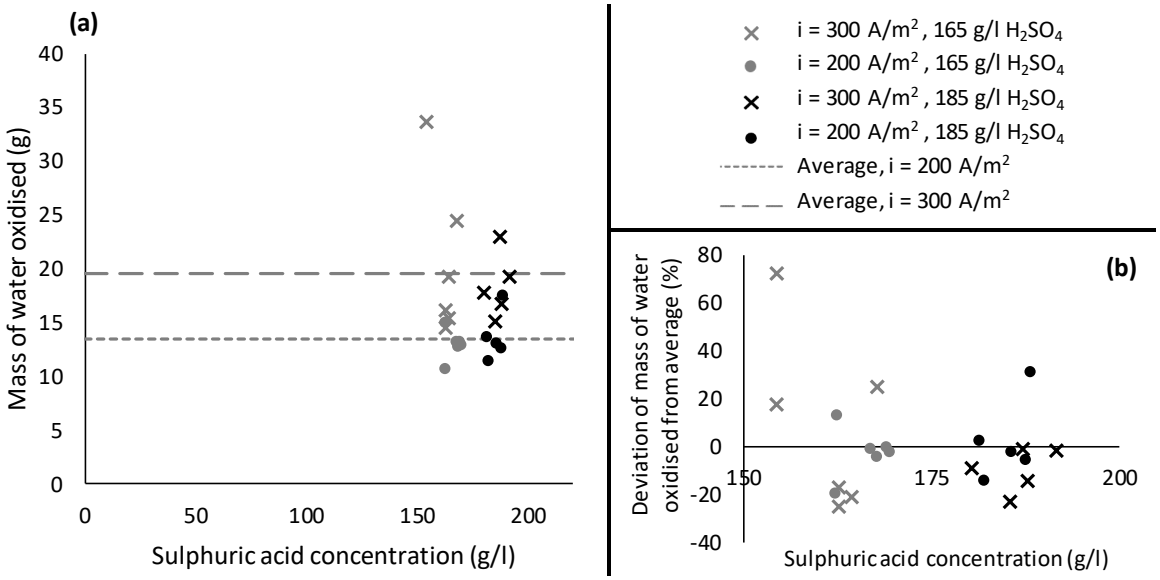

Figure 5.5: *Mass of water oxidised as a function of the sulphuric acid concentration (165 & 185 g/l) of the bench-scale experiments at two levels of current density (200 & 300 A/m^2)* ***(a)****, and percentage deviation from the average mass of water oxidised* ***(b)****.*

5.2.3.3 Effect of Iron Concentration

As part of the parameter fitting approach, the effect of the concentration of iron on the mass of iron reacted (reduced and oxidised) was investigated. Shown in *Figure 5.6 (a)* is the mass of iron reduced as a function of the initial iron concentration at two levels of current density (~200 and ~300 A/m^2), and similar in *Figure 5.6 (b)* for the mass of iron oxidised. It was noted that the concentration of iron affected the mass reacted, with a higher mass of iron reduced and oxidised at a higher concentration of iron in the electrolyte, at both current densities tested. The sum of the current densities of copper and iron reduction must be equal to the sum of the current densities of the water and iron oxidation (see Section *2.4.2 Power Contributions* of *Chapter 2 Literature Review*). The higher mass of iron reduced in comparison to iron oxidised can therefore be attributed to a lower current density utilised in copper reduced than in water oxidation. There is more scatter in the iron oxidation data due to higher deviation in water oxidation data possibly due to the sensitivity of the sulphuric acid measurements.

The major finding from *Figure 5.6* is that the dependence of the quantity of reduced or oxidised iron on the iron concentration indicated that the reactions are strongly mass transfer limited, and that they occurred above the limiting current density for iron. Therefore, the mass transfer modified Butler-Volmer equation and diffusion equation were necessary for parameter fitting, as discussed in *Chapter 4 Parameter Fitting Approach*. The mass transfer dependency of the iron kinetics in electrowinning is supported by Aminian *et al.* (2000) and Moats and Khouraibchia (2009).

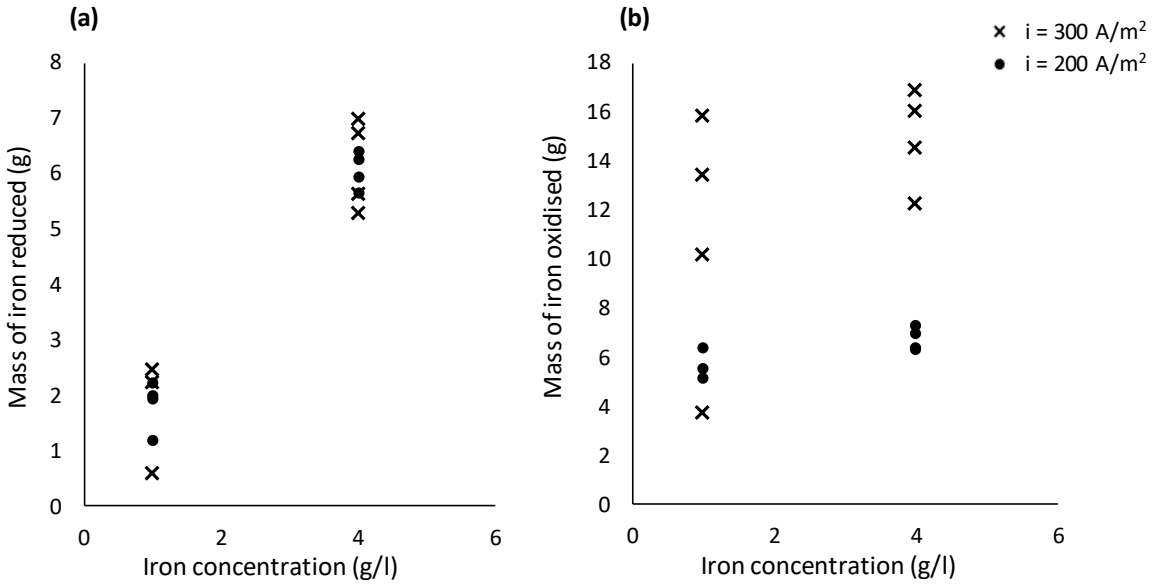

Figure 5.6: *Mass of iron reduced and mass of iron oxidised as a function of the iron concentration in the bench-scale electrowinning experiments, at current densities of 200 and 300 A/m^2.*

5.2.4 Limiting Current Density Test

The independence of the mass of copper plated and water oxidised from the electrolytic copper and sulphuric acid concentrations respectively (discussed in Section *5.2.3 Effect of Electrolyte Composition*) implies that these reactions were operating below the limiting current density at the current densities tested (~200 and ~300 A/m^2). In order to determine whether all current densities tested (from 100 to 600 A/m^2) were below the limiting current density, and therefore that mass transfer effects could be neglected, the mass of copper plated was plotted as a function of the current density, shown in *Figure 5.7*. A linear relationship was observed from the figure, meaning the assumption that operation was below the limiting current density was valid. The data points for each current density tested were grouped together (because the different copper concentrations tested did not affect the mass of copper plated) with the error bars showing the uncertainty. The linear relationship between the mass of copper plated and the current density represents Faraday's Law.

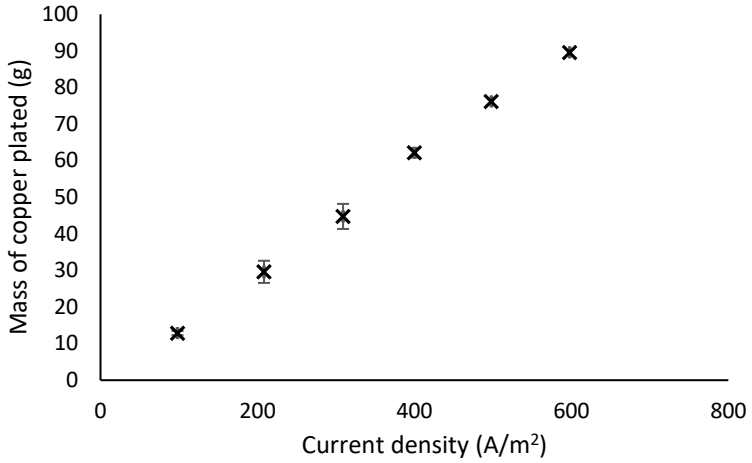

Figure 5.7: *Mass of copper plated at different levels of current density, with grouped data points from the bench-scale electrowinning experiments.*

5.3 Parameter Fitting

5.3.1 Current Loss Parameter

The current loss parameter for the bench-scale electrowinning experiments was estimated as the average loss in current for each of the control experiments without the presence of iron. Equation 43 from *Chapter 3 Model Development* indicates how the current loss was incorporated into the model to find a total scaled up current, by adding the current loss parameter, I_{loss}, to the effective current (that used in copper plating). Current loss is plotted against the total current in *Figure 5.8*, with the associated data and residual plots provided in *Appendix C Experimental and Model Results*. The current loss is independent from the total current, and is a random reflection of stray currents, insufficient electrode contacts or side reactions that may have occurred in each electrowinning experiment. The value of the current loss parameter is 0.145 A, which made up between 0.85 % and 4.5 % of the total current. It is noted that the current loss is specific to, and needs to be estimated for, each electrowinning system to which the model is applied.

$$I_{scale\ up} = I_{effective} + I_{loss} \qquad [43]$$

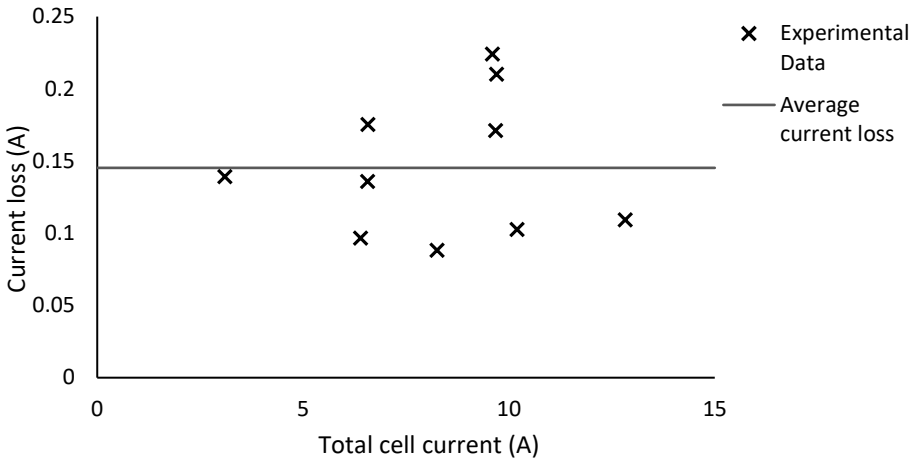

Figure 5.8: *Current loss versus total cell current for the electrowinning experiments, the average of which is the current loss parameter.*

5.3.2 Parameters Associated with Copper Reduction

The Butler-Volmer equation, Equation 14 of *Chapter 2 Literature Review*, was used to model the reduction of copper by calculating the current density as a function of the overpotential. The Butler-Volmer equation specific to copper reduction in displayed in Equation 59 and incorporates the parameters of exchange current density ($i_{0,Cu}$) and charge transfer coefficient (α_{Cu}). Sufficient mass transfer of cupric ions occurred such that the mass transfer limitation to kinetics was considered negligible and therefore a mass transfer coefficient was unnecessary (Section *5.2.3 Effect of Electrolyte Composition*).

$$i_{Cu} = i_{0,Cu}\left[\exp\left(\frac{-\alpha_{Cu}n_{Cu}F}{RT}\eta\right) - \exp\left(\frac{(1^{*}-\alpha_{Cu})n_{Cu}F}{RT}\eta\right)\right] \quad [59]$$

The model was calibrated to the data generated from the bench-scale electrowinning experiments using a nonlinear regression to find the best fitting parameters. The model for the determination of current density for copper reduction from the overpotential is presented in *Figure 5.9* together with the experimental data points used in its calibration. The cathode (where the copper plating occurs) is the negative electrode, and the experimental data and model indicate that the more negative the overpotential, the higher the current density for copper reduction and therefore the mass plated. The experimental data includes all electrolyte compositions, because it was found that changes in electrolyte composition do not affect the kinetics for copper reduction. The scatter between experimental data points may however be due to slight differences in composition and experimental error.

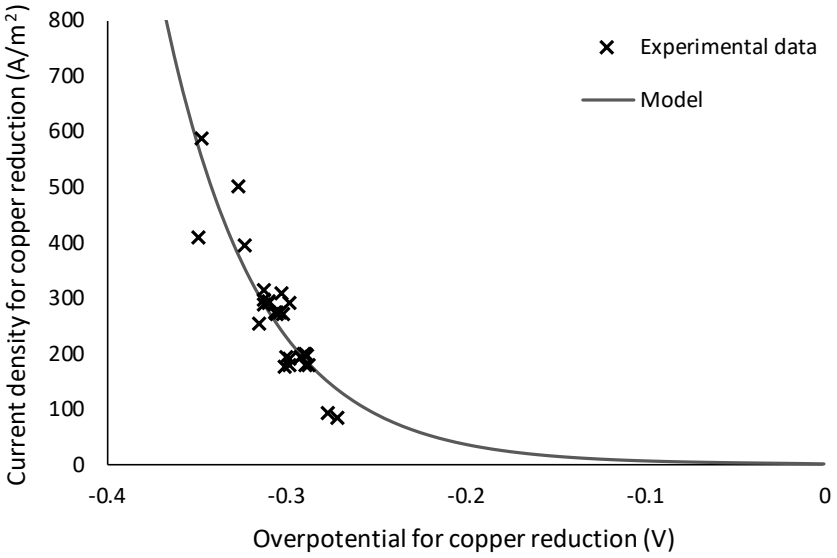

Figure 5.9: *Current density for copper reduction as a function of the overpotential, showing the Butler-Volmer model calibrated to the experimental data points by the best fitting parameters.*

The best fitting value of the exchange current density was determined to be 8.39 x 10^{-5} A/cm^2, with a charge transfer coefficient of 0.256. The model fit with an R^2 of 0.869 and adjusted R^2 of 0.864, indicating a relatively good fit. The parameters fall into the typical ranges suggested by Newman and Thomas-Alyea (2004), that the exchange current density could fall anywhere from less than 10^{-7} mA/cm^2 to over 1 mA/cm^2, and the charge transfer coefficient between 0.2 and 2. These parameter ranges are large, which explains why the parameters found in this research vary from those found by Aminian *et al.* (2000) for their electrowinning model. The values found by Aminian *et al.* were an exchange current density of 2.3x10^{-3} A/cm^2 and alpha value of 0.62 in their basic fit of parameters. The residuals for the model compared to the experimental data illustrated a heteroscedastic distribution, and therefore a weighted nonlinear regression was used. All model data and residuals are provided in *Appendix C Experimental and Model Results.*

The 95% confidence and prediction bands that accompany the copper kinetics model were determined in MATLAB. The confidence and prediction intervals are specific to the range of experimental data that was captured in the model and are illustrated in *Figure 5.10*. It was implied that at a 95% level of confidence, the results of a single additional experiment would fall in the prediction interval, and that the mean of additional experimental results would fall in the confidence interval. The relatively tight confidence interval, and the fact that majority of the experimental data fell into the prediction interval, indicate a good model fit.

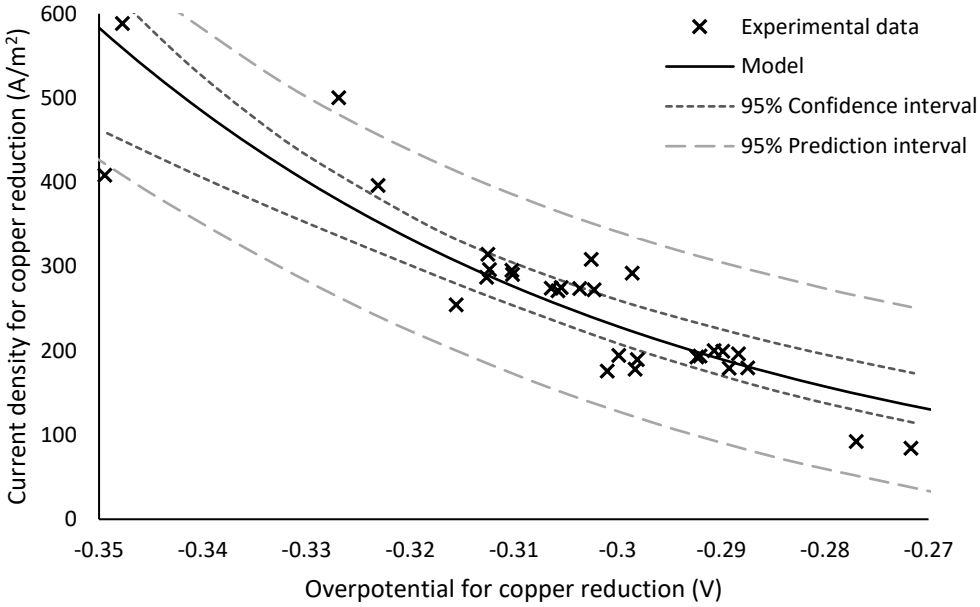

Figure 5.10: *95% confidence and prediction intervals for the Butler-Volmer equation for copper reduction, over the range of experimental data points.*

5.3.3 Parameters Associated with Water Oxidation

The parameters associated with the oxidation kinetics of water to hydrogen ions and oxygen gas were found using a nonlinear regression in a similar manner to that of the copper reduction parameters. The Butler-Volmer equation (Equation 14) applied to water oxidation is provided in Equation 60, with the relevant parameters of the exchange current density (i_{0,H_2O}) and charge transfer coefficient (α_{H_2O}). Once again, the mass transfer coefficient was neglected because operation was below the limiting current density and the concentration of sulphuric acid did not affect the mass of water that evolved.

$$i_{H_2O} = i_{0,H_2O}\left[\exp\left(\frac{-\alpha_{H_2O} n_{H_2O} F}{RT}\eta\right) - \exp\left(\frac{(1^* - \alpha_{H_2O}) n_{H_2O} F}{RT}\eta\right)\right] \quad [60]$$

The current density for water oxidation was plotted as a function of the overpotential in *Figure 5.11*, showing the model and the experimental data to which it was calibrated. The anode, where the oxidation of water occurred, was the positive electrode, and the more positive the overpotential, the higher the current density and therefore mass of water oxidised. The best fitting exchange current density for the bench-scale electrowinning experiments had a value of 1.05×10^{-5} A/cm^2, and the charge transfer coefficient had a value of 0.573. The model fit to the data with an R^2 of 0.748 and adjusted R^2 of 0.739, indicating that the model fit relatively well.

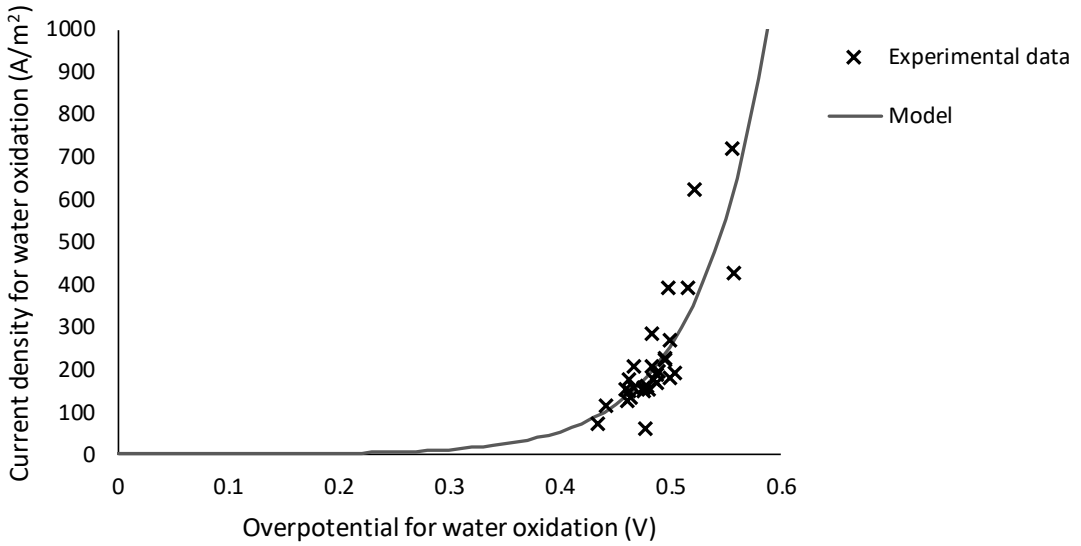

Figure 5.11: *Current density for water oxidation as a function of the overpotential, showing the Butler-Volmer model calibrated to the experimental data points by the best fitting parameters.*

The confidence and prediction bands at a 95% level of significance are specific to the range of experimental data captured, and are plotted in *Figure 5.12*. The relatively tight confidence and prediction intervals indicate that the model encapsulated the experimental data well. All model data and residuals comparing the model and experiments are provided in *Appendix C Experimental and Model Results.*

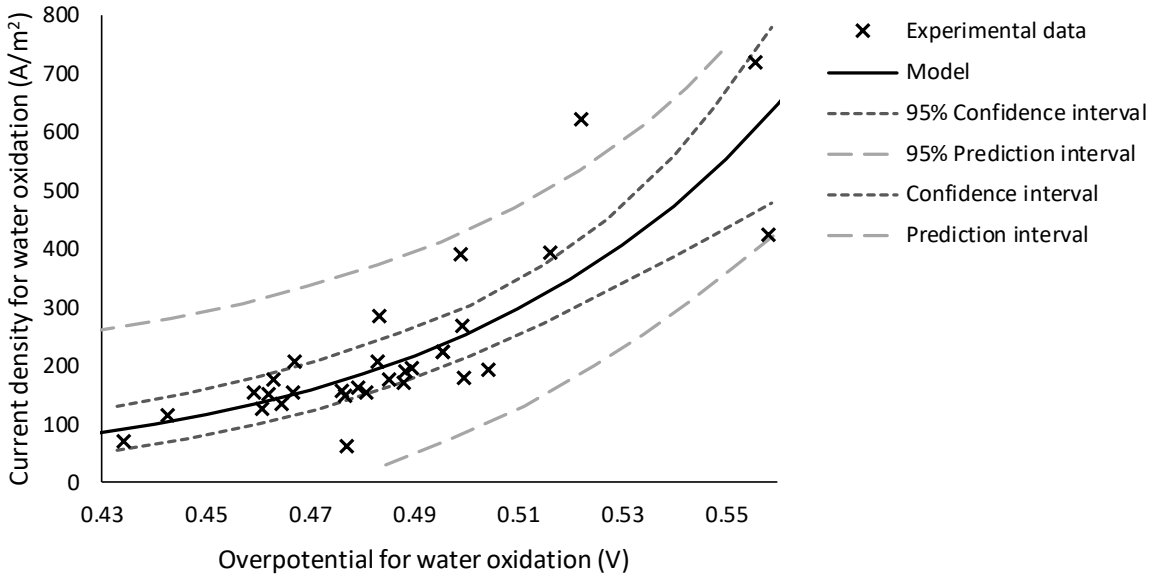

Figure 5.12: *95% confidence and prediction intervals for the Butler-Volmer equation for water oxidation, over the range of experimental data points.*

5.3.4 Parameters Associated with Iron Reduction

The kinetics for the reduction of iron comprised of both mass transfer and reaction kinetics, because the reduction of iron occurred above its limiting current density and it was found that the concentration of iron had an effect on the mass of iron reduced (Section *5.2.3.3 Effect of Iron Concentration*). The iron reduction kinetics were determined using the Butler-Volmer Equation incorporating mass transfer (Equation 15 from *Chapter 2 Literature Review*). The Butler-Volmer equation specific to iron reduction is provided in Equation 53 introduced in *Chapter 4 Parameter Fitting Approach*, including the parameters of exchange current density ($i_{0,Fe^{3+},red}$) and charge transfer coefficient ($\alpha_{Fe^{3+},red}$). The diffusion of iron was determined using Equation 13 for the approximation of a linear concentration profile in the boundary layer. Equation 61 indicates the diffusion specific to the flux of ferric ions to, or ferrous ions from the electrode, and incorporates the mass transfer coefficients ($m_{Fe^{3+},red}$ and $m_{Fe^{2+},red}$), where *i* in the equation refers to either Fe^{3+} or Fe^{2+}. A multivariate nonlinear regression was used to calibrate the parameters to the model equations, and the resulting Butler-Volmer model and experimental data are plotted in *Figure 5.13*, showing the current density utilised for iron oxidation as a function of the overpotential, at iron concentrations of 1 g/l and 4 g/l.

$$i_{Fe^{3+},red} = i_{0,Fe^{3+},red}\left[C_R \exp\left(\frac{-\alpha_{Fe^{3+},red} n_{Fe} F}{RT}\eta\right) - C_O \exp\left(\frac{\left(1^{*}-\alpha_{Fe^{3+},red}\right) n_{Fe} F}{RT}\eta\right)\right] \quad [53]$$

With $C_R = \frac{C_{Fe^{2+},surface}}{C_{Fe^{2+},bulk}}$ and $C_O = \frac{C_{Fe^{3+},surface}}{C_{Fe^{3+},bulk}}$

$$i_{Fe^{2/3+},red} = m_{i,Fe\ red}\left(C_{i,Fe\ red,bulk} - C_{i,Fe\ red,surface}\right) nFA \quad [61]$$

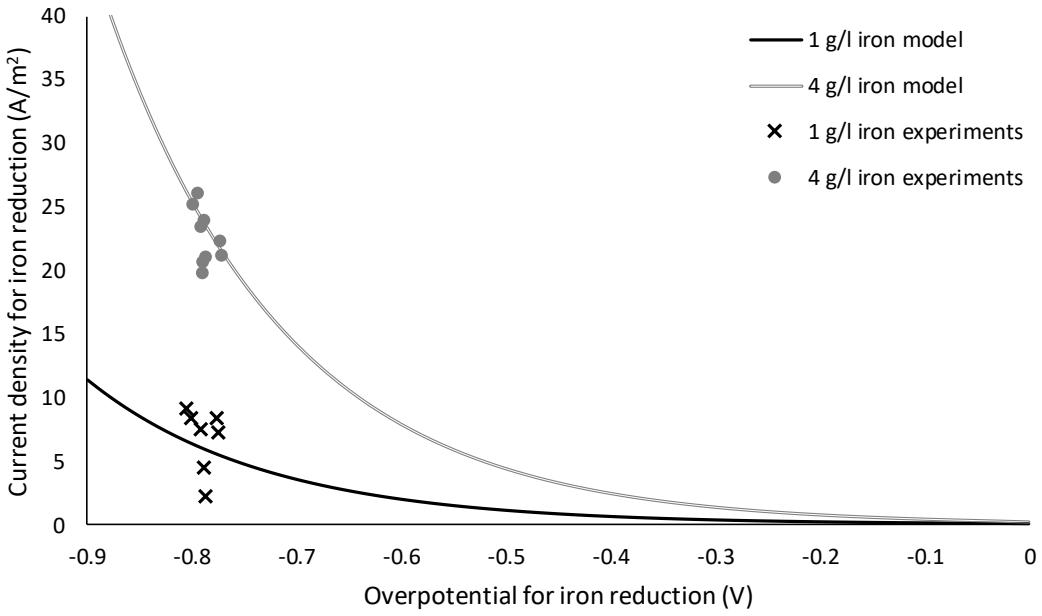

Figure 5.13: *Current density for iron reduction as a function of the overpotential, showing the Butler-Volmer model at two levels of iron concentration.*

The reduction of iron occurred at the negative cathode, and the more negative the overpotential of the cathode, the higher the current density associated with iron reduction and associated mass of iron reduced. The model fit the experimental data relatively well, with an R^2 of 0.741 and adjusted R^2 of 0.724. The value of the exchange current density fit to the bench-scale experiments was 3.81×10^{-4} A/cm^2, charge transfer coefficient was 0.160, mass transfer coefficient for ferric ions ($m_{Fe^{3+},red}$) was 27.9 cm/s, and mass transfer coefficient for ferrous ions ($m_{Fe^{2+},red}$) was 1.46 cm/s.

5.3.5 Parameters Associated with Iron Oxidation

The kinetics for the oxidation of ferrous to ferric ions was treated in a similar manner to that of the iron reduction, using a multivariate nonlinear regression. The equations for the reaction kinetics and diffusion equations associated with the oxidation of iron are provided in Equation 56 from *Chapter 4 Parameter Fitting Approach* and Equation 62. The mass of iron oxidised as a function of the overpotential is provided in *Figure 5.14* for iron concentrations of 1 g/l and 4 g/l, showing the best fitting Butler-Volmer model to the experimental data.

$$i_{Fe^{2+},ox} = i_{0,Fe^{2+},ox}\left[\mathrm{C}_R \exp\left(\frac{-\alpha_{Fe^{2+},ox} n_{Fe} F}{RT}\eta\right) - \mathrm{C}_\mathrm{O} \exp\left(\frac{\left(1^* - \alpha_{Fe^{2+},ox}\right) n_{Fe} F}{RT}\eta\right)\right] \quad [56]$$

With $C_R = \frac{C_{Fe^{2+},surface}}{C_{Fe^{2+},bulk}}$ and $C_O = \frac{C_{Fe^{3+},surface}}{C_{Fe^{3+},bulk}}$

$$i_{Fe^{2/3+},ox} = m_{i,Fe\ ox}\left(C_{i,Fe\ ox,bulk} - C_{i,Fe\ ox,surface}\right) nFA \quad [62]$$

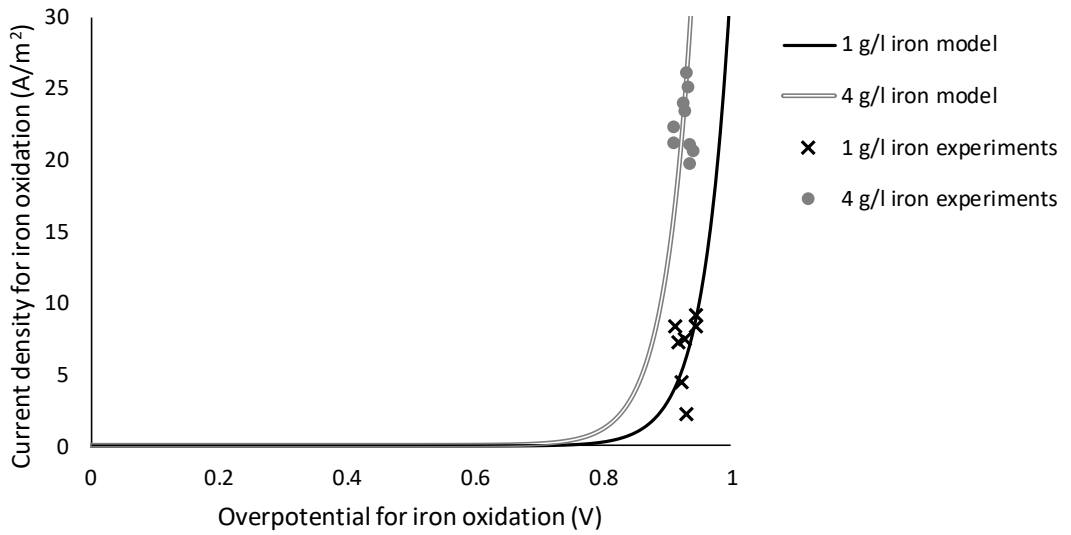

Figure 5.14: *Current density for iron oxidation as a function of the overpotential, showing the Butler-Volmer model at two levels of iron concentration.*

The Butler-Volmer model that predicted the current density for iron oxidation as a function of the current density and iron concentration showed to fit relatively well, with an R^2 of 0.661 and adjusted R^2 of 0.661. The

oxidation of iron occurred at the positive anode, which is why the more positive the overpotential, the higher the current density and associated mass of iron oxidised. The value of the exchange current density fit to the bench-scale experiments was 6.49×10^{-11} A/cm^2, charge transfer coefficient was 0.348, mass transfer coefficient for ferric ions ($m_{Fe^{3+},ox}$) was 1.46 cm/s, and mass transfer coefficient for ferrous ions ($m_{Fe^{2+},ox}$) was 43.2 cm/s.

5.3.6 Parameter Sensitivity Analysis

Sensitivity analyses were conducted to study the effect of altering the parameters on the electrowinning model. The experimentally determined parameters pertaining to the reaction kinetics (exchange current densities and charge transfer coefficients) were independently increased and decreased to investigate their effect on the Butler-Volmer equation and calculated current density for each reduction and oxidation equation. Thereafter, the parameters were input into the original predictive model, and the sensitivity of the performance indicators on changes in the parameters was observed.

Figure 5.15 shows the Butler-Volmer equation for the plating of copper that was best fit to the bench-scale experimental data, with current density for copper reduction as a function of the overpotential. The results of increasing or decreasing the parameters by 20% are illustrated on the graph, and it was observed that the charge transfer coefficient had the largest effect and could potentially alter the kinetics to a large extent. An increase in both parameters provided a model with a steeper gradient, in which higher current densities were obtained at less negative overpotentials, and vice versa for a decrease in both parameters.

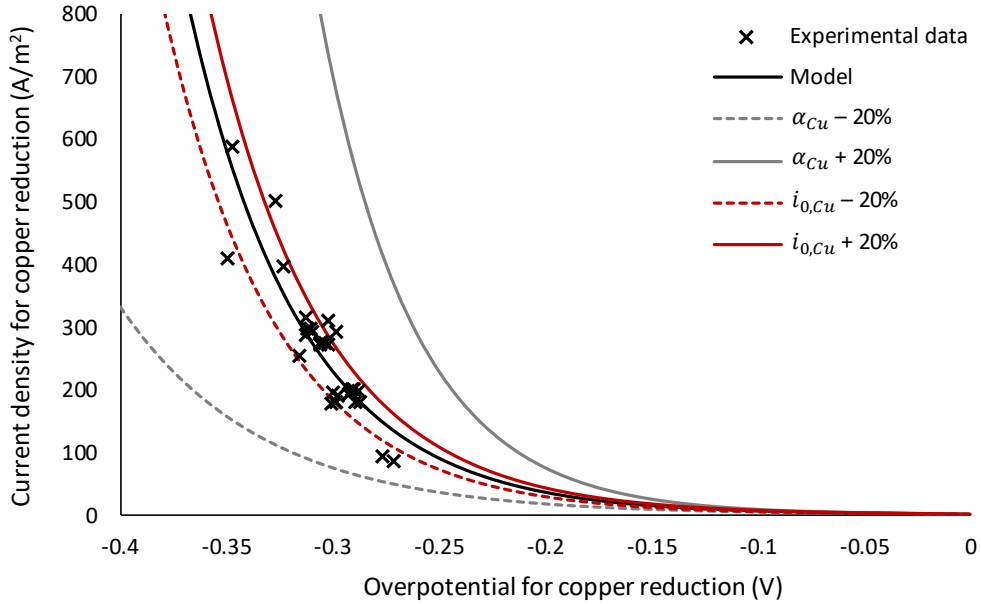

Figure 5.15: *Sensitivity of the copper reduction Butler-Volmer model to changes in its parameters.*

Similarly for the water evolution kinetics, the current density as a function of the overpotential is illustrated in *Figure 5.16* with the model fit to the experimental data and the effect of changes in the parameters. The

model is sensitive to the charge transfer coefficient in particular, while the exchange current density would have to change by a few orders of magnitude if a larger impact on the model was required. For this oxidation reaction, increasing the exchange current density and decreasing the charge transfer coefficient shifted the model such that a higher current density would be obtained from a lower overpotential.

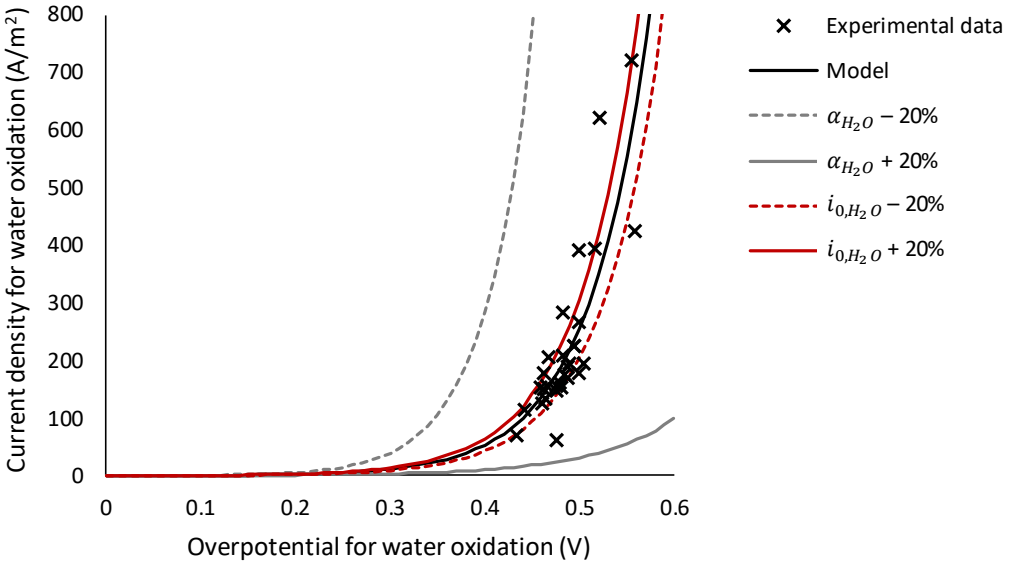

Figure 5.16: *Sensitivity of the Butler-Volmer model for water oxidation rate kinetics to changes in its parameters.*

Similar sensitivity analyses were conducted for the iron reduction (*Figure 5.17*) and iron oxidation (*Figure 5.18*) Butler-Volmer models. The 1 g/l iron model is represented in *Figure 5.18 (a)* and the 4 g/l iron model is represented in *Figure 5.18 (b)* for clarity purposes. The effects of the iron reduction parameter changes mirror those of the copper reduction, and the effects of the iron oxidation parameter changes mirror those of the water oxidation. All changes in the Butler-Volmer model equations due to increases and decreases in associated parameters reflect the theory discussed in Section *2.3.3 Reaction Rate* of *Chapter 2 Literature Review.* It was concluded from the sensitivity analyses that the kinetics were highly sensitive to shifts in the charge transfer coefficients, and therefore if accurate rate kinetics would be required for the model application, the accurate quantification of parameters would be important.

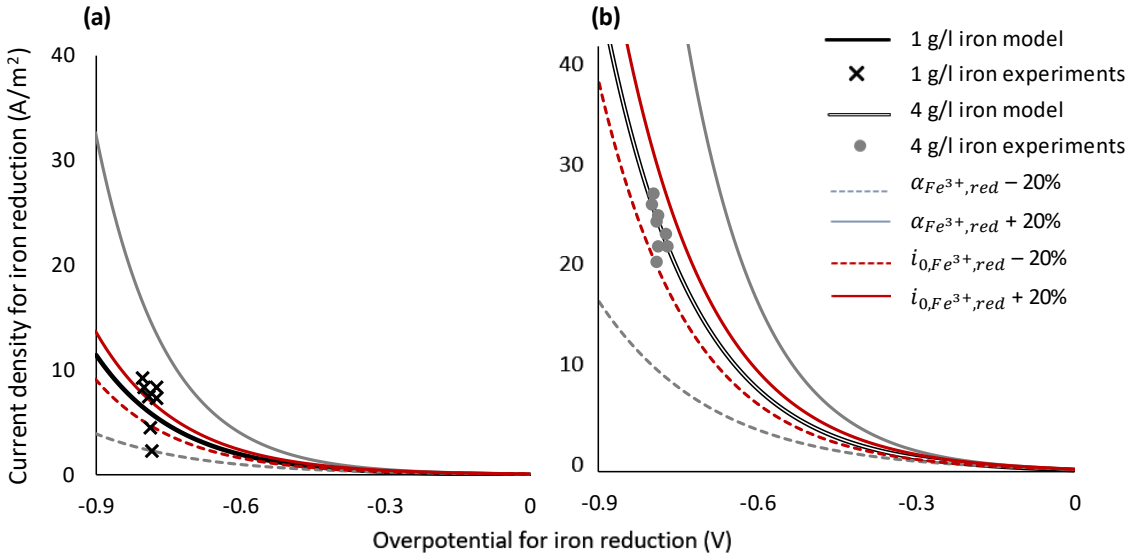

Figure 5.17: *Sensitivity of the Butler-Volmer model for iron reduction rate kinetics to changes in the rate kinetics parameters, at 1 g/l iron* ***(a)*** *and 4 g/l iron* ***(b)****.*

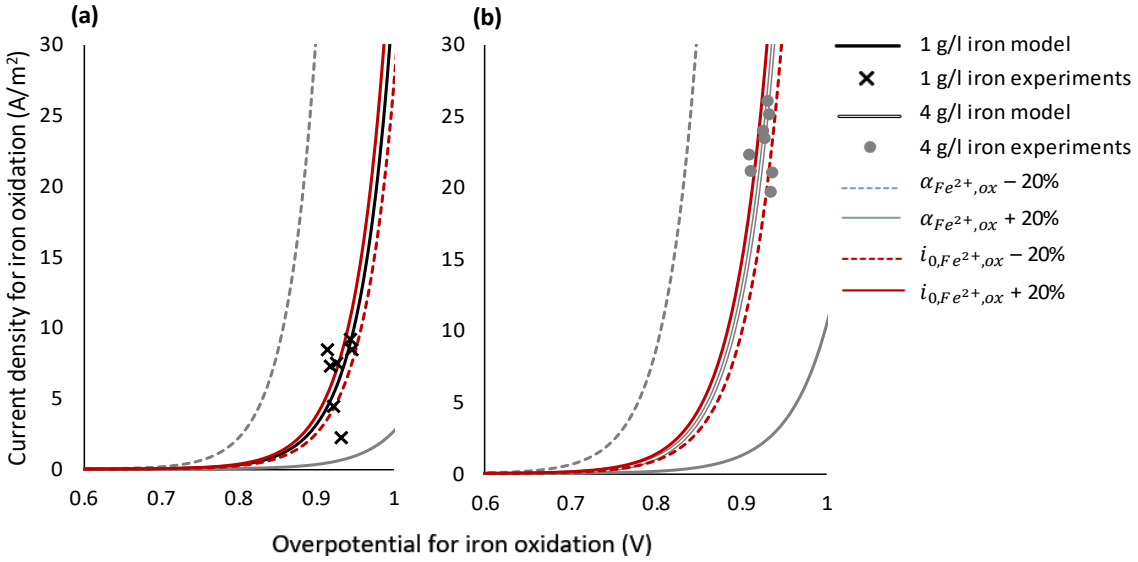

Figure 5.18: *Sensitivity of the Butler-Volmer model for iron oxidation rate kinetics to changes in the rate kinetics parameters, at 1 g/l iron* ***(a)*** *and 4 g/l iron* ***(b)****.*

The experimentally determined model parameters were input into the original electrowinning model, with average experimental input data, and used as a basis for comparison of the sensitivity of performance indicators to changes in parameters. Independent increases and decreases of 20% and 30% on each parameter were conducted, and *Figure 5.19* indicates their effect on the copper plating rate (a), current efficiency (b) and specific energy consumption (c). The copper plating rate was impacted significantly by the copper reduction charge transfer coefficient (α_{Cu}) as noted from *Figure 5.15* above indicating the sensitivity of the isolated model for copper plating current density. When the copper charge coefficient decreased by 30% as indicated on the *Figure 5.19*, it translated to a total decrease in copper plated of 38% less than it

would have been at the original rate. Copper plating rate was sensitive to the water and iron oxidation charge transfer coefficients (α_{H_2O} and $\alpha_{Fe^{2+},ox}$) because oxidation kinetics constrain the current used for copper reduction. In *Figure 5.19* b it was observed that the electrowinning current efficiency was the most sensitive to the charge transfer coefficients for copper and iron reduction (α_{Cu} and $\alpha_{Fe^{3+},red}$), which directly relate to the calculation of the current efficiency. The impact of the charge transfer coefficients on current efficiency is significant, with the potential of decrease from 88.6% current efficiency to 75.6% corresponding to a 30% decrease in the alpha value for copper. It was noted that the current efficiency was much more sensitive to the presence of iron than it was to the current loss parameter for this specific electrowinning system. This being said, the current loss parameter (I_{loss}) is still vital in the calculation of the current efficiency and could change drastically between different electrowinning setups and operations. The sensitivity of the specific energy consumption was similar to that of the current efficiency, with the specific energy consumption increasing by 17% with a 30% decrease in the charge transfer coefficient for copper reduction (α_{Cu}) and 34% increase in specific energy consumption with a 30% increase in alpha for iron reduction ($\alpha_{Fe^{3+},red}$). Overall, the electrowinning model performance was the most sensitive to the charge transfer coefficients of each electrochemical reaction. The remaining parameters would have to be varied to a larger extent to have as high an impact on the model results.

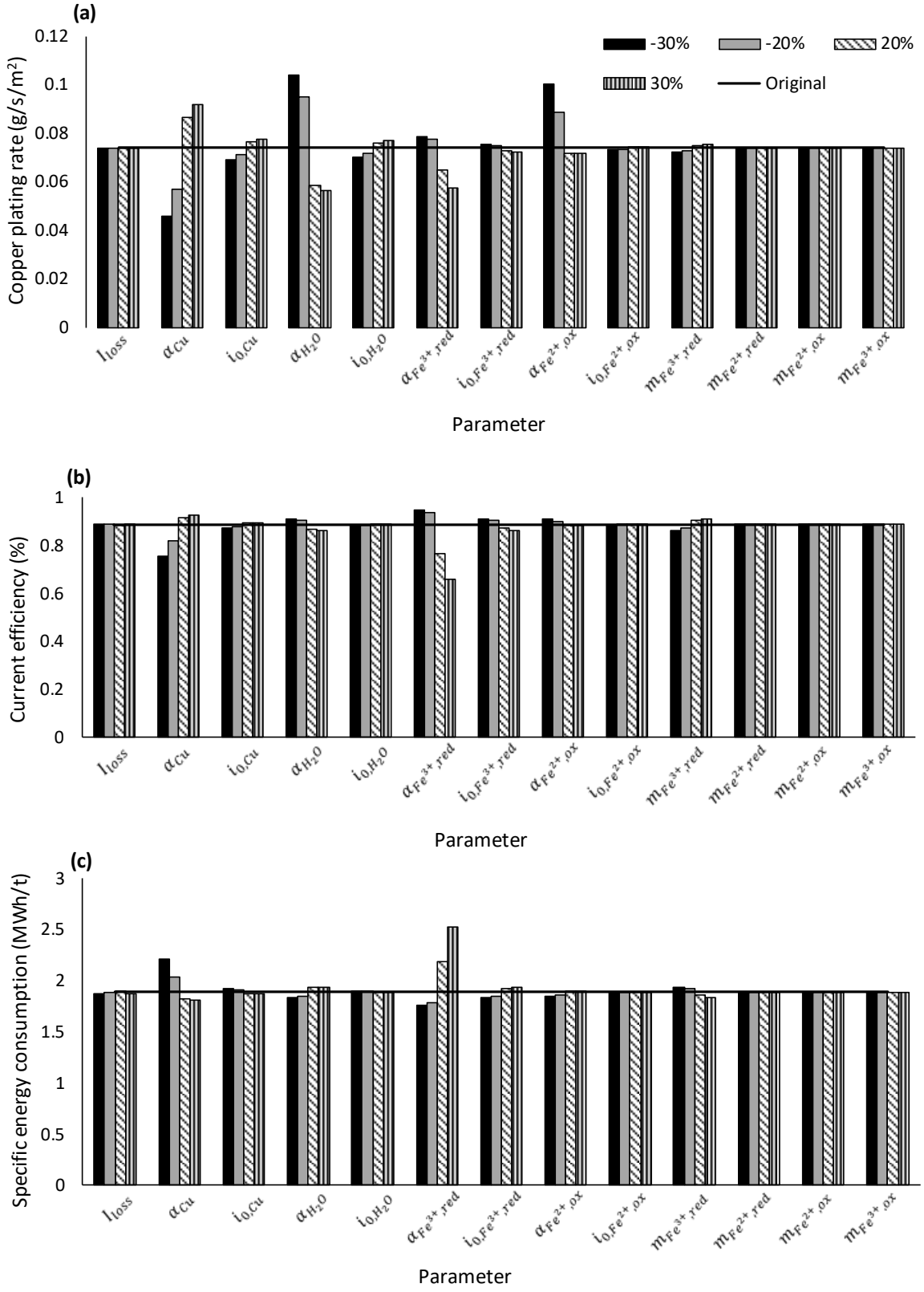

Figure 5.19: *Sensitivity of the copper plating rate* ***(a)****, current efficiency* ***(b)*** *and specific energy consumption* ***(c)*** *to percentage changes in the model parameters.*

5.3.7 Parameter Fitting Applied to Industry Data

The sensitivity analyses of the electrowinning model results, presented in Section *5.3.6 Parameter Sensitivity Analysis* above, highlight the extent that the model kinetics and performance could be altered through variation in the parameters. The variation of the performance of electrowinning tankhouses was illustrated by plotting the average plating rate as a function of the overpotential from 17 plants worldwide (Robinson *et al.*, 2013b) (using the 0.145 A current loss parameter generated from the bench-scale experiments) and comparing to the bench-scale electrowinning experimental data and associated model in *Figure 5.20*. While much of the industrial data lay relatively close to the model, some of the data suggests that on average, the desired copper plating rate would be achieved only at a more negative overpotential, and therefore more energy would have to be supplied to the system. The higher energy requirement for industrial tankhouses could be because the current losses are higher than in the bench-scale setup. In industry, there is less control over contact resistance and short circuits, and more likely to be side reactions and inefficiencies which increase the overpotential requirement. The range of industrial data points highlights the necessity of the fitting of parameters specific to each electrowinning plant.

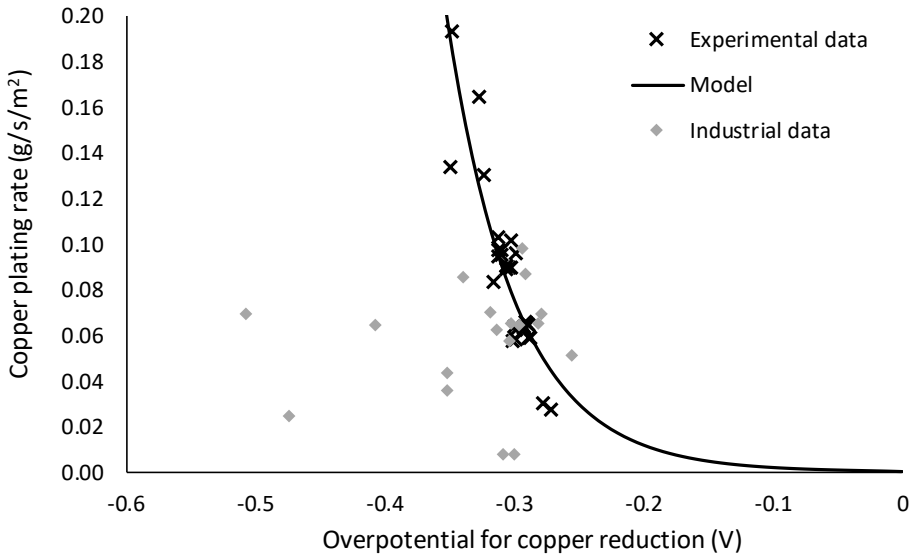

Figure 5.20: *Comparison of industrial operating values to the bench-scale experiment calibrated model for the plating rate of copper per cathode surface area.*

Similarly, the average current density for water oxidation from the global electrowinning tankhouses was compared to the model generated from the bench-scale experiments, in *Figure 5.21*. The spread of industrial data once again shows the variability between plants and the requirement for specific parameters to be fit to each scenario.

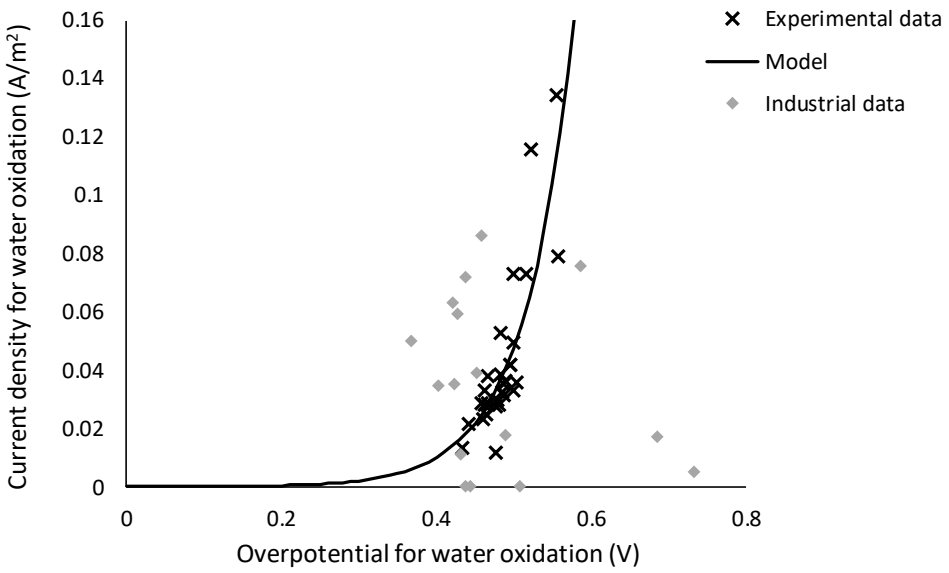

Figure 5.21: *Comparison of industrial operating values to the bench-scale experiment calibrated model for the current density used up in water oxidation.*

5.3.8 Summary of Parameters Fit to Bench-Scale Experiments

The parameters that were fit to the bench-scale electrowinning experiments are summarised in *Table 4.5*, and were found by isolating the reaction kinetics equations from within the model and performing a series of nonlinear regressions. The goodness of fit of the parameters in terms of adjusted R^2 values ranged from 0.661 to 0.864, indicating a relatively high degree of accuracy. All of the exchange current density parameters fall within the range provided by Newman and Thomas-Alyea (2004), between 10^{-7} mA/cm^2 and 1 mA/cm^2. The parameters are specific to the bench-scale electrowinning setup, which is why they differ from those found by Aminian *et al.* (2000) in their basic parameter fit. The wide range of possible parameter values means that each electrowinning system would have to be calibrated to its model for the most accurate prediction of performance. The key performance indicators were the most sensitive to increases and decreases of the charge transfer coefficients, while the remaining parameters would have to be altered by larger percentages in order to have a prominent effect.

Table 5.1: *Summary of the parameters fit to the bench-scale electrowinning experiments.*

Model equation(s)	Parameter	Value	Goodness of fit (R^2_{adj})
Current loss	I_{loss}	0.145 A	n/a
Copper reduction	$i_{0,Cu}$	8.39×10^{-5} A/cm^2	0.864
	α_{Cu}	0.256	
Water oxidation	i_{0,H_2O}	1.05×10^{-5} A/cm^2	0.739
	α_{H_2O}	0.573	
Iron reduction	$i_{0,Fe^{3+},red}$	3.81×10^{-4} A/cm^2	0.724
	$\alpha_{Fe^{3+},red}$	0.160	
	$m_{Fe^{3+},red}$	27.9 cm/s	
	$m_{Fe^{2+},red}$	1.46 cm/s	
Iron oxidation	$i_{0,Fe^{2+},ox}$	6.49×10^{-11} A/cm^2	0.661
	$\alpha_{Fe^{2+},ox}$	0.348	
	$m_{Fe^{2+},ox}$	43.2 cm/s	
	$m_{Fe^{3+},ox}$	1.46 cm/s	

5.4 Model Performance

5.4.1 Actual versus Predicted Electrowinning Performance

The performance of the semi-empirical electrowinning model was evaluated by comparing measured performance indicators of the copper plating rate (which directly correlates to the yield), current efficiency and specific energy consumption. The performance evaluation was completed by first implementing the parameters generated from the bench-scale electrowinning experiments into the original predictive model. Subsequently, the model input information was populated by data from each electrowinning experiment that was utilised for the parameter fitting, electrowinning experiments that were not used in parameter fitting, and average data obtained from electrowinning plants in industry.

The actual (measured) copper plating rate per cathode surface area was compared to the copper plating rate per surface area that was predicted in the electrowinning model, and illustrated in *Figure 5.22*. The additional experiments conducted fall in close proximity to the y=x line, indicating that the model was able to accurately predict the copper plating rate for experiments conducted in the laboratory scale electrowinning cell, within

an average absolute error of 7%. The data points from the tankhouses in industry (Robinson *et al.*, 2013b) are scattered over both sides of the y=x line, with an average absolute error of 22%. The higher error associated with the industrial data is expected, as the parameters are fit specifically to the bench-scale cell and would have to be fit to each specific plant for the most accurate results.

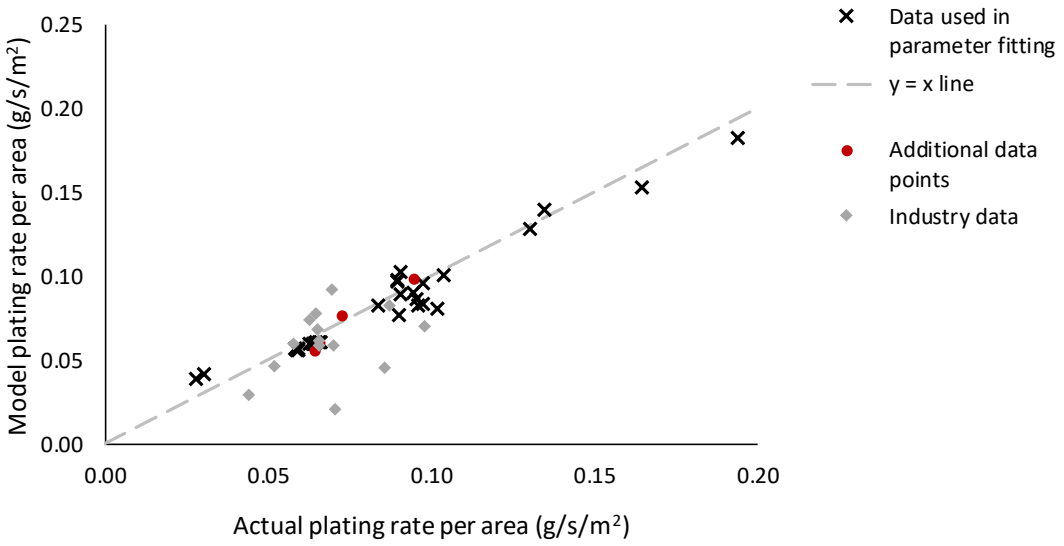

Figure 5.22: *Actual versus predicted copper plating rate for experimental and industrial data.*

The accuracy of the model prediction of current efficiency was evaluated by comparing the model output to the measured result at the same input conditions, and this is depicted in *Figure 5.23*. The electrowinning model predicted the current efficiencies of the additional experiments on the electrowinning cell to a high degree of accuracy, with the model overpredicting the current density by a maximum of 1.0% error, and underpredicting the current efficiency by a maximum error of 5.3%, with an average absolute error of 3.2%. Once again, the average current efficiencies taken from industrial tankhouses are more scattered, and mainly overpredicted by the electrowinning model by up to 21.6%. The model current efficiencies may be higher than the actual values because of the value of the current loss parameter, with more energy likely to be lost to side reactions, stray currents, insufficient electrode contact, short circuits and process inefficiencies in industry. However, the predictive model was still able to predict industrial current efficiencies to a reasonable extent, with an average absolute error of 7.6%.

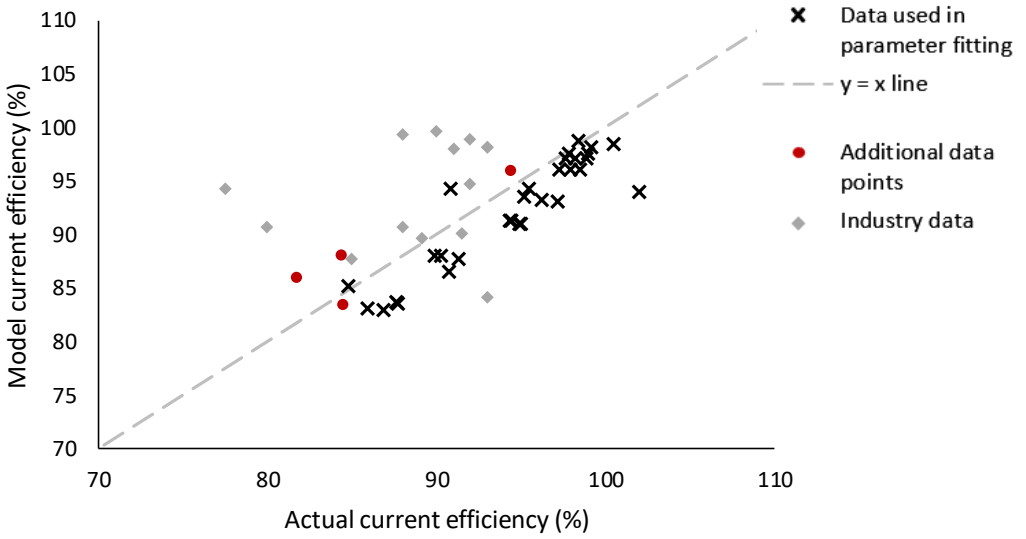

Figure 5.23: *Actual versus predicted current efficiency for experimental and industrial data.*

The final electrowinning performance indicator was the specific energy consumption, and the model prediction thereof is compared to the measured values in *Figure 5.24*. The additional experiments conducted on the bench-scale electrowinning cell indicate that the model can predict specific energy consumption to within an accurate degree, with an average absolute percentage error of 3.0%. The model seemed to underpredict the specific energy consumption of the industrial data somewhat, and this is also noted by the two outliers, but again this could be explained by the current loss parameter that would be higher for industry purposes than in the laboratory scale setup. The maximum deviation of the model from the industrial data had an error of 26.9%, but the average absolute error was 11.3% of the actual specific energy consumption, indicating that the model could still predict industrial specific energy consumption to a large extent.

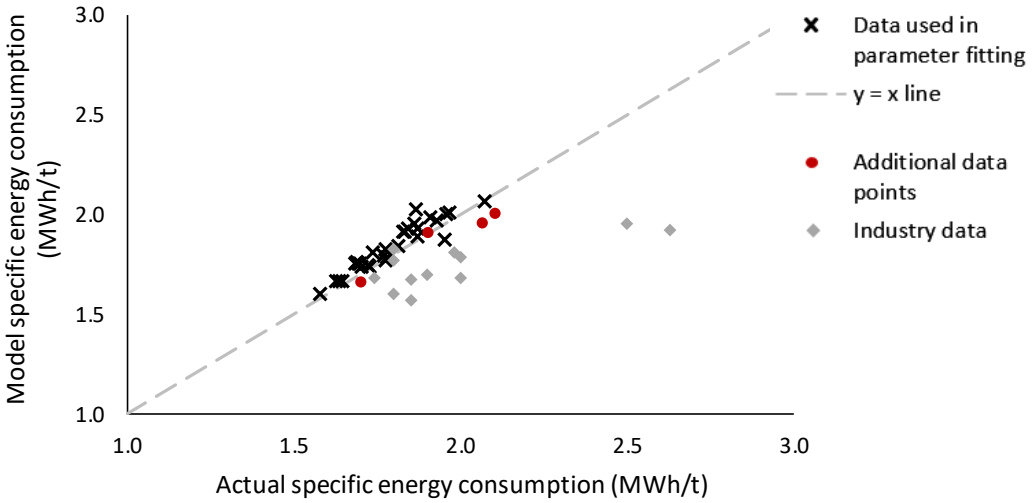

Figure 5.24: *Actual versus predicted specific energy consumption for experimental and industrial data.*

Overall, the electrowinning model with parameters obtained from the bench-scale electrowinning experiments predicted the key performance indicators of the copper plating rate, current efficiency and specific energy consumption to a high degree of accuracy. The performance of industrial electrowinning tankhouses varied, but the model was still able to predict it within a reasonable accuracy. All experimental, industrial and model data values, residual graphs and percentage accuracies, and accuracy evaluations of other process outputs (current density and spent electrolyte composition) are provided in *Appendix C Experimental and Model Results*.

5.4.2 Relationships Between Electrowinning Input and Output Variables

In order to ensure that the model accurately portrayed the physical electrowinning system, validity checks were performed to test the relationships between the input and output variables. Effects of the input variables with the largest impact on the three key performance indicators of the plating rate per area, current efficiency and specific energy are presented in this section.

The first relationship tested was the effect of the voltage applied on the plating rate of copper per area, at two different levels of hardware resistance, as provided in *Figure 5.25*. The range of voltages tested were those reported by Robinson *et al.* (2013b) for industrial tankhouses worldwide. The global averages of the remaining input variables were utilised (see *Table 3.4* of *Chapter 3 Model Development*), with the parameters found from the bench-scale electrowinning experiments conducted in this research. The plating rate of copper increased with an increase in voltage applied to the cell, which can be attributed to an increase in overpotential and hence driving force for the reaction, and this reflects the Butler-Volmer equation. The hardware resistance was vital for the determination of an accurate plating rate, with a higher resistance lowering the reaction rate as some of the potential would be lost to the hardware resistance. Illustrated on *Figure 5.25* is the range and average of typical plating rate per area in industry, from Robinson *et al.* (2013b). The predicted plating rate fell within the typical industrial range depending on the hardware resistance, and this provides an indication of the model validity.

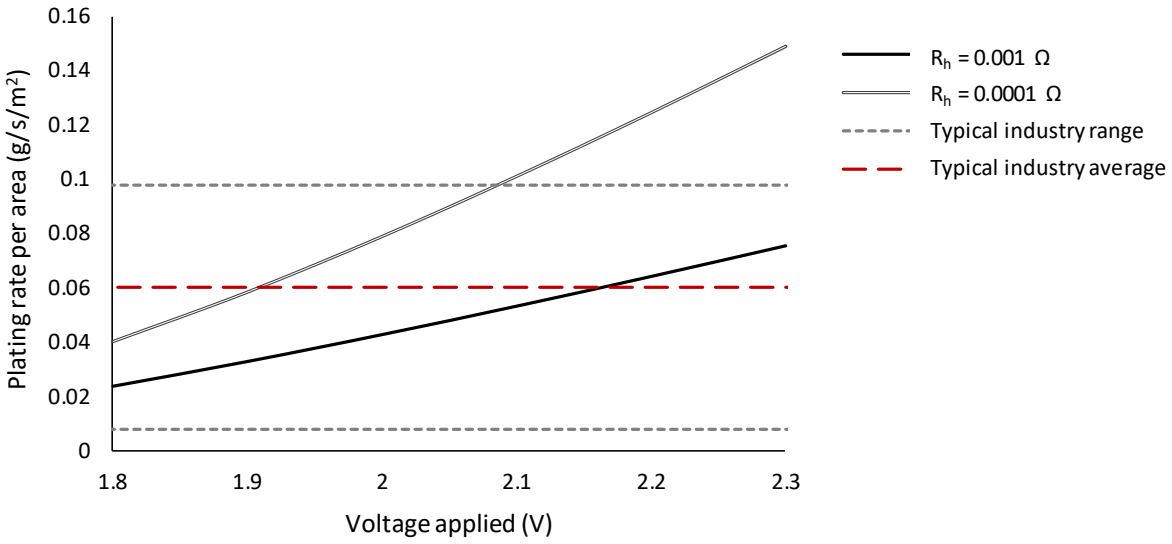

Figure 5.25: *Copper plating rate predicted in the model as a function of the applied voltage at two different input hardware resistance values, with typical industrial plating rates.*

The second model relationship that was validated was the effect of applied voltage and iron concentration on the current efficiency of the electrowinning operation. The current efficiency is provided as a function of the applied voltage (in the range of industry operation), at two levels of iron concentration in *Figure 5.26*. The higher the voltage applied to the system, the higher the current efficiency because the quantity of energy lost to iron reactions, hardware resistance, and other current losses remained similar even at higher voltages. The iron concentration of 1.7 g/l represented the average concentration of iron in an electrowinning system, and the associated current efficiencies fell within the typical industry range at all applied voltages, showing the validity of the relationship. At a higher iron concentration of 5 g/l (representing an industry maximum), the current efficiency was lower because some of the total current was being used up by the reduction and oxidation of iron instead of in the copper plating reaction. The relationship between the voltage, iron concentration and current efficiency that is presented in the electrowinning model is supported in the relevant literature (Das and Gopala Krishna, 1996; Khouraibchia and Moats, 2010). The rule of thumb in electrowinning that the current efficiency decreases by 2.5 % for every 1 g/l increase in iron concentration is also reflected in the model results (Das and Gopala Krishna, 1996).

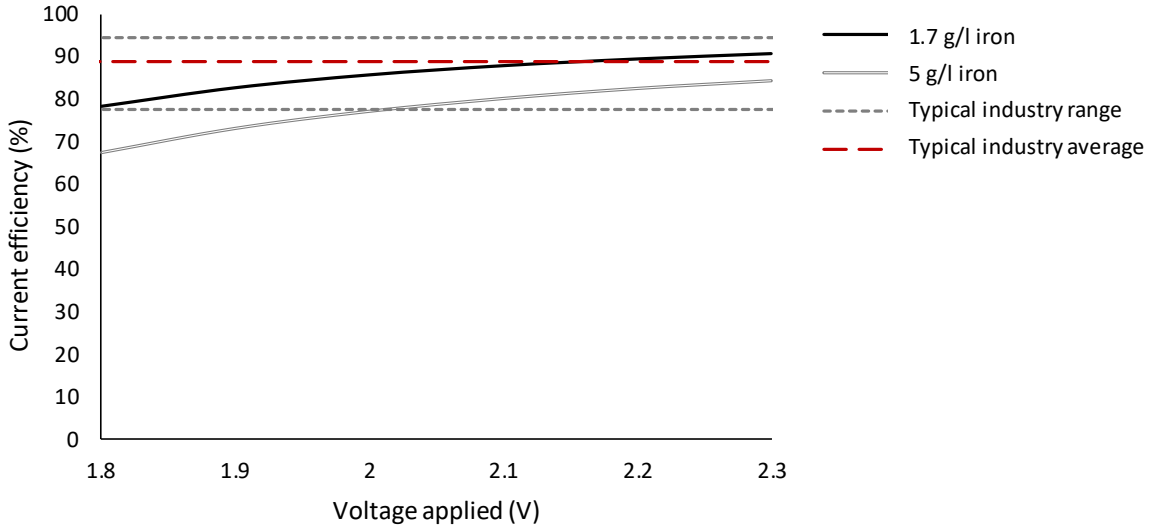

Figure 5.26: *Current efficiency predicted in the model as a function of the applied voltage at two different iron concentrations, with typical industrial operating values.*

Finally, the effect of the applied voltage and iron concentration on the specific energy consumption was demonstrated, as illustrated in *Figure 5.27* showing the specific energy consumption as a function of the applied voltage at two levels of iron concentration. At lower voltage levels, the specific energy decreased with an increase in voltage which corresponded to an increase in current efficiency. At higher voltages, however, the specific energy consumption tended to remain fairly constant or increased slightly. The trend in specific energy consumption can possibly be explained by the energy consumption being driven by copper reduction kinetics at lower voltages, while at higher voltages the energy consumption is controlled by water evolution kinetics due to large anodic overpotentials (Free *et al.*, 2006). The high sensitivity of current efficiency to voltage at the lower voltage levels matches this theory (see *Figure 5.26*).

The concentration of iron had a significant effect on the specific energy consumption, with an increased amount of iron in the electrolyte using up additional current. The electrowinning model predicted a specific energy consumption in the range of voltages applied and the average iron concentration of 1.7 g/l which is within close accuracy of the industry average energy consumption of approximately 2 MWh/t. The specific energy consumption pertaining to both the average (1.7 g/l) and high (5 g/l) iron concentrations fell well within the typical industry range, indicating that the model can be considered valid in its prediction of energy consumption.

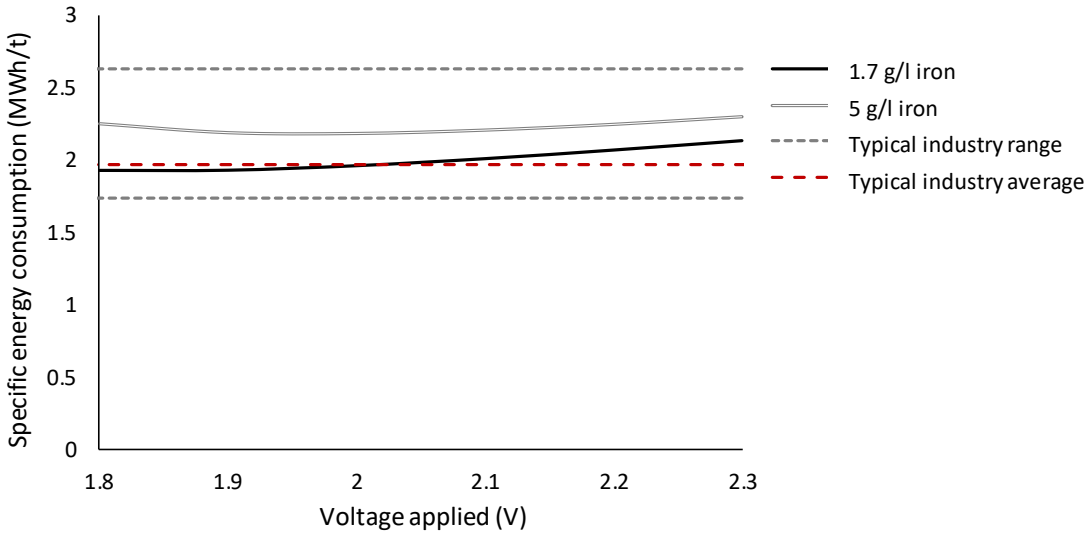

Figure 5.27: *Specific energy consumption predicted in the model as a function of the applied voltage at two different iron concentrations, with typical industrial operating values.*

5.5 Industrial Application

The results of the electrowinning model and parameter fitting to the bench-scale experiments indicate that the performance of electrowinning can be predicted to a high extent from the set of input variables chosen. Furthermore, the variability of the performance of electrowinning tankhouses in industry has been highlighted. While the parameters found during this research are well suited to the laboratory scale electrowinning system, they might not be as accurate when applied to an industrial process, and hence it is clear that for the most accurate performance prediction, tankhouses should make use of the electrowinning model in conjunction with the parameter fitting approach. It is important to consider the application of the model when deciding how accurate the parameters are required to be. If the steady state simulation is to be used in operator training or to gain a better understanding of the electrowinning operation, the parameters found in this research would be suitable. However, if the model is to be used in process control, it is recommended that parameters be fit specific to the electrowinning plant.

If a tankhouse has well recorded data of historical input and output variables that pertain to the model and these have varied significantly enough, they could be used for the determination of specific parameters. If not all critical historical data is available, the parameter fitting approach could be applied by running the experimental design on a pilot plant or varying the current or voltage in a cell and measuring its performance. Running experiments on a pilot plant setup could allow the current loss parameter to accurately be determined by testing the response of iron in the system. A more forward-thinking possibility could be to implement a self learning system for parameter fitting as the electrowinning operation runs, so that parameters correct themselves over time to provide the most accurate predictions of performance. In order

to successfully implement the electrowinning model in a tankhouse, a few critical variables need to be measured and requirements met as outlined in *Table 5.2*.

Table 5.2: *Requirements for industrial application of the electrowinning model.*

Category	Requirement	Details
Input variables to be measured regularly	Advance electrolyte composition Cell voltage and current	Variables may vary significantly and require regular monitoring for input into model.
	Cell temperature Electrolyte flowrate	Variables should remain relatively constant, therefore less regular recording should be performed.
Once off measurements	Hardware resistance	Measure hardware resistance between the electrodes and power supply. Although this could be performed once, it is suggested that regular maintenance checks be conducted to ensure it remains constant.
	Electrode surface area Interelectrode spacing Number of cathodes per cell	Should have on record from tankhouse design.
Output variables to be measured regularly	Output electrolyte composition Mass of copper plated	These variables will be used to compare to the model predictions.
Electrowinning model	Software	Electrowinning modelling software is required, with a user interface.
	Operator/Automated procedure	A plant operator is required to be responsible for monitoring actual versus predicted plant performance and inputting relevant information into the software. There is also scope for automatic process monitoring.
Electrowinning parameter fitting approach	Methodology	The methodology provided in this research would be provided as a set of instructions.
	Software	Software is required to conduct nonlinear regressions for parameter determination, with a user interface.

The electrowinning model is restricted to standard ranges of electrowinning input and output variables and should not be used outside of these ranges for the most accurate results. The model is also limited to steady state applications and electrowinning operations that maintain similar performance to the bench-scale cell in order for the parameters to be applicable. The model does not claim to be accurate under all operating circumstances, but can be used as tool together with the parameter fitting approach for use in future applications for the most accurate results to be obtained.

5.6 Summary

The results of the electrowinning model and parameter fitting approach were assessed in this chapter to ensure that the model was valid and accurate in its prediction of process performance. In addition, the fourth objective of this research was met, to compare the model predicted electrowinning performance indicators with data obtained from industrial plants. The results obtained from the bench-scale experiments validated the assumptions used in the model of a constant copper plating rate, and that the operation occurred below the limiting current density for copper reduction and water oxidation. The hardware resistance was also determined for use as an input into the model. The parameter fitting approach proved successful in the fitting of parameters to the experiments, with all rate kinetics parameters showing a high accuracy of fit. The performance of the model showed to be particularly sensitive to the charge transfer coefficients of each oxidation and reduction reaction, and these could be manipulated in order to fit the model to data from industrial electrowinning plants. When the parameters were input back into the original electrowinning model, it was found that the performance of electrowinning in the same system could be accurately predicted, but the model was less accurate in predicting the performance of industrial electrowinning cells. However, the model was still able to simulate the relationships between input and output variables as per literature, and within the industrial operating performance ranges.

6

CONCLUSIONS AND RECOMMENDATIONS

6.1 Conclusions

A semi-empirical model to predict electrowinning performance was developed in this research, from a first principles approach combined with the fitting of parameters to experimental data. The four major objectives were achieved: the first to develop an electrowinning model that could predict key performance indicators, the second objective to conduct bench-scale electrowinning experiments as part of a parameter fitting approach, the third objective to calibrate the bench-scale experimental data to the electrowinning model by parameter fitting, and the fourth objective to compare the model predicted electrowinning performance indicators with data obtained from industrial plants.

The development of the electrowinning model for the completion of the first research objective was achieved by coding a set of equations into MATLAB that could predict the key performance indicators of copper plating rate, current efficiency and specific energy consumption. Input variables into the model were available or easily measurable in industrial tankhouses and consisted of operational variables and those fixed due to cell design. A circuit diagram representation of an electrowinning cell formed the backbone to the model, which was scaled up from a single electrode pair to a cell. The circuit diagram concept allowed for determination of the anodic and cathodic voltages, voltages lost to hardware and electrolyte resistances and the split of current between reactions occurring at each electrode. Modelling consisted of rate calculations for each electrochemical reaction, thermodynamic and electrochemical equations, mass balances and property correlations. The electrowinning model was limited to steady state operation and was valid under standard industrial electrowinning operating conditions.

An experimental procedure was developed as the second objective of this research, the results of which would allow parameters to be fit to the model and the validation of the model assumptions to be made. The experimental procedure consisted of a full factorial design testing the effect of copper, sulphuric acid and iron concentrations and current density on electrowinning performance. From plating rate experiments, it was concluded that the copper plating rate remained constant over time, and therefore the steady state assumption was valid. It was found that the concentrations of both copper and sulphuric acid had no significant effect on the mass of species reacted in each reaction at copper concentrations of 35 and 55 g/l, and sulphuric acid concentrations of 165 and 185 g/l. It was therefore concluded that the copper reduction and water evolution reactions were reaction rate limited under standard electrowinning operating conditions, and therefore mass transfer of copper was neglected in the predictive model. This assumption was validated through a limiting current density test, which proved that the copper reduction reaction indeed

operated below the current density and that mass transfer effects could safely be ignored. The current density for the oxidation and reduction of iron was significantly impacted by the concentration of iron, therefore reaction kinetics and mass transfer effects were incorporated into the parameter fitting.

The third objective of this research, to fit parameters to the bench-scale experimental data, was met by developing a MATLAB code which could calibrate the experimental data to the electrowinning model equations through a series of nonlinear regressions. The parameters that were fit were exchange current densities and charge transfer coefficients for each electrochemical reaction (copper reduction, water oxidation, iron reduction and iron oxidation), mass transfer coefficients associated with the diffusion of ferric and ferrous ions to and from each electrode, and the current loss parameter. Average current loss was found to be 0.145 A, which accounted for losses in current due to stray currents, ineffective electrode contact and possible side reactions. The parameters associated with the rate kinetics all fit well to the experimental data, with relatively high R^2 and adjusted R^2 values (R^2_{adj} of 0.864 for copper reduction, 0.739 for water oxidation, 0.724 for iron reduction and 0.661 for iron oxidation). The electrowinning performance indicators were most sensitive to changes in the charge transfer coefficients of each of the electrochemical equations, but all electrowinning operations that differ from the bench-scale setup used in this research would require their own parameters to be fit for the most accurate model to be obtained.

The final objective was to evaluate the performance of the model with reference to data obtained from industrial plants, and this was achieved by comparing average electrowinning data from global industrial tankhouses to the model calibrated to the bench-scale cell. When parameters fit to the bench-scale experiments were incorporated back into the original model, performance of the bench-scale setup was predicted relatively accurately. The average absolute errors between actual and predicted performance in the bench-scale setup were 7.0% for the copper plating rate, 3.2% for the current efficiency, and 3.0% for the specific energy consumption. The relatively low percentage errors demonstrate the potential of the model to accurately predict performance in an electrowinning system with specifically fit parameters. When used to predict performance of the industrial tankhouses, the average absolute percentage error was 22% for the plating rate, 7.6% for the current efficiency and 11.4% for the specific energy consumption. The performance data for the industrial tankhouses were scattered, but the model was able to predict the performance to some extent without specifically altering parameters. It was concluded that the most accurate performance results would be obtained by combining the parameter fitting approach with the electrowinning model.

Overall, the steady state electrowinning model has been shown to provide relatively accurate results, with assumptions validated through bench-scale experiments and the relationships between input and output variables carried through into the model. The model could be used as is (with current parameters) for a rough estimate of plant performance and to gain insight into the effect of changing input variables on the electrowinning output variables and performance measures. Should a more accurate model be required, the

parameter fitting approach could be applied. Overall, the model has the potential to form a backbone to many industrial applications, possibly changing the way that electrowinning tankhouses operate to become safer, more economical and more efficient.

6.2 Recommendations

6.2.1 Further Modelling Considerations

The electrowinning model developed in this research could be extended to include additional relationships and considerations to account for more of the physical phenomena that occur in the system. One such major consideration that could potentially be incorporated into the model is a quality performance indicator. The quality indicator could include the determination of current maldistribution throughout the cell, calculation of the thickness of copper deposited per cathode over time, detection of dendrite formation and warnings for possible short circuits. These morphology predictions could potentially aid in the determination of a more accurate current loss parameter by estimating the potential for short circuits to occur. There is a possibility of including the effect of smoothing agents on the electrolyte properties, copper deposit quality and reaction rates through empirical relationships.

Further additions to the electrowinning model could be the inclusion of mass transfer effects for both copper reduction and water oxidation. These mass transfer effects could be taken into account using the extended Butler-Volmer equation (Equation 15). In addition, limiting current densities could be included for each reaction to accurately reflect the system boundaries beyond the standard electrowinning system conditions used in this research. That being said, additional experiments on the bench-scale electrowinning cell are suggested to determine the upper and lower bounds of input variables that can be accurately reflected in the model (extrapolations from the levels tested in this research). Additional experiments could be conducted to simulate electrowinning conditions without the presence of a solvent-extraction stage, and corresponding model performance evaluated.

Further recommendations are to incorporate losses of electrolyte due to evaporation of water and the production of acid mist and scale up calculations for different electrical configurations between cells or electrodes. Also, different methods of scale-up from a single electrode pair to a cell could be investigated to depict different electrical and electrolytic flow configurations. The existing electrowinning model created as part of this research is not compromised by neglecting these additional considerations, but their inclusion into the model would provide deeper insight into the electrowinning operation and extend its usefulness.

6.2.2 Current Model Applications

It is recommended that the electrowinning model with parameters determined from the bench-scale experiments be used as is for operator training, to assist with operator decision making and for cell design purposes. A more accurate representation of a specific electrowinning system could be obtained by applying the parameter fitting approach to fit specific parameters to process data. The electrowinning model together with specifically fit parameters could be used in electrowinning tankhouses as an accurate guide for operators to investigate the effect of changing input variables on the system performance in order to meet requirements.

The electrowinning model with specifically fit parameters could be used as a comparison tool for operators to gauge whether actual performance meets the standard, or the predicted output. The model as a comparative tool could aid in fault determination: should electrowinning be operating below the predicted performance, operators could locate faults such as short circuits and improve plant efficiency in a much quicker time than in current industrial practice. The electrowinning model and parameter fitting approach developed in this research could therefore form a meaningful contribution to the field by assisting in operator training, tankhouse design, the manual control process and fault determination to make the process more efficient, effective and economical.

6.2.3 Future Model Applications

The electrowinning model developed in this research could form a basis for the implementation of process control and updated monitoring systems in electrowinning tankhouses. For control purposes, the steady state model would have to be converted to a dynamic model through the inclusion of time into the mass balance equations. An appropriate control strategy would also need to be decided upon and implemented. The parameters would need to be as accurate as possible should the predictive model be used for control purposes. It is therefore recommended that the parameter fitting approach be applied to experiments on a pilot plant setup in order to accurately represent the kinetics of the specific tankhouse to which it pertains. There is also the possibility of implementing a self-learning system for parameter fitting as the electrowinning operation runs, to ensure that the fit parameters are as accurate and up to date as possible. Overall, the model together with parameter fitting approach form a foundation for a diverse range of applications, others of which include electrowinning process optimisation, and the prediction and detection of hazards and faults so that preventative measures can be implemented. These many applications have the potential to positively impact the operation of hydrometallurgical plants even further in economical, practical and safety related areas.

7

REFERENCES

Alfantazi, A. M. and Valic, D. 2003. A study of copper electrowinning parameters using a statistically designed methodology. *Journal of Applied Electrochemistry*, 33(2): 217-225.

Al Shakarji, R., He, Y. and Gregory, S. 2013. Performance evaluation of acid mist reduction techniques in copper electrowinning. *Hydrometallurgy*. 131-132: 76-80.

Aminian, H., Bazin, C., Hodouin, D and Jacob, C. 2000. Simulation of a SX – EW pilot plant. *Hydrometallurgy*, 56(1): 13-31.

Aminian, H., Bazin, C. and Hodouin, D. 1998. Residence time distributions in SX-EW equipment. *International Journal of Mineral Processing*, 54(3–4): 235-242.

Anderson, C. G. 2014. Innovations in Hydrometallurgy. in Anderson, C.G., Dunne, R. and Uhrie, J. (eds.). *Mineral Processing and Extractive Metallurgy: 100 Years of Innovation*. Colorado: Society for Mining, Metallurgy, and Exploration, Inc. 467-501.

Aqueveque, P. E., Wiechmann, E. P., Herrera, J. and Pino, E. J. 2015. Measurable variables in copper electrowinning and their relevance to predicting process performance. *IEEE Transactions on Industry Applications*, 51(3): 2607-2614.

Armstrong, R. D. 1972. Equivalent Circuits for Electrochemical Cells. *Journal of Electroanalytical Chemistry and Interfacial Electrochemistry*, 40(2): 437-439.

Bard, A. J. and Faulkner, L. R. 2001. *Electrochemical Methods: Fundamentals and Applications*. United States of America: John Wiley & Sons, Inc. 1-833.

Beukes, N. T. and Badenhorst, J. 2009. Copper electrowinning: theoretical and practical design. *Journal of the Southern African Institute of Mining and Metallurgy*, 109(6): 213-240.

Blackett, A. and Nicol, M. 2010. The simulation of current distribution in cells during the electrowinning of copper, in *Proceedings of Copper 2010*, (4), Hamburg: 1291-1292.

Coetzee, C., Tadie, M. and Dorfling, C. 2018. *Characterizing the Role of Polyacrylamide Additives in Copper Electrowinning*. Published Master's Thesis. Stellenbosch: Stellenbosch University.

Chang, J. H. 2009. *Modeling of an Electrochemical Cell*. Published masters thesis. Toronto: University of Toronto. [Online]. Available: https://tspace.library.utoronto.ca/bitstream/1807/18247/6/ Chang_JinHyun _200911_MASc_Thesis.pdf [Accessed March 2018].

Choi, N. S., Kim, D. W., Cho, J. and Kim, D. H. 2014. A Fully Optimized Electrowinning Cell for Achieving a Uniform Current Distribution at Electrodes Utilizing Sampling-Based Sensitivity Approach. *Journal of Electrical Engineering and Technology*, 10: 742–747.

Cifuentes, L. and Simpson, J. 2005. Temperature dependence of the cathodic and anodic kinetics in a copper electrowinning cell based on reactive electrodialysis. *Chemical Engineering Science*, 60(17): 4915-4923.

Cifuentes, L., Castro, J.M., Crisóstomo, G., Casas, J.M. and Simpson, J. 2007. Modelling a Copper Electrowinning Cell Based on Reactive Electrodialysis. *Applied Mathematical Modelling*, 31(7): 1308-1320.

Dao, T. S. and McPhee, J. 2011. Dynamic Modeling of Electrochemical Systems Using Linear Graph Theory. *Journal of Power Sources*, 196: 10442-10454.

Das, S. C. and Gopala Krishna, P. 1996. Effect of Fe(III) during copper electrowinning at higher current density. *International Journal of Mineral Processing*, 46(1–2): 91-105.

Davenport, W. G., King, M., Schlesinger and M., Biswas, A.K. 2002. *Extractive Metallurgy of Copper: Fourth Edition*. Oxford: Pergamon. 399 pages.

Dini, J. W. and Snyder, D. D. 2011. Electrodeposition of Copper, in Schlesinger, M. and Paunovic, M. (eds.). *Modern Electroplating: Fifth Edition*. New Jersey: John Wiley & Sons, Inc. 33-78.

Ehsani, A., Yazici, E. Y. and Deveci, H. 2016. The Effect of Temperature on the Electrowinning Of Copper, in *Proceedings of the 18th International Metallurgy & Materials Congress*, 114: 521-523.

Fabian, C. 2005. *Copper electrodeposition in the presence of guar or activated polyacrylamide*. Published doctoral dissertation. Queensland: James Cook University. 76-114.

Free, M. L., Bhide, R., Rodchanarowan, A. and Phadke, N. 2006. Electrochemical modeling of electrowinning performance, in Kongoli, F. and Reddy, R. G. (eds.). *Sohn International Symposium: Advanced Processing of Metals and Materials*, (6), The Minerals, Metals and Materials Society. 479-491.

Free, M. L., Bhide, R. and Rodchanarowan, A. 2013. Evaluation of mass transport effects on the nucleation and growth of electrodeposits. *Transactions of the Institutions of Mining and Metallurgy, Section C: Mineral Processing and Extractive Metallurgy*, 122(4): 223-228.

Georgiadou, M. 2003. Modeling current density distribution in electrochemical systems. *Electrochimica Acta*, 48(27): 4089-4095.

Hiskey, J. B. 2009. Principles and Practical Considerations of Copper Electrorefining and Electrowinning, in Jergensen, G. V. (ed.). *Copper Leaching, Solvent Extraction, and Electrowinning Technology*. United States of America: Society for Mining, Metallurgy and Exploration, Inc. 169-186.

Kafumbila, J. 2017. *Design of Copper Electrowinning Circuit Using Conventional Cells.* Independently Published: Democratic Republic of the Congo. 57 pages.

Kalliomäki, T., Aromaa, J. and Lundström, M. 2016. Modeling the Effect of Composition and Temperature on the Conductivity of Synthetic Copper Electrorefining Electrolyte. *Minerals*, 6(59): 1-11.

Kawai, S. and Miyazawa, T. 2014. CFD Modelling and Simulation of Industrial-Scale Copper Electrorefining Process. *Minerals Engineering*. (63): 81-90.

Khouraibchia, Y. and Moats, M. S. 2010. Evaluation of the Effect of Copper Electrowinning Parameters on Current Efficiency and Energy Consumption Using Surface Response Methodology, in *217th Electrochemical Society Meeting*. 295-306.

Kim, K. R., Choi, S. Y., Paek, S., Park, J. Y., Hwang, I. S. and Jung. 2013. Electrochemical hydrodynamics modeling approach for a copper electrowinning cell. *International Journal of Electrochemical Science*, 8(11): 12333-12347.

Laitinen, I. S. and Tanttu, J. T. 2008. Modelling and Simulation of a Copper Electrolysis Cell Group. *Simulation Modelling Practice and Theory*, 16: 900-909.

Leahy, M. J. and Schwarz, M. P. 2014. Flow and Mass Transfer Modelling for Copper Electrowinning: Development of Instabilities Along Electrodes. *Hydrometallurgy*. (147-148): 41-53.

Lie, B. and Hauge, T. A. 2008. Modeling of an Industrial Copper Leaching and Electrowinning Process, With Validation Against Experimental Data, in *Proceedings of the 49th Scandinavian Conference on Simulation & Modeling*. Oslo.

Loutfy, R. O. and Leroy, R. L. 1978. Energy efficiency in metal electrowinning. *Journal of Applied Electrochemistry*, 8(6): 549-555.

Lower, S. K. 1994. Chem1 Electrochemistry Class Notes. Simon Fraser University [Online]. Available: http://www.chem1.com/acad/webtext/elchem/index2.html [2018, June 6].

Mahon, M. J. 2016. Dynamic Process Simulation of Zinc Electrowinning. Unpublished doctoral dissertation. Vancouver: The University of British Columbia. 247 pages.

Martis, M. S. 2006. Validation of simulation based models: A theoretical outlook. *Electronic Journal of Business Research Methods*, 4(1): 39-46.

Mathew, R. J. 2012. Increasing Oxygen Charge Transfer Resistance on the Anode in Copper Electrowinning, in Free, M. L., Moats, M., Houlachi, G. Asselin, E.A., Allanore, A., Yurko, J. and Wang, S. (eds.). *Electrometallurgy 2012*. Ontario: John Wiley & Sons, Inc. 41–46.

Mirza, A., Burr, M., Ellis, T., Evans, D., Kakengela, D., Webb, L., Gagnon, J., Leclercq, F. and Johnston, A. 2016. Corrosion of lead anodes in base metals electrowinning. *The Journal of the South African Institute of Mining and Metallurgy*, 116: 533-538.

Mishra, K. and Cooper, W. C. 2016. Electrochemical Aspects of the Direct Electrowinning of Copper from Sulphuric Acid Leach Solutions in the Presence of Iron Using Gas Sparging, in *International Metallurgy and Materials Congress*. Istanbul. 13-36.

Moats, M. S. and Khouraibchia, Y. 2009. Effective Diffusivity of Ferric Ions and Current Efficiency in Stagnant Synthetic Copper Electrowinning Solutions. *Minerals & Metallurgical Processing*, 26(4): 179-186.

Moats, M. S., Luyima, A. and Cui, W. 2016. Examination of copper electrowinning smoothing agents. Part 1: A review. *Minerals and Metallurgical Processing*, 33(1): 7-13.

Murray, A., Khakbaz, H., Pranowo, A., Aslin, N. and Kannan, M. B. 2016. Effects of process parameters on the adhesive strength of copper electrodeposits in a bench-scale electrowinning cell. *Transactions of the Institutions of Mining and Metallurgy, Section C: Mineral Processing and Extractive Metallurgy*, 125(1): 10-16.

Najim, S. T. 2016. Estimation of Mass Transfer Coefficient for Copper Electrowinning Process. *The Journal of Engineering*, 4(22): 158-168.

Najminoori, M., Mohebbi, A., Arabi, B. G. and Daneshpajouh, S. 2015. CFD Simulation of an Industrial Copper Electrowinning Cell. *Hydrometallurgy*. 153: 88-97.

Newman, J. and Thomas-Alyea, K. E. 2004. *Electrochemical Systems: Third Edition*. New Jersey: John Wiley & Sons, Inc. 207-602.

Panda, B. and Das, S. C. 2001. Electrowinning of copper from sulfate electrolyte in presence of sulfurous acid. *Hydrometallurgy*, 59(1): 55-67.

Pasa, A. A. and Munford, M. L. 2006. Electrodeposition. *Encyclopedia of Chemical Processing*. 821-832.

Paunovic, M. and Schlesinger, M. 2005. *Fundamentals of Electrochemical Deposition: Second Edition.* New Jersey: John Wiley & Sons, Inc. 113-138.

Paynter, J. C. 1973. A review of copper hydrometallurgy. *Journal of the South African Institute of Mining and Metallurgy*, (November): 158-170.

Pfalzgraff, C. L. 2009. Do's and Don'ts of Tankhouse Design and Operation. *Society for Mining, Metallurgy and Exploration*: 217-221.

Pradhan, N., Krishna, P. G. and Das, S. C. 1996. Influence of chloride ion on electrocrystallization of copper. *Plating and Surface Finishing*, 83(3): 56-63.

Price, D. C. and Davenport, W. G. 1980. Densities, Electrical Conductivities and Viscosities of CuSO4/H2SO4 Solutions in the Range of Modern Electrorefining and Electrowinning Electrolytes. *Metallurgical Transactions*, 11B(March): 159-160.

Reade, G., Ottewill, G. and Walsh, F. 1992. Electrolytic conductivity and its measurement. *Transactions of the Institute of Metal Finishing*, 70(1): 45-49.

Robinson, T., Sole, K. C., Sandoval, S., Moats, M., Siegmund, A. and Davenport, W. E. 2013a. Copper Electrowinning: 2013 World Tankhouse Operating Data, in *Proceedings of Copper 2013.* Santiago.

Robinson, T., Sole, K.C., Sandoval, S., Moats, M., Siegmund, A. and Davenport, W. E. 2013b. *Global Cu EW survey Copper 2013*. Excel Spreadsheet.

Rodrigues, J. C. P. 1983. *Modelling the Performance of Manganese Electrowinning Cells*. Published masters thesis. Johannesburg: University of the Witwatersrand. 48 pages.

Samson, E., Lemaire, G., Marchand, J. and Beaudoin, J. J. 1999. Modeling chemical activity effects in strong ionic solutions. *Computational Materials Science*, 15(3): 285-294.

Schlesinger, M. E., King, M.J., Sole, K. C. and Davenport, W. G. 2011. *Extractive Metallurgy of Copper. Fifth Edition*. Oxford: Elsevier. 439 pages.

Scott, A. C., Pitblado, R. M. and Barton, G. W. 1987. A Mathematical Model of a Zinc Electrowinning Cell, in *Twentieth International Symposium on the Application of Computers and Mathematics in the Mineral Industries*, 2: 51-62.

Shukla, A. 2013. *Modeling and Measuring Electrodeposition Parameters Near Electrode Surfaces to Facilitate Cell Performance Optimization.* Published Masters Thesis. Utah: University of Utah. 120 pages.

Su, C., Zhang, W., Ghali, E., and Houlachi, G. 2017. Electrochemical investigation of electrolyte composition and electrolysis parameters during zinc electrowinning. *Journal of Applied Electrochemistry*, 47(8): 941-958.

Thermo Fischer Scientific. 2012. Conductivity and Concentration Relationship. Thermo Fischer Scientific.

Werner, J. M., Zeng, W., Free, M. L., Zhang, Z. and Cho, J. 2018. Modeling and Validation of Local Electrowinning Electrode Current Density Using Two Phase Flow and Nernst-Planck Equations. *Journal of The Electrochemical Society*, 165(5): 190-207.

Wiechmann, E. P., Munoz, L. G., Aqueveque, P. E., Vidal, G. A. and Henriquez, J. A. 2014. Introducing a bypass-backup connection system for current-mode copper electrowinning intercell bars. *IEEE Transactions on Industry Applications*, 50(2): 1490-1495.

Wiechmann, E. P., Morales, A. S., Aqueveque, P., Pino, E. J., Munoz, L. and Henriquez, J. A. 2016. Intercell busbar design for copper electrowinning. *IEEE Transactions on Industry Applications*, 52(5): 4480-4488.

Wiechmann, E. P., Morales, A. S. and Aqueveque, P. 2009. Full Measuring System for Copper Electrowinning Processes Using Optibar Intercell Bars. *IEEE Transactions on Industry Applications*, 45(5): 1575-1582.

Wiechmann, E. P., Morales, A. S. and Aqueveque, P. 2010. Improving Productivity and Energy Efficiency in Copper Electrowinning Plants. *IEEE Transactions on Industry Applications*, 46(4): 1264-1270.

Winand, R. 1992. Electrocrystallization- theory and applications. *Hydrometallurgy*. 29: 567-598.

Yuwono, J. A., Clancy, M., Chen, X. and Birbilis, N. 2018. Exploring As-Cast PbCaSn-Mg Anodes for Improved Performance in Copper Electrowinning. *Metallurgical and Materials Transactions B: Process Metallurgy and Materials Processing Science*. 49(3): 1453-1463.

Zeng, W., Free, M. L., Werner, J. and Wang, S. 2015. Simulation and Validation Studies of Impurity Particle Behavior in Copper Electrorefining. *Journal of The Electrochemical Society*, 162(14): E338–E352.

Zhang, Z., Werner, J. and Free, M. 2018. A Current Efficiency Prediction Model Based on Electrode Kinetics for Iron and Copper During Copper Electrowinning, in Lambotte, G., Lee, J., Allanore, A. and Wagstaff, S.R. (eds.). *Mineral Processing Fundamentals 2018*. Minerals, Metals and Materials Series. 111-131.

APPENDIX A

SAMPLE CALCULATIONS

Stoichiometric Calculations: Mass of Chemicals Required in Experiments

The bench-scale electrowinning experiments included the preparation of a synthetic advance electrolyte. The electrolyte composition included copper, iron and sulphuric acid in water, which was created by dissolving copper sulphate and ferric sulphate in the electrolyte. The masses of each of the chemicals required to provide the desired electrolyte composition are calculated as follows.

Copper sulphate

The mass of copper sulphate ($CuSO_4 \cdot 5H_2O$) that is required to provide the desired copper concentration is calculated using Equation 63.

$$m_{CuSO_4 \cdot 5H_2O} = x_{Cu} V \frac{M_{CuSO_4}}{M_{Cu}} \frac{\upsilon_{Cu}}{\upsilon_{CuSO_4}} \quad [63]$$

Where m = Mass of species (g)

M = Molar mass of species (g/mol)

V = Volume (l)

x = Concentration (g/l)

υ = Stoichiometric coefficient ($\upsilon_{Cu} = 1;\ \upsilon_{CuSO_4} = 1$)

Ferric sulphate

The mass of ferric sulphate ($Fe_2(SO_4)_3 \cdot xH_2O$) that is required to provide the desired iron concentration is calculated using Equation 64.

$$m_{Fe_2(SO_4)_3 \cdot xH_2O} = x_{Fe} V \frac{M_{Fe_2(SO_4)_3 \cdot xH_2O}}{M_{Fe}} \frac{\upsilon_{Fe_2(SO_4)_3 \cdot xH_2O}}{\upsilon_{Fe}} \quad [64]$$

With $\upsilon_{Fe} = 2;\ \upsilon_{Fe_2(SO_4)_3 \cdot xH_2O} = 1$

Sulphuric acid

The mass of sulphuric acid (H_2SO_4) that is required in the electrolyte to provide the desired sulphuric acid concentration is calculated using Equation 65.

$$m_{H_2SO_4} = \frac{x_{H_2SO_4} V}{grade} \quad [65]$$

Where $grade$ = Purity of sulphuric acid (98.08%)

Mass of Water Oxidised

The mass of water that gets oxidised during the electrowinning of copper can be calculated from the difference in sulphuric acid concentrations in the advance and spent electrolyte, as per Equation 66.

$$m_{H_2O} = V(x_{H_2SO_4,spent} - x_{H_2SO_4,advance}) \frac{M_{H_2O}}{M_{H_2SO_4}} \frac{\upsilon_{H_2O}}{\upsilon_{H_2SO_4}} \quad [66]$$

With $\upsilon_{Fe} = 1$; $\upsilon_{Fe_2(SO_4)_3 \cdot xH_2O} = 1$ from the overall cell reaction (Equation 6):

$$Cu^{2+}_{(aq)} + SO^{2-}_{4(aq)} + H_2O_{(l)} \rightarrow Cu_{(s)} + \frac{1}{2}O_{2(g)} + 2H^{+}_{(aq)} + SO^{2-}_{4(aq)} \qquad E^0 = -0.89\ V \quad [6]$$

APPENDIX B

EXPERIMENTAL PROCEDURE

Appendix B includes information relating to procedural aspects of the bench-scale electrowinning experiments, and comprises the design of experiments with detailed methodology, determination of flowrate and the calibration curve used in the sulphuric acid concentration measurement.

Experimental Design

Table B.1: *Design of input operating conditions for electrowinning experiments conducted in the bench-scale electrowinning cell.*

Type of Experiment	Number	Current density (A/m^2)	Copper concentration (g/l)	Sulphuric acid concentration (g/l)	Iron concentration (g/l)
Full factorial design (2 levels of each factor)	1	300	55	185	4
	2	300	55	185	1
	3	300	55	165	4
	4	300	35	185	4
	5	200	55	185	4
	6	300	55	165	1
	7	200	35	185	4
	8	300	35	185	1
	9	200	55	165	4
	10	300	35	165	4
	11	200	55	185	1
	12	300	35	165	1
	13	200	55	165	1
	14	200	35	185	1
	15	200	35	165	4
	16	200	35	165	1
Full factorial design (control, excluding iron)	17	300	55	185	0
	18	300	55	165	0
	19	300	35	185	0
	20	200	55	185	0
	21	300	35	165	0
	22	200	55	165	0
	23	200	35	185	0
	24	200	35	165	0
Additional current density	25	100	45	175	2
	26	100	45	175	0
	27	400	45	175	2
	28	400	45	175	0
	29	500	45	175	0
	30	600	45	175	0

Table B.1 (continued):

Type of Experiment	Number	Current density (A/m²)	Copper concentration (g/l)	Sulphuric acid concentration (g/l)	Iron concentration (g/l)
24 h plating rate (2 repeats)	31 32	200	55	185	4
Model validation	33	340	55	185	4
	34	230	55	165	4
	35	270	35	185	4
	36	210	55	165	0

Detailed Methodology

A detailed approach to the execution of the electrowinning experiments in the bench-scale setup is outlined as follows:

1. Insert two anodes into the electrowinning cell such that 2 cm between the anode and cathode is maintained. Bolt the positive wires from the power source to the anode hanger bars using lugs. This step only needs to be performed for the first experiment.
2. Switch on thermostat for water bath (set to approximately 60°C to maintain a cell temperature of 45°C). Ensure that the level in the water bath is sufficient.
3. Prepare 9.5 l of advance electrolyte by weighing the correct mass of copper sulphate, ferric sulphate and sulphuric acid and dissolving in tap water.
4. Take a 500 ml sample of advance electrolyte and set aside for analysis.
5. Place stock solution container of advance electrolyte into water bath and connect pipes.
6. Circulate the electrolyte throughout the electrowinning system until a steady temperature in the cell has been reached (approximately 20 minutes). Ensure that the extraction system is running.
7. Rinse blank cathode with acetone and distilled water and let air dry.
8. Weigh blank cathode and insert into the electrowinning cell.
9. Bolt the negative terminal of the power source to the cathode hanger bar.
10. Reduce pump speed to the desired setting of 20% of the maximum, to achieve an electrolyte flowrate of 3.5 l/h.
11. Switch the power supply on to the desired constant current setting and start the timer.
12. Measure the voltage over the power source, anode and cathode wires and between each anode and cathode hanger bar for use in resistance calculations (repeat this step every hour).
13. After four hours of plating, switch the power supply and pump off.
14. Remove the cathode from the electrowinning cell, rinse with distilled water and leave to air dry.
15. Weigh the cathode plate to determine the mass of copper that had plated.
16. Take 500 ml of spent electrolyte as a sample for analysis.

17. Open the valves in the setup that will allow the spent electrolyte to be discarded in the waste container.
18. Rinse the electrowinning setup with water and allow to dry before initiating the proceeding experimental run.

Electrolyte Flowrate

The electrolyte flowrate was set to provide the desired interfacial velocity of 0.1 $m^3/(h \cdot m^2)$ over the electrode surface to meet industry standards. The volumetric flowrate required was calculated using Equation 67.

$$Q = uA \quad [67]$$

Where Q = Volumetric flowrate (m^3/h)

u = Interfacial velocity ($m^3/(h \cdot m^2)$)

A = Electrode surface area (m^2)

The desired volumetric flowrate was set by adjusting the percentage speed of the peristaltic pump and measuring the associated flowrate in an iterative manner. The flowrates were determined using the time it took to fill up a volume in a measuring cylinder, with the desired flowrate of 3.5 l/h achieved at a pump speed of 20%. The flowrate measurements used to calculate the average are provided in *Table B.2.*

Table B.2: *Electrolyte flowrates measured in the bench-scale electrowinning setup at a pump speed of 20% to provide the desired interfacial velocity of 0.1 $m^3/(h \cdot m^2)$.*

Flowrate test number	Flowrate (m^3/h)	Average flowrate (l/h)
1	3.36	
2	3.95	3.50
3	3.19	

Determination of Experimental Sulphuric Acid Concentration

Each electrowinning experiment on the bench-scale setup required the determination of sulphuric acid concentration in the advance and spent electrolyte. A calibration curve was created indicating the sulphuric acid concentration based on the solution conductivity, iron and copper concentration. The calibration curve was determined by preparing a variety of synthetic solutions with known composition and measuring their conductivity at 45°C, and is shown in *Figure B.1*. If the copper or iron concentration was not specifically represented on the graph, interpolation was performed between the two closest points.

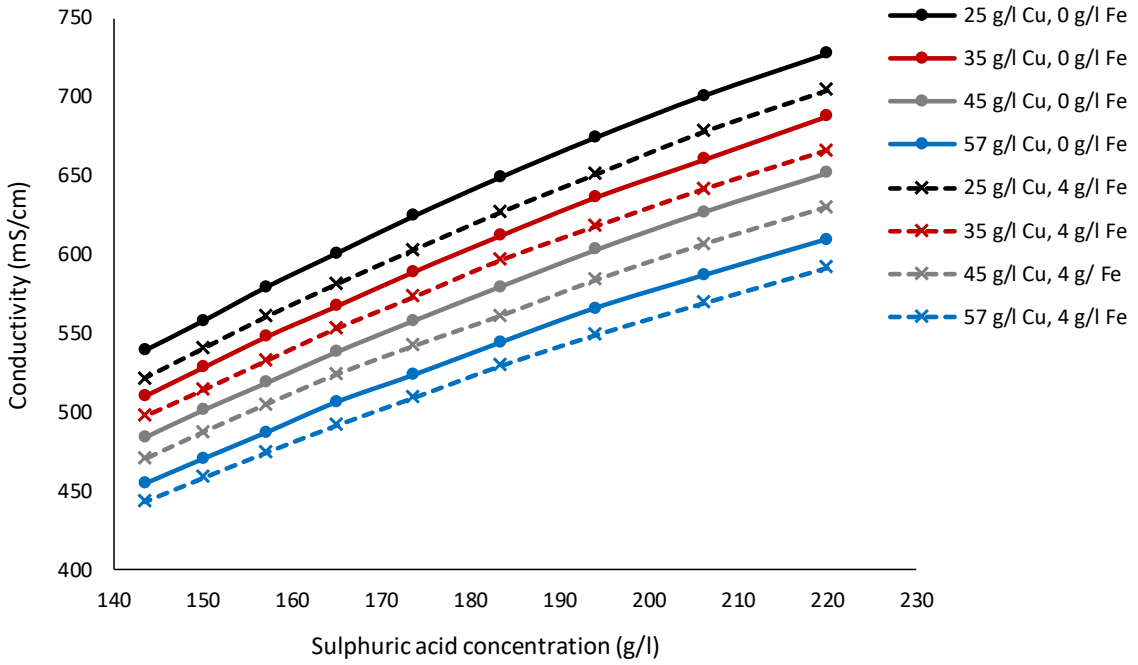

Figure B.1: *Calibration curve of electrolyte conductivity (at 45°C) as a function of sulphuric acid concentration, at copper concentrations of 25, 35, 45 and 57 g/l and iron concentrations of 0 and 4 g/l.*

APPENDIX C

EXPERIMENTAL AND MODEL RESULTS

Appendix C includes information relating to the results of the bench-scale electrowinning experiments, the fitting of parameters and determination of model accuracy (*Chapter 5 Results and Discussion*).

Experimental Results

Table C.1: *Electrowinning performance and related output data obtained in the bench-scale experiments. Experiment numbers correspond to the experimental design in Table B.1.*

Experiment number	Voltage (V)	Current (A)	Current density (A/m^2)	Mass copper plated (g)	Current efficiency (%)	Specific energy consumption (MWh/t)
1	2.00	9.70	302	41.7	90.7	1.86
2	2.10	9.69	302	41.8	90.8	1.95
3	2.06	9.68	302	41.9	91.3	1.91
4	2.10	9.69	302	41.5	90.3	1.96
5	1.90	6.59	205	27.4	87.7	1.83
6	2.00	10.2	317	47.0	97.2	1.74
7	1.90	6.58	205	27.1	86.9	1.84
8	2.02	9.70	302	44.2	96.2	1.77
9	1.90	6.57	205	27.3	87.7	1.83
10	2.10	9.69	302	41.3	89.9	1.97
11	1.90	6.55	204	29.3	94.3	1.70
12	2.05	9.69	302	43.7	95.2	1.81
13	1.90	6.59	205	29.5	94.5	1.70
14	1.90	6.57	205	29.6	94.9	1.69
15	1.91	6.58	205	26.8	85.9	1.87
16	1.90	6.40	199	28.8	95.0	1.69
17	2.00	9.60	299	44.5	97.7	1.73
18	2.07	9.70	302	45.0	97.9	1.78
19	2.08	10.2	318	47.9	99.0	1.77
20	1.90	6.57	205	30.5	97.9	1.64
21	2.01	9.68	302	45.1	98.2	1.72
22	1.90	6.40	199	29.9	98.5	1.63
23	2.00	8.26	257	38.8	98.9	1.71
24	1.90	6.58	205	30.4	97.3	1.65
25	1.79	3.20	99.7	12.9	99.7	1.78
26	1.79	3.10	96.6	14.0	96.6	1.58
27	2.26	12.8	400	62.2	100	1.87
28	2.20	12.8	400	60.3	99.1	1.87
29	2.30	16.0	498	76.2	100	1.93
30	2.42	19.2	598	89.6	98.5	2.07

Table C.2: *Advance and spent electrolyte copper concentration per sample, determined by AAS and converted from a 1000 times dilution factor. Experiment numbers correspond to the experimental design in Table B.1*

Experiment number	Copper concentration (g/l)					
	Advance electrolyte			Spent electrolyte		
	Sample 1	Sample 2	Average	Sample 1	Sample 2	Average
1	53.7	53.3	53.5	49.1	50.3	49.7
2	54.7	54.9	54.8	52.5	54.0	53.2
3	52.4	52.3	52.4	49.4	48.3	48.8
4	31.3	31.1	31.2	29.8	29.0	29.4
5	51.3	53.4	52.3	49.5	51.9	50.7
6	56.9	56.4	56.7	50.1	51.4	50.7
7	36.7	35.6	36.1	31.6	31.7	31.7
8	36.0	37.1	36.5	32.3	29.8	31.0
9	54.4	56.3	55.4	46.7	49.5	48.1
10	32.5	30.5	31.5	29.1	30.0	29.6
11	56.1	55.6	55.8	52.4	52.2	52.3
12	34.6	31.3	32.9	30.0	32.3	31.2
13	54.0	56.0	55.0	50.6	53.3	52.0
14	33.7	32.0	32.8	25.9	27.9	26.9
15	36.4	36.3	36.3	33.1	34.4	33.7
16	36.6	36.0	36.3	33.0	33.2	33.1
17	51.9	54.8	53.4	47.6	51.6	49.6
18	54.2	53.1	53.6	39.7	42.6	41.2
19	34.5	35.1	34.8	31.6	30.8	31.2
20	51.8	52.7	52.2	42.1	39.3	40.7
21	34.6	33.0	33.8	29.3	28.2	28.8
22	50.7	50.6	50.6	50.7	51.2	50.9
23	34.6	36.9	35.7	30.9	31.1	31.0
24	32.3	31.5	31.9	31.5	31.6	31.5

Table C.3: *Advance and spent electrolyte conductivities and copper and iron concentrations, for use in the determination of sulphuric acid concentration per the calibration curve in Figure B.1. Experiment numbers correspond to the experimental design in Table B.1.*

Experiment number	Iron concentration (g/l)	Advance electrolyte			Spent electrolyte		
		Conductivity (mS/cm)	Concentration (g/l)		Conductivity (mS/cm)	Concentration (g/l)	
			Copper	Sulphuric acid		Copper	Sulphuric acid
1	4	542.6	53.5	185.6	574.0	49.7	195.3
2	1	555.3	55.0	187.9	594.4	53.2	198.7
3	4	498.5	52.4	162.9	532.4	48.8	172.2
4	4	600.0	31.2	180.3	640.8	29.4	191.7
5	4	545.3	52.3	185.5	569.8	50.7	194.0
6	1	509.6	56.7	167.9	556.7	50.7	183.5
7	4	600.6	36.1	187.4	627.0	31.7	195.6
8	1	620.5	36.5	191.6	664.0	31.0	203.9
9	4	501.6	55.4	167.8	527.6	48.1	176.1
10	4	557.0	31.5	162.8	596.7	29.6	173.2
11	1	552.7	55.8	188.0	583.5	52.3	199.3
12	1	568.4	32.9	164.5	610.2	31.2	174.4
13	1	511.7	55.0	167.0	539.0	52.0	175.5
14	1	609.8	32.8	181.2	642.0	26.9	190.0
15	4	559.1	36.3	169.5	588.7	33.7	177.9
16	1	568.5	36.3	169.0	601.1	33.1	177.6
17	0	564.8	53.4	188.4	587.0	49.6	191.8
18	0	512.4	53.6	164.1	554.4	41.2	176.5
19	0	621.6	34.8	187.2	674.1	31.2	201.9
20	0	554.8	52.2	182.0	580.6	40.7	189.4
21	0	544.5	33.8	154.5	617.3	28.8	176.1
22	0	515.8	50.6	162.3	541.8	50.9	169.2
23	0	626.0	35.7	190.6	664.5	31.0	201.2
24	0	570.3	31.9	162.3	607.5	31.5	172.0

Table C.4: *Mass of species that reacts per side of electrode in each bench-scale electrowinning experiment and associated current density. Experiment numbers correspond to the experimental design in Table B.1.*

Experiment number	Mass of species reacted per electrode side (g)				Current density per reaction (A/m^2)			
	Copper	Water	Iron (reduction)	Iron (oxidation)	Copper reduction	Water oxidation	Iron reduction	Iron oxidation
1	20.9	7.56	2.82	16.1	274	175	21.1	120
2	20.9	8.39	2.76	13.4	274	195	20.6	100
3	21.0	7.29	2.64	16.9	275	169	19.7	126
4	20.7	8.93	3.49	12.3	273	207	26.1	92
5	13.7	6.60	2.83	6.43	180	153	21.2	48
6	23.5	12.2	0.30	3.74	309	283	2.26	28
7	13.6	6.37	3.21	7.31	178	148	24.0	55
8	22.1	9.62	1.12	10.2	291	223	8.40	76
9	13.7	6.44	2.98	7.00	179	149	22.3	52
10	20.7	8.11	3.36	14.5	271	188	25.1	109
11	14.7	8.84	0.97	0.00	193	205	7.26	0
12	21.9	7.69	1.23	15.8	287	178	9.2	118
13	14.8	6.66	1.13	6.42	194	154	8.42	48
14	14.8	6.90	1.01	5.61	194	160	7.53	42
15	13.4	6.55	3.14	6.38	176	152	23.5	48
16	14.4	6.70	0.59	5.17	189	155	4.44	39
17	22.2	2.66	-	-	292	61.6	-	-
18	22.5	9.66	-	-	296	224	-	-
19	23.9	11.5	-	-	315	266	-	-
20	15.3	5.77	-	-	200	134	-	-
21	22.5	16.9	-	-	296	391	-	-
22	14.9	5.38	-	-	196	125	-	-
23	19.4	8.30	-	-	255	192	-	-
24	15.2	7.59	-	-	200	176	-	-
25	6.4	3.04	-	-	84.5	70.4	-	-
26	7.0	18.3	-	-	408	424	-	-
27	31.1	26.8	-	-	500	621	-	-
28	30.2	4.94	-	-	92.2	115	-	-
29	38.1	16.9	-	-	396	392	-	-
30	44.8	31.1	-	-	589	720	-	-

Hardware Resistance Measurements

The resistance of the hardware used in the bench-scale electrowinning experiments was determined every hour for every experiment. The hardware resistance remained constant over each experiment but differed slightly between experiments. The residual plot indicates difference from the average resistance per experiment, and the large uniform scatter shows that the average resistance value is reliable.

Table C.5: *Resistances in the anodic and cathodic components of the bench-scale electrowinning cell, measured in each experiment. Experiment numbers correspond to the experimental design in Table B.1.*

Experiment number	Resistance (Ω)			
	Total	Anodic connections	Cathodic connections	Other
1	0.0345	0.0097	0.0244	0.0004
2	0.0533	0.0105	0.0291	0.0136
3	0.0456	0.0098	0.0260	0.0098
4	0.0548	0.0099	0.0283	0.0166
5	0.0440	0.0095	0.0213	0.0132
6	0.0314	0.0095	0.0190	0.0030
7	0.0340	0.0094	0.0230	0.0017
8	0.0362	0.0096	0.0214	0.0052
9	0.0414	0.0095	0.0250	0.0069
10	0.0528	0.0098	0.0294	0.0136
11	0.0388	0.0096	0.0227	0.0064
12	0.0386	0.0098	0.0216	0.0073
13	0.0393	0.0096	0.0221	0.0076
14	0.0327	0.0095	0.0287	0.0000
15	0.0342	0.0096	0.0246	0.0000
16	0.0363	0.0092	0.0219	0.0052
17	0.0376	0.0100	0.0237	0.0040
18	0.0433	0.0097	0.0255	0.0080
19	0.0430	0.0095	0.0207	0.0127
20	0.0404	0.0096	0.0279	0.0029
21	0.0306	0.0096	0.0226	0.0000
22	0.0438	0.0101	0.0314	0.0023
23	0.0369	0.0093	0.0213	0.0063
24	0.0409	0.0096	0.0239	0.0075
25	0.0688	0.0106	0.0334	0.0248
26	0.0420	0.0105	0.0296	0.0020
27	0.0422	0.0107	0.0251	0.0064
28	0.0645	0.0106	0.0284	0.0256
29	0.0436	0.0106	0.0254	0.0076
30	0.0386	0.0107	0.0244	0.0035

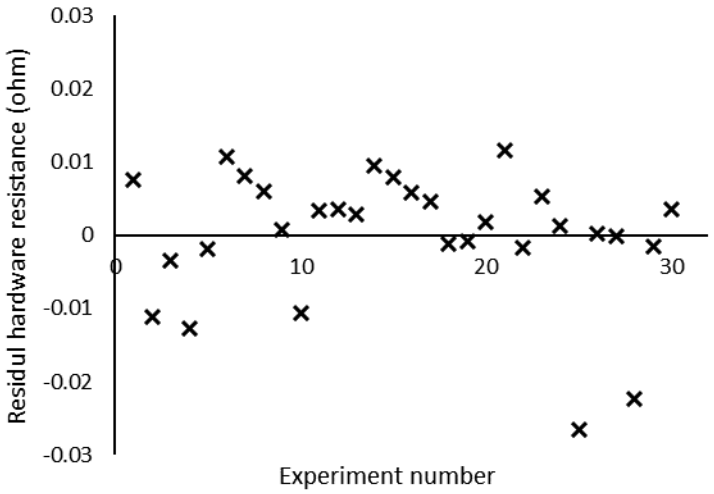

Figure C.1: *Residual hardware resistance per bench-scale electrowinning experiment, or the difference between average hardware resistance (used in the electrowinning model) and resistance per experiment.*

Plating Rate Experiments

The plating rate experiments consisted of measuring the mass of copper plated per hour in two repeat 24 hour experiments. Comparison between the two plating rates is provided, with hypothesis tests indicating that the plating rate remained constant over the period.

Table C.6: *Mass of copper plated over time for each bench-scale electrowinning plating rate experiment, with a current density of 200 A/m^2, initial copper concentration of 55 g/l, initial sulphuric acid concentration of 185 g/l and iron concentration of 4 g/l.*

Time (h)	Mass plated Experiment 1 (g)	Mass plated Experiment 2 (g)	Average mass plated (g)	Average plating rate per area (g/s/m^2)
0	0	0	0	0
1	6.450	7.930	7.190	0.0558
2	13.49	15.78	14.64	0.0584
3	21.35	24.06	22.71	0.0616
4	29.06	29.62	29.34	0.0629
5	37.00	36.13	36.57	0.0640
6	44.63	-	44.63	0.0644
7	52.01	-	52.01	0.0643
22	154.5	141.6	148.0	0.0608
23	161.7	147.5	154.6	0.0608
24	169.2	153.4	161.3	0.0610

Table C.7: *Details on the hypothesis tests conducted for the plating rate experiments, to determine whether there was a significant difference in plating rates per hour, and between the two experiments conducted.*

Test	Is there a significant difference between plating rates in the two experiments?	Is there a significant difference between the average plating rate in each hour to the constant plating rate?
Null hypothesis	H_0: $\mu_1 = \mu_2$	H_0: $\mu_{per\ hour} = \mu_{average}$
Alternate hypothesis	H_1: $\mu_1 \neq \mu_2$	H_1: $\mu_{per\ hour} \neq \mu_{average}$
Significance level	$\alpha = 0.05$	$\alpha = 0.05$
P value	0.69	0.91
Conclusion	0.686 > 0.05 Therefore, cannot reject null hypothesis that the plating rates between samples are equal.	0.91 > 0.05 Therefore, cannot reject null hypothesis that the plating rate each hour is equal to the constant overall plating rate.

Parameter Fitting

This section provides additional information relating to the fitting of model parameters to the bench-scale experimental data. For each electrochemical reaction, residual plots are provided indicating the difference between experimental current density and the Butler-Volmer model.

MATLAB Function: 'fitnlm'

The built-in MATLAB function used in the fitting of model parameters was 'fitnlm'. Input variables to the 'fitnlm' function are the experimental data (X and Y variables) to which the model needs to be fit, the model equation (Y as a function of X) with unknown parameters, and an initial guess of parameters. The function uses the method of least squares in an iterative manner to calculate the best fitting parameters such that the model equation matches the data as accurately as possible. The function requires the data to which the model This function makes use of an iterative procedure using the method of least-squares to calculate best fitting parameters.

Current Loss Parameter

Table C.8: *Current loss (the difference between total current and current used to plate copper) for each control experiment with no iron present. Experiment numbers correspond to the experimental design in Table B.1.*

Experiment Number	Total Current (A)	Current Loss (A)	Current used to plate copper (A)	Current loss as a percentage of total current (%)
17	9.60	0.224	9.38	2.33
18	9.70	0.210	9.49	2.17
19	10.2	0.103	10.1	1.01
20	6.57	0.136	6.43	2.07
21	9.68	0.171	9.51	1.77
22	6.40	0.097	6.30	1.51
23	8.26	0.088	8.17	1.07
24	6.58	0.175	6.40	2.67
25	3.10	0.139	2.96	4.49
27	12.8	0.109	12.7	0.85

Reduction of Copper

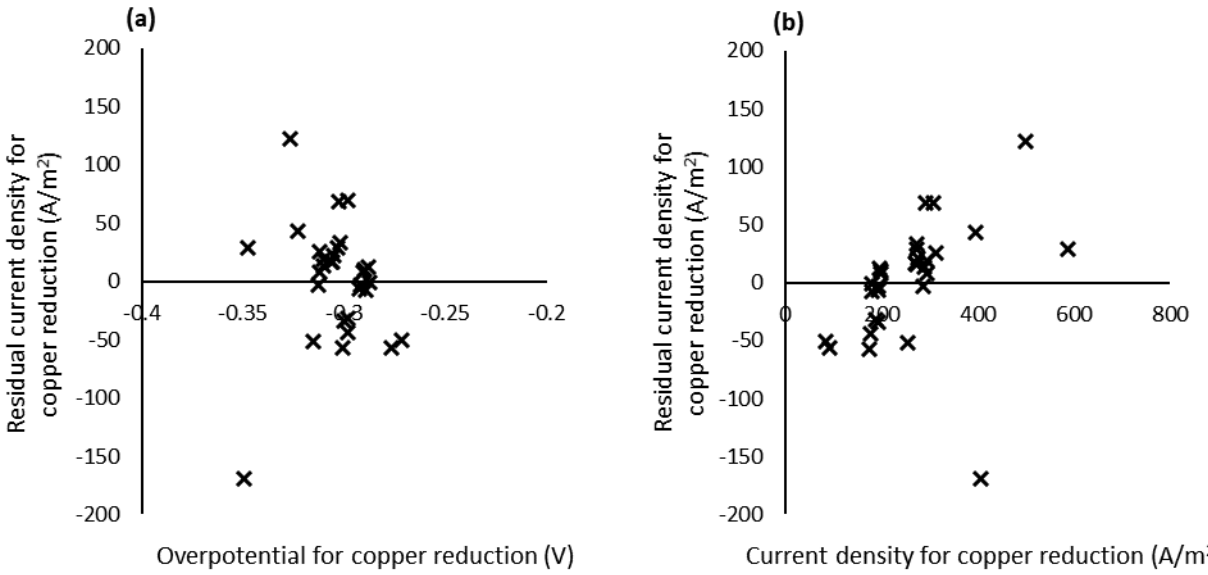

Figure C.2: *Residual current density for copper reduction as a function of the overpotential* ***(a)*** *and current density* ***(b)****, in the comparison of bench-scale experimental data to the model Butler-Volmer equation.*

The confidence intervals for the exchange current density parameter for copper reduction ($i_{0,Cu}$) are [-4.03x10^{-6}; 2.81x10^{-4}], and confidence intervals for the charge transfer coefficient (α_{Cu}) are [0.190; 0.279]. These confidence intervals are illustrated in *Figure 5.10*.

Oxidation of Water

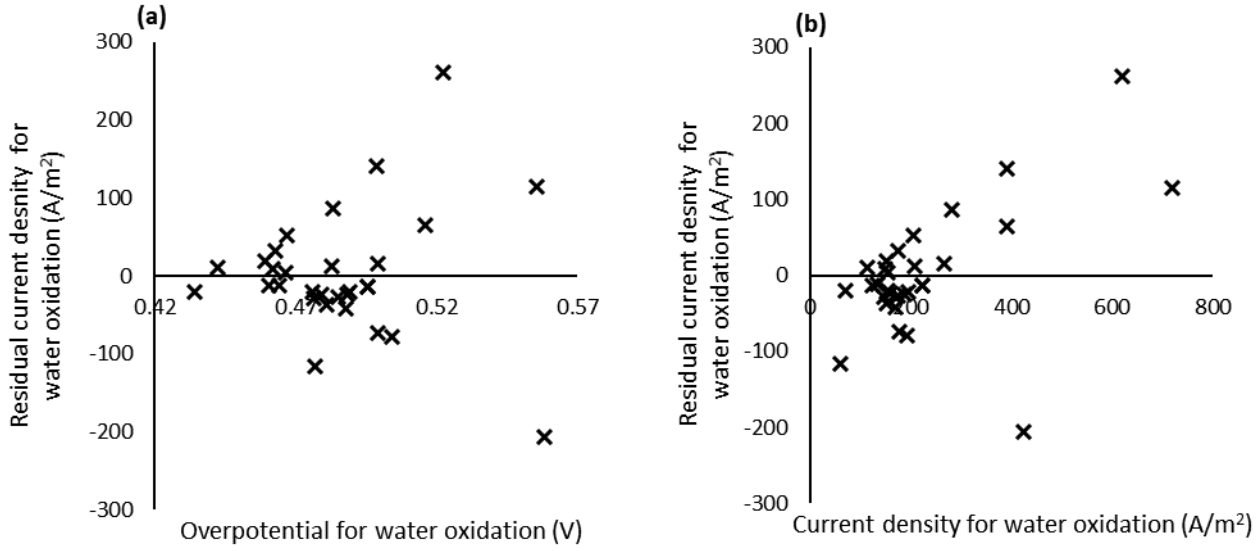

Figure C.3: *Residual current density for water oxidation as a function of the overpotential* ***(a)*** *and current density* ***(b)****, in the comparison of bench-scale experimental data to the model Butler-Volmer equation.*

The confidence intervals for the exchange current density parameter for water oxidation ($i_{0,H_{20}}$) are [-1.06x10^{-5}; 3.73x10^{-5}], and confidence intervals for the charge transfer coefficient (α_{H_20}) are [0.490; 0.680]. These confidence intervals are illustrated in *Figure 5.12*.

The heteroscedastic residual plots for copper reduction and water oxidation meant that a weighted nonlinear regression was used to fit model parameters within their kinetics equations.

Reduction of Iron

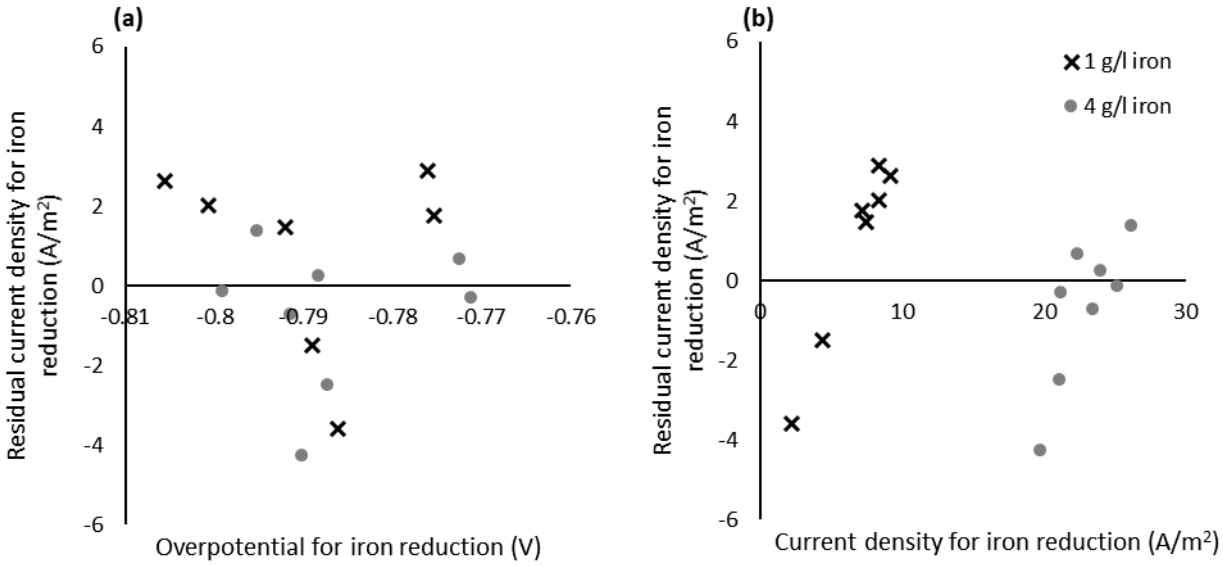

Figure C.4: *Residual current density for iron reduction as a function of the overpotential* ***(a)*** *and current density* ***(b)*** *for 1 and 4 g/l iron, in the comparison of bench-scale experimental data to the model Butler-Volmer equation.*

Oxidation of Iron

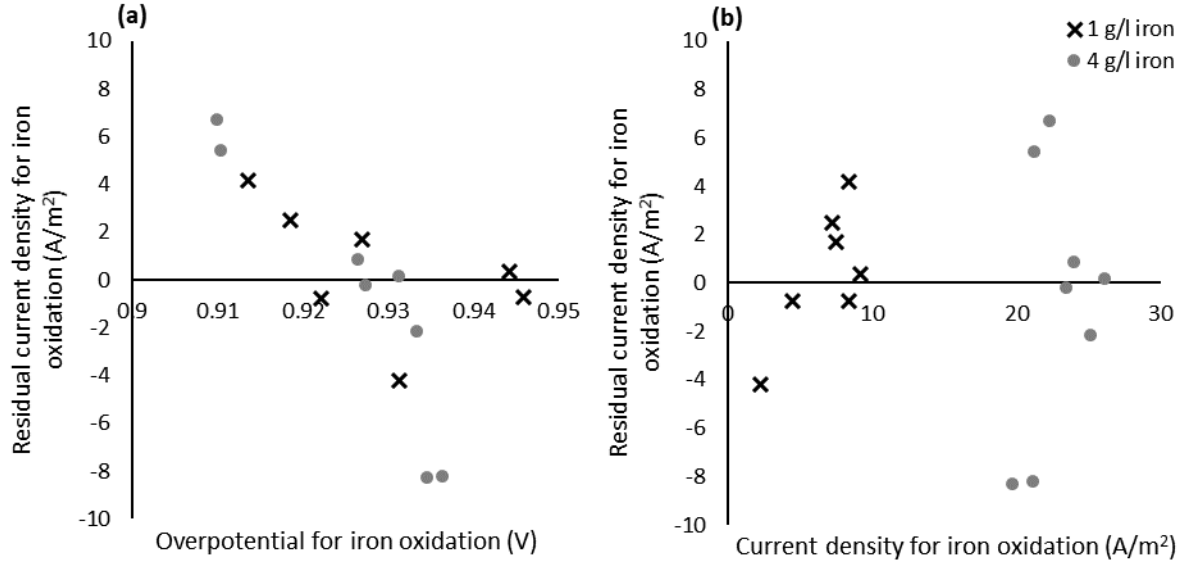

Figure C.5: *Residual current density for iron oxidation as a function of the overpotential* ***(a)*** *and current density* ***(b)*** *for 1 and 4 g/l iron, in the comparison of bench-scale experimental data to the model Butler-Volmer equation.*

Sensitivity Analyses

Table C.9: *Values of the performance indicators of plating rate, current efficiency and specific energy consumption with percentage increases and decreases in each parameter, for average bench-scale experimental data at 45 g/l copper, 175 g/l sulphuric acid, 2 g/l iron and a current density of 250 A/m^2.*

Parameter	Percentage change in parameter (%)	Key performance indicator		
		Plating rate (g/s/m^2)	Current efficiency (%)	Specific energy consumption (MWh/t)
	Original	0.0738	0.886	1.885
I_{loss}	-30	0.0738	0.891	1.875
	-20	0.0738	0.889	1.878
	+20	0.0738	0.883	1.891
	+30	0.0738	0.891	1.875
α_{Cu}	-30	0.0459	0.756	2.209
	-20	0.0567	0.820	2.037
	+20	0.0865	0.917	1.821
	+30	0.0915	0.926	1.803
$i_{0,Cu}$	-30	0.0692	0.872	1.916
	-20	0.0709	0.878	1.903
	+20	0.0762	0.893	1.870
	+30	0.0773	0.896	1.865
α_{H_2O}	-30	0.1041	0.910	1.835
	-20	0.0951	0.904	1.847
	+20	0.0584	0.867	1.926
	+30	0.0563	0.864	1.933
i_{0,H_2O}	-30	0.0702	0.883	1.893
	-20	0.0715	0.884	1.889
	+20	0.0759	0.889	1.880
	+30	0.0768	0.890	1.878
$\alpha_{Fe^{3+},red}$	-30	0.0784	0.950	1.758
	-20	0.0775	0.938	1.781
	+20	0.0650	0.764	2.185
	+30	0.0574	0.661	2.526
$i_{0,Fe^{3+},red}$	-30	0.0756	0.911	1.834
	-20	0.0750	0.903	1.850
	+20	0.0727	0.870	1.919
	+30	0.0722	0.863	1.936
$\alpha_{Fe^{2+},ox}$	-30	0.1005	0.908	1.839
	-20	0.0889	0.900	1.856
	+20	0.0716	0.884	1.889
	+30	0.0715	0.884	1.889
$i_{0,Fe^{2+},ox}$	-30	0.0732	0.886	1.885
	-20	0.0734	0.886	1.885
	+20	0.0743	0.887	1.883
	+30	0.0745	0.887	1.883

Table C.9 (continued):

Parameter	Percentage change in parameter (%)	Key performance indicator		
		Plating rate (g/s/m^2)	Current efficiency (%)	Specific energy consumption (MWh/t)
$m_{Fe^{3+},red}$	-30	0.0721	0.863	1.936
	-20	0.0727	0.871	1.919
	+20	0.0750	0.903	1.850
	+30	0.0756	0.911	1.834
$m_{Fe^{2+},red}$	-30	0.0738	0.886	1.885
	-20	0.0738	0.886	1.885
	+20	0.0738	0.886	1.885
	+30	0.0738	0.886	1.885
$m_{Fe^{3+},ox}$	-30	0.0738	0.886	1.885
	-20	0.0738	0.886	1.885
	+20	0.0738	0.886	1.885
	+30	0.0738	0.886	1.885
$m_{Fe^{2+},ox}$	-30	0.0740	0.887	1.884
	-20	0.0739	0.887	1.884
	+20	0.0738	0.886	1.885
	+30	0.0737	0.886	1.885

Industrial Data

Table C.10: *Input data required for the electrowinning model in 18 industrial electrowinning plants, obtained from Robinson* et al. *(2013b).*

Plant number	Tankhouse name and location	Number of Cathodes	Area per electrode side (m^2)	Cell temperature (°C)	Interelectrode distance (mm)	Flowrate (m^3/h)
1	Minera El Abra, Chile	66	1.25	41.5	47.5	19.2
2	Escondida Oxide, Chile	60	0.97	50	50.8	16.2
3	Escondida Sulfide, Chile	60	1	52	50.8	16.8
4	Mantos Blancos, Chile	51	1.25	49	52.3	18
5	Radomiro Tomic, Chile	60	1.25	47.5	50	16.8
6	Salvador, Chile	45	1.22	48	50	
7	Minera Cerro Verde, Peru	50	1.24	45	50	13.6
8	Toquepala, Peru	62	1.29	46	47.625	18
9	Mineral Park, USA	21	1.32	35	50.8	1.8
10	Morenci Central, USA	63	1.31	46.5	50.8	8.4
11	Safford, USA	73	1.3	47	50.8	36
12	Hellenic Copper, Cyprus	30	1.12	35	50	6.6
13	Kamoto Copper EW1, DRC	228	1.25	45	45	6
14	Kansanshi, Zambia	69	1.1	40	47.5	15
15	Mutanda, DRC	48	1.32	45	47.5	
16	Tenke Fungurume, DRC	66	1.16	50	50	27
17	Rustenburg BMR, South Africa	63	1.14	55	47.5	
	Bench-scale cell	1	0.032	45	20	0.0035

Table C.11: *Electrolyte composition data in advance and spent electrolyte for industrial electrowinning plants, obtained from Robinson* et al. *(2013b). For specific tankhouse names and locations, refer to Table C.10.*

Plant number	Iron concentration (g/l)	Advance electrolyte		Spent electrolyte	
		Copper concentration (g/l)	Sulphuric acid concentration (g/l)	Copper concentration (g/l)	Sulphuric acid concentration (g/l)
1	1.7	36	185	34	195
2	1.4	42.5	180	40	185
3	1.2	42.5	182.5	40.5	185
4	1.23	31	200	30	210
5	1.15	40	195	38	180
6	0.75	56	175	41	195
7	2.61	34	170	32	172
8	2.2	45	165	35	180
9	2.75	43	167.5	26	178
10	2.75	41	185	35	200
11	2.64	36	185	33.8	188.6
12	2	30	165	26	175
13	2	48	170	35	180
14	5	55	175	35	190
15	1.75	42.5	160	32.5	190
16	1.2	43	180	40	187
17	2.25	70	90	35	120

Table C.12: *Electrowinning power data and mass of copper plated in the electrowinning duration for industrial electrowinning plants, obtained from Robinson* et al. *(2013b). For specific tankhouse names and locations, refer to Table C.10.*

Plant number	Voltage at electrodes (V)	Current per cell (kA)	Current density (A/m^2)	Mass copper plated per side (kg)	Electrowinning duration (days)
1	1.89	36	285	35	5
2	1.95	33	303	37	4.5
3	2.1	39.25	350	37	5
4	1.86	20	214	37.5	6
5	1.87	34	260	42.5	6
6	1.9	22.5	250	45	6.5
7	1.89	23.975	220	7	8
8	1.95	35	285	55	7
9	2.25	4.5	114	40	14
10	1.95	38	290	42.5	6
11	1.88	47	253	55	7
12	1.8	14	212.5	55	11
13	2.3	30.5	270	37.5	5
14	2	0.6875	280	40	6.5
15	2	22.5	235	40	8
16	2	54.5	356.5	61	7
17	1.8	11	156	7	9

Comparison between Actual and Predicted Data

Table C.13: *Comparison between actual electrowinning plating rates and plating rates predicted by the electrowinning model using identical input conditions, for bench-scale experiments and industrial data.*

Category	Number	Plating rate (g/s/m^2)			Percentage error (%)
		Actual	Predicted	Error	
Bench-scale experimental data used in parameter fitting	1	0.0903	0.077	0.013317	-14.7552
	2	0.0903	0.103	-0.01246	13.8
	3	0.0906	0.089	0.001474	-1.63
	4	0.0898	0.097	-0.00773	8.61
	5	0.0592	0.057	0.002435	-4.11
	6	0.1016	0.080	0.021415	-21.1
	7	0.0587	0.055	0.003202	-5.45
	8	0.0957	0.086	0.009729	-10.2
	9	0.0591	0.056	0.003249	-5.50
	10	0.0894	0.097	-0.00756	8.46
	11	0.0634	0.059	0.004112	-6.49
	12	0.0946	0.090	0.004339	-4.59
	13	0.0638	0.060	0.004176	-6.54
	14	0.0640	0.059	0.00474	-7.40
	15	0.0580	0.057	0.001191	-2.05
	16	0.0624	0.059	0.002916	-4.67
	17	0.0962	0.082	0.014238	-14.8
	18	0.0974	0.095	0.001899	-1.95
	19	0.1036	0.100	0.003581	-3.46
	20	0.0660	0.061	0.005294	-8.02
	21	0.0975	0.083	0.01437	-14.7
	22	0.0647	0.061	0.004011	-6.20
	23	0.0838	0.082	0.001805	-2.15
	24	0.0657	0.061	0.004857	-7.39
	25	0.1345	0.139	-0.00501	3.72
	26	0.0278	0.039	-0.01095	39.3
	27	0.1648	0.153	0.012163	-7.38
	28	0.0304	0.041	-0.0106	34.9
	29	0.1938	0.183	0.0113	-5.82
	30	0.1305	0.128	0.0026	-2.01
Additional bench-scale experiments	31	0.0985	0.099	-0.0039	-4.07
	32	0.0560	0.056	0.0081	12.6
	33	0.0609	0.061	0.0044	6.79
	34	0.0763	0.076	-0.0037	-5.1

Table C.13 (continued):

Category	Number	Plating rate (g/s/m²)			Percentage error (%)
		Actual	Predicted	Error	
Industry data	1	0.0676	0.068	-0.0028	4.27
	2	0.0697	0.070	0.0284	-29.0
	3	0.0448	0.045	0.0409	-47.7
	4	0.0591	0.059	-0.0012	2.15
	5	0.0615	0.061	0.0041	-6.25
	6	0.0583	0.058	0.0074	-11.2
	7	0.0082	0.061	-0.0524	n/a
	8	0.0209	0.021	0.0496	n/a
	9	0.0251	0.073	-0.0482	n/a
	10	0.0736	0.074	-0.0110	17.6
	11	0.0586	0.059	0.0113	-16.2
	12	0.0465	0.046	0.0052	-10.1
	13	0.0917	0.092	-0.0223	32.1
	14	0.0777	0.078	-0.0130	20.0
	15	0.0287	0.029	0.0151	-34.5
	16	0.0827	0.083	0.0043	-4.92
	17	0.0079	0.039	-0.0309	n/a

Table C.14: *Comparison between actual electrowinning current efficiencies and current efficiencies predicted by the electrowinning model using identical input conditions, for bench-scale experiments and industrial data.*

Category	Number	Plating rate (g/s/m^2)			Percentage error (%)
		Actual	Predicted	Error	
Bench-scale experimental data used in parameter fitting	1	90.7	86.5	4.20	-4.63
	2	90.8	94.2	-3.40	3.75
	3	91.3	87.7	3.58	-3.92
	4	90.3	88.0	2.23	-2.47
	5	87.7	83.7	4.00	-4.56
	6	97.2	93.0	4.22	-4.34
	7	86.9	82.9	3.94	-4.54
	8	96.2	93.2	2.98	-3.10
	9	87.7	83.5	4.21	-4.80
	10	89.9	88.0	1.91	-2.13
	11	94.3	91.2	3.13	-3.32
	12	95.2	93.4	1.72	-1.81
	13	94.5	91.3	3.20	-3.39
	14	94.9	91.0	3.91	-4.12
	15	85.9	83.1	2.79	-3.25
	16	95.0	91.0	4.02	-4.23
	17	97.7	97.1	0.59	-0.60
	18	97.9	97.5	0.37	-0.38
	19	99.0	97.6	1.41	-1.42
	20	97.9	96.0	1.86	-1.90
	21	98.2	97.1	1.13	-1.15
	22	98.5	96.0	2.46	-2.50
	23	98.9	97.0	1.86	-1.89
	24	97.3	96.1	1.24	-1.27
	25	102.0	94.0	8.02	-7.87
	26	84.8	85.2	-0.40	0.48
	27	100.5	98.4	2.06	-2.05
	28	95.5	94.2	1.26	-1.31
	29	98.5	98.7	-0.21	0.22
	30	99.1	98.1	1.00	-1.01
Additional bench-scale experiments	31	84.3	88.2	-3.83	-4.54
	32	84.4	83.5	0.87	1.03
	33	94.3	96.1	-1.72	-1.82
	34	81.7	86.0	-4.35	-5.33

Table C.14 (continued):

Category	Number	Plating rate (g/s/m²)			Percentage error (%)
		Actual	Predicted	Error	
Industry data	1	92.0	94.7	-2.74	2.97
	2	91.0	98.0	-7.05	7.75
	3	92.0	98.9	-6.89	7.49
	4	90.0	99.6	-9.61	10.68
	5	93.0	98.2	-5.16	5.55
	6	93.0	87.6	-5.16	5.55
	7	87.9	89.6	-1.76	2.00
	8	93.0	84.1	8.86	-9.53
	9	80.0	89.8	-9.80	12.25
	10	88.0	90.7	-2.69	3.05
	11	89.1	89.6	-0.48	0.53
	12	91.5	90.1	1.39	-1.52
	13	77.5	94.3	-16.76	21.62
	14	85.0	87.8	-2.76	3.25
	15	80.0	90.7	-10.72	13.41
	16	88.0	99.3	-11.28	12.82
	17	90.0	89.7	0.32	-0.36

Table C.15: *Comparison between actual electrowinning specific energy consumption and specific energy consumption predicted by the electrowinning model using identical input conditions, for bench-scale experiments and industrial data.*

Category	Number	Plating rate (g/s/m^2)			Percentage error (%)
		Actual	Predicted	Error	
Bench-scale experimental data used in parameter fitting	1	1.86	1.95	-0.09	4.87
	2	1.95	1.88	0.07	-3.60
	3	1.91	1.99	-0.08	4.09
	4	1.96	2.01	-0.05	2.54
	5	1.83	1.92	-0.09	4.79
	6	1.74	1.82	-0.08	4.54
	7	1.84	1.93	-0.09	4.76
	8	1.77	1.83	-0.06	3.21
	9	1.83	1.92	-0.09	5.05
	10	1.97	2.01	-0.04	2.18
	11	1.70	1.75	-0.06	3.44
	12	1.81	1.85	-0.03	1.85
	13	1.70	1.76	-0.06	3.51
	14	1.69	1.76	-0.07	4.31
	15	1.87	1.93	-0.06	3.37
	16	1.69	1.76	-0.07	4.42
	17	1.73	1.74	-0.01	0.62
	18	1.78	1.79	-0.01	0.39
	19	1.77	1.80	-0.03	1.45
	20	1.64	1.67	-0.03	1.95
	21	1.72	1.74	-0.02	1.18
	22	1.63	1.67	-0.04	2.57
	23	1.71	1.74	-0.03	1.93
	24	1.65	1.67	-0.02	1.30
	25	1.87	2.03	-0.16	8.55
	26	1.78	1.77	0.01	-0.47
	27	1.93	1.97	-0.04	2.10
	28	1.58	1.60	-0.02	1.34
	29	2.07	2.07	0.00	-0.21
	30	1.87	1.89	-0.02	1.03
Additional bench-scale experiments	31	2.10	2.01	0.09	4.34
	32	1.90	1.92	-0.02	-1.05
	33	1.70	1.67	0.03	1.78
	34	2.07	1.96	0.10	5.05

Table C.15 (continued):

Category	Number	Plating rate (g/s/m²)			Percentage error (%)
		Actual	Predicted	Error	
Industry data	1	1.74	1.68	0.06	-3.28
	2	1.85	1.68	0.17	-9.32
	3	2.00	1.79	0.21	-10.43
	4	1.85	1.58	0.27	-14.86
	5	1.80	1.61	0.19	-10.72
	6	1.80	1.83	-0.03	1.66
	7	2.02	1.78	0.24	-11.96
	8	2.50	1.95	0.55	-21.80
	10	1.98	1.81	0.17	-8.39
	11	1.80	1.77	0.03	-1.64
	12	2.00	1.68	0.32	-15.75
	14	2.63	1.92	0.71	-26.91
	16	1.90	1.70	0.20	-10.57
	17	2.04	1.69	0.35	-17.00

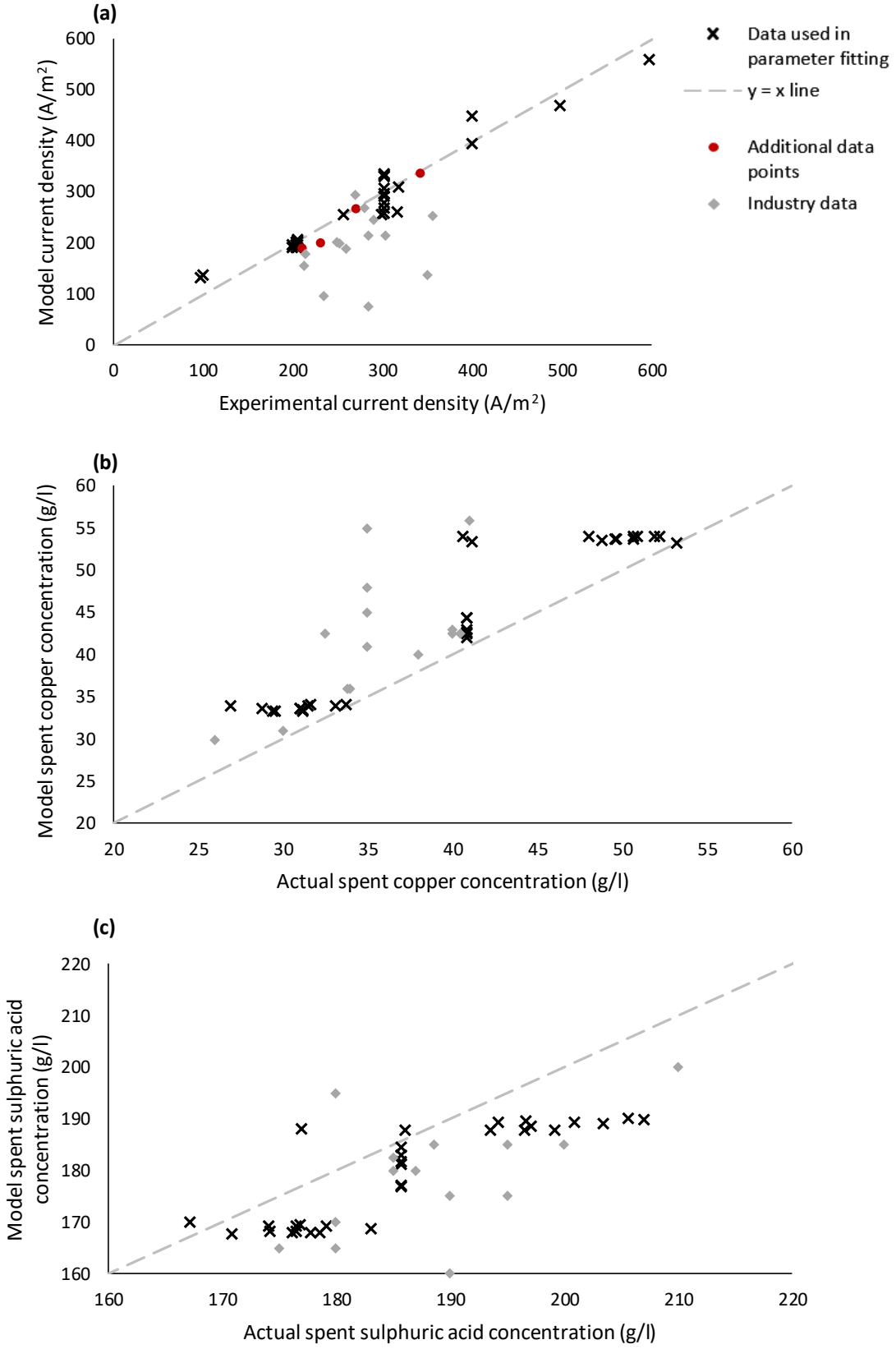

Figure C.6: *Additional comparisons of predicted electrowinning output data to actual electrowinning output data for* ***(a)*** *current density,* ***(b)*** *spent copper concentration and* ***(c)*** *spent sulphuric acid concentration.*

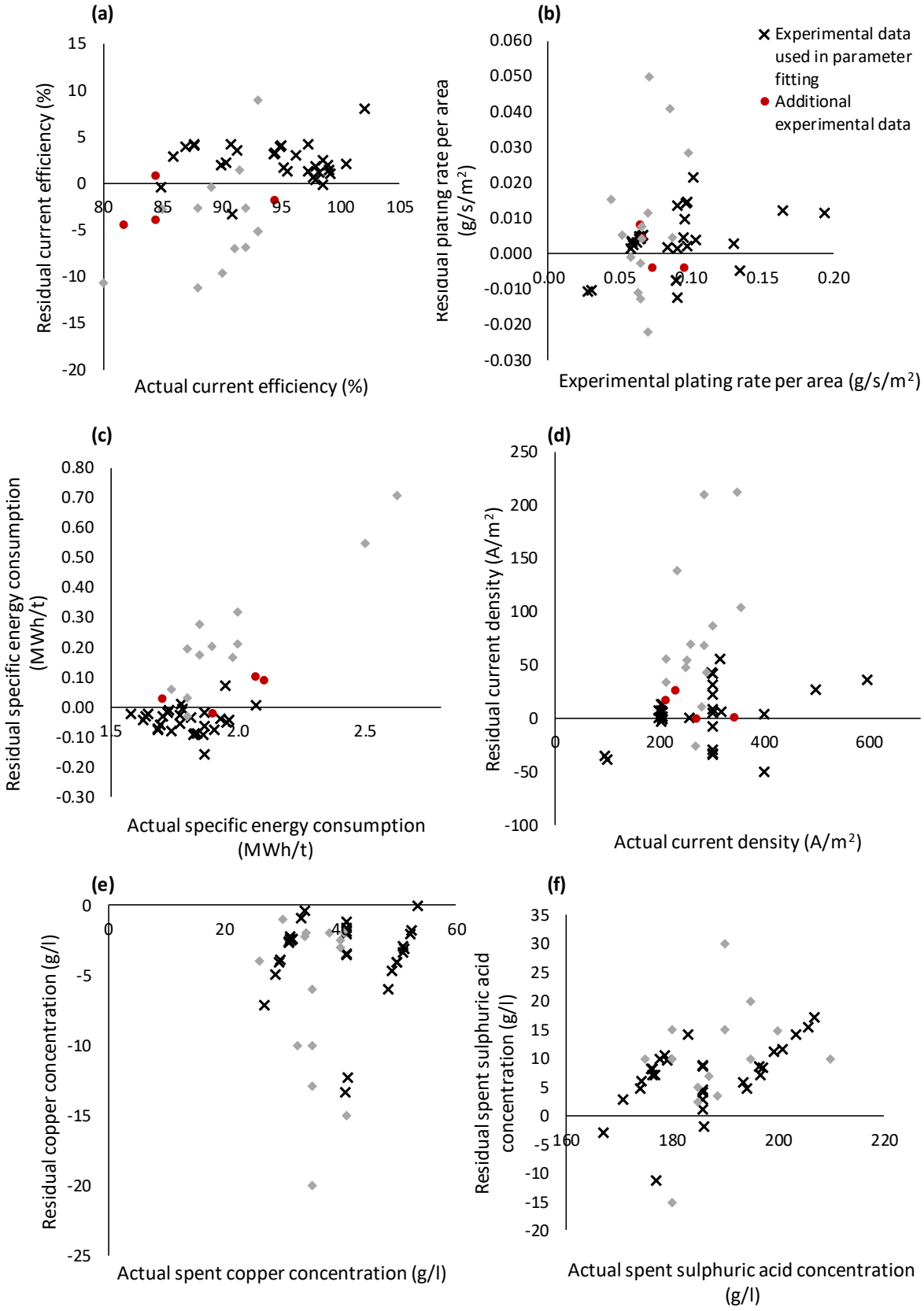

Figure C.7: *Residual graphs (difference between actual and predicted value) for* ***(a)*** *current efficiency,* ***(b)*** *copper plating rate,* ***(c)*** *specific energy consumption,* ***(d)*** *current density,* ***(e)*** *spent copper concentration and* ***(f)*** *spent sulphuric acid concentration.*